信州大学審査学位論文

Biofunctionalization of Carbon Nanotubes

March 2012

JINHEE KIM

Summary

CNTs hold great promise as a next-generation vehicle for biomolecules in biosensors, drug carriers and biocatalysts because they are optically active, electrically conductive, mechanically strong and small enough in diameter. However, CNTs are insoluble in an aqueous solution and exhibit a low degree of biocompatibility because of their strongly bundled structure as well as the hydrophobic nature of their sidewalls. In my PhD. thesis, to solve such intrinsic problems as well as to exploit their excellent physical and chemical properties at a molecular level, I carried out the biofunctionalization of CNTs by attaching biomolecules to the sidewall of the tubes, and then provided the promising uses of DNA-wrapped CNTs as reinforcing filler in the biomolecule-based nanofiber web using the electrospinning system and the template for the hybrid-type biocatalysts.

In chapter 3, I revealed the role of defects in dispersibility of CNTs in aqueous DNA solutions using as-grown defective and high-temperature thermally treated tubes. We found that the dispersibility of nanotubes depended strongly on the density of the defect on the sidewall. DNA was helically wrapped around the sidewall of the tubes in an irregular pattern. Structural defects on the sidewall of nanotubes are found to provide additional sites for binding with DNA. Theoretical calculations support the conclusion that defect sites exhibit high reactivity toward the adsorption of DNA.

In chapter 4, I reported experimental and theoretical evidence to demonstrate that the nitrogen doped CNTs are highly dispersed in DNA solution compared to pure and hydroxyl group-decorated CNTs. I observed the anomalously two-fold high dispersion of nitrogen doped carbon nanotubes as compared with those of pure and hydroxyl group-decorated CNTs. Such a result is rationalized by the larger amount of adsorbed DNA that is observed in nitrogen doped CNTs as well as the higher binding energy between nucleobases and nitrogen doped CNTs.

In chapter 5, I have prepared individually dispersed DWNT aqueous solutions using ssDNA, and studied the interaction between DNA molecules and the outer tubes of DWNTs in solution. I observed that the inner tubes are structurally shielded by outer tubes, and charge transfer occurs from the outer tubes to the inner tubes by observing the completely depressed RBMs associated with the outer tubes via the mechanical wrapping and the strong charge transfer between DNA and the outer tubes. I demonstrated that the bright fluorescence as well as the sharp absorption peaks arises from the inner tubes of DWNTs, and not from isolated SWNTs. I believe that the inner tubes of DWNTs could be more efficient than SWNTs in the fabrication of

photoluminescent materials.

In chapter 6, I demonstrated a simple way of preparing optically and biologically active protein/nanotube multifunctional materials with the help of a bio-inspired multifunctional mussel adhesive protein. The optical studies revealed that the semitransparent DWNT aqueous suspension thus prepared exhibited strong optical signals from the inner tubes of the DWNT. Mussel protein are coated homogeneously and completely on the sidewall of the DWNTs by creating covalent bridge between the hydroxyl groups on the outer tubes of the DWNTs and the amine groups of dopamine. The optically active, electrically conductive, mechanically strong, waterproof and biologically active mussel protein coated DWNT will find their applications in bio and medical applications as well as electronic devices.

In chapter 7, I fabricated mechanically tough, electrically conductive PEO nanofiber web using the electrospinning system by incorporating DNA or DNA-wrapped CNTs. Strong luminescent signal from the inner tubes in DWNTs indicates that nanotubes were individually dispersed in DNA solution. Newly developed mechanically tough, electrically conductive PEO nanofiber web with a high porosity will find their applications in biomedical fields.

In chapter 8, I developed a novel type of cellulase that is both alkali- and thermo-stable by immobilizing cellulose on the sidewall of SWNTs dispersed by helically wrapped DNA. The hydrophobic interactions between the sidewall of the tubes and the cellulases are helpful for maintaining the shape of the cellulase molecules in the temperature range of 40～80°C, while the helically wrapped DNA along the sidewall of the tube imparts high stability at high pH. I envisage that this alkali- and thermo-stable form of cellulase can be used over a wide range of temperatures and environmental conditions.

In this thesis, I demonstrated the effectiveness of biomolecules as dispersing agent and surface modifier for the intrinsically bundled and hydrophobic CNTs by clarifying the interaction between the sidewall of CNTs and biomolecules and then suggested the novel uses of biomolecules-decorated CNTs as reinforcing filler in PEO-based nanofiber web and as the template for the hybrid-type biocatalysts. It is envisaged that my accomplished results will contribute to the development of multi-functional scaffolds for growing cells, high-performance coating material for biomedical devices and novel-type drug delivery system.

Abbreviation

CNT	carbon nanotube
SWNT	single walled carbon nanotube
DWNT	double walled carbon nanotube
M tube	metallic tube
S tube	semiconducting tube
S@S	a semiconducting inner tube and a semiconducting outer tube
S@M	a semiconducting inner tube and a metallic outer tube
M@S	a metallic inner tube and a semiconducting outer tube
M@M	a metallic inner tube and a metallic outer tube
MWNT	multi-walled carbon nanotube
DNA	deoxyribonucleic acid
ssDNA	single stranded deoxyribonucleic acid
dsDNA	double stranded deoxyribonucleic acid
Dopa	3, 4-dihydroxy-L-phenylalanine
Mgfp	mytilus galloprovincialis foot protein
CVD	chemical vapor deposition
CCVD	catalytic chemical vapor deposition
Peapod	single walled carbon nanotube encapsulating fullerenes
SDBS	sodium dodecyl benzene sulfonate
SEM	scanning electron microscopy
TEM	transmission electron microscopy
XPS	x-ray photoelectron spectroscopy
UV-vis-NIR	ultraviolet-visible-near Infrared
PL	photoluminescence
TGA	thermogravimetric analysis
RBM	radial breathing mode
I_D	the intensity of the D band
I_G	the intensity of the G band
BWF	Breit-Wigner-Fano
PEO	polyethylene oxide
Ex-1	cellobiohydrolase

Contents

CHAPTER 1

General Introduction

Chapter 1 General Introduction

1.1 Background

Over the past 15 years, nanotechnology has received lots of attention from our society as innovative solutions for the global problems. Simply speaking, nanotechnology could be defined as the capability to understand and design complex things on nanoscale. CNT is considered as the most intensively studied nanotechnology-related materials of this decade. Geometrically, CNT is a seamless long hollow tubule by rolling graphene layer. Such unique configuration at the atomic level renders it to show unique structural, chemical, mechanical, thermal, optical and electronic properties[1-3]: Young's modulus is higher than any other material, and tensile strength is 100 times stronger than steel, the electrical current density is 100 times higher than for copper and carrier mobility is *ca.* 105 cm^2/Vs. Those theoretically expected and experimentally confirmed properties allow us to study their fundamental properties in detail, and make them promising in a wide range of applications.

1.1.1 What is Carbon Nanotube?

CNT could be visualized by rolling sheets of graphene (sp^2 carbon honeycomb lattice) into a cylinder of nanometer size diameter (Fig. 1 (a)). The structure of CNT has been explored early on by high-resolution transmission electron microscopy (Fig. 1 (b)),[4] yielding direct information that the nanotubes are seamless nanoscale tubule derived from the honeycomb lattice representing a single atomic layer of crystalline graphite, so-called a graphene sheet. The curvature of the nanotubes incorporates a small amount of sp^3 bonding so that the force constant in the circumferential direction is slightly weaker than along the nanotube axis. SWNT is only one atom thick and has a small number of atoms around its circumference, only a few wave vectors are needed to describe the periodicity of the nanotubes. These constraints lead to quantum confinement of the wave functions in the radial and circumferential directions, with plane wave motion occurring only along the nanotube axis, corresponding to a large number or closely spaced allowed wave vectors. CNTs (*n, m*) can be either metallic or semiconducting, and likewise the individual constituents of MWNTs or SWNT bundles can be metallic or semiconducting.[5] In the case of MWNTs of which diameter smaller than around 100 nm, no graphitic three-dimensional stacking is established,[6] even though an individual shell of the multi layers consists of perfect graphene sheets. Also each tube has different and independent chirality, which might contribute to a larger inter-shell spacing than is found in graphite. These characteristic structures of single-

and MWNTs indicate that they are unique one-dimensional materials with fascinating electronic, chemical, mechanical, and thermal properties.

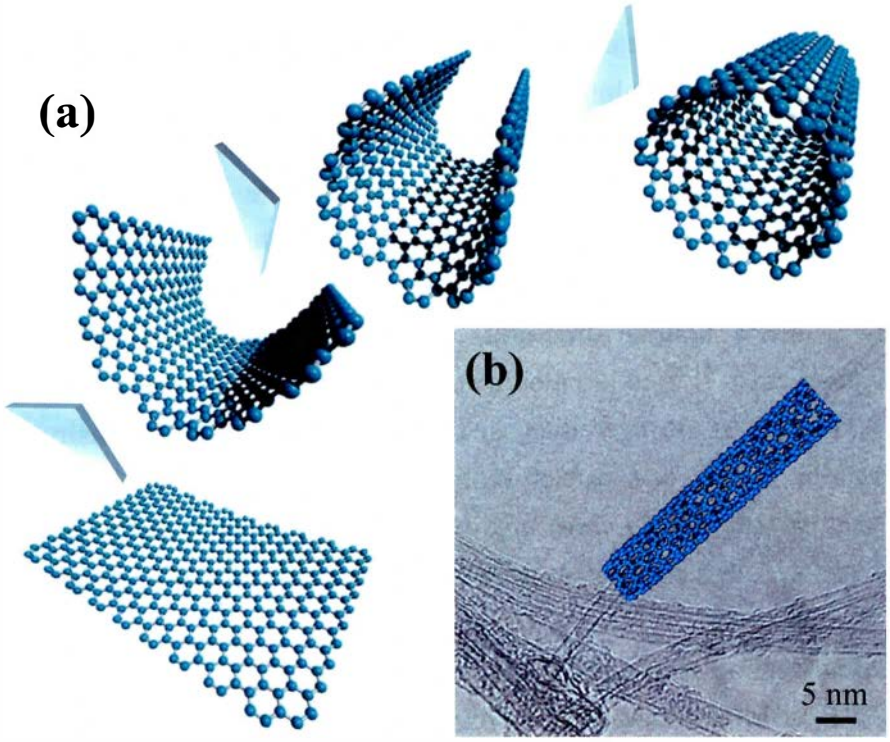

Figure 1 (a) A schematic diagram describing how CNT is made by rolling a single graphene (sp^2 carbon honeycomb lattice). (b) A typical high-resolution transmission electron microscope image of CNT.

1.1.2 Electronic Properties of Carbon Nanotube

Since CNTs can be rolled from a graphene sheet in many ways, there are numerous possible orientations of the hexagons on the nanotubes (Fig. 2), even though the basic shape of the CNT wall is a cylinder, where the two indices (n, m) fully identify each unique CNT.[1, 2] CNTs (n, m) can be either metallic ($n - m = 3q$, $q = 0, 1, 2, \ldots$) or semiconducting ($n - m = 3q \pm 1$, $q = 0, 1, 2, \ldots$).[5] These remarkable electronic properties follow from the electronic structure of 2D graphite under the constraints of quantum confinement in the circumferential direction.[5] The unique electronic properties of CNTs are caused by the quantum confinement of electrons normal to the nanotube axis. In the radial direction, electrons are confined by the monolayer thickness of the graphene sheet. Consequently, electrons can propagate only along the nanotube axis, and so to their wave vector points. The resulting number of one-dimensional conduction and valence bands effectively depends on the standing waves that are set up around the circumference of the CNTs. The sharp intensities (spikes) in the density of states of the tubes are known as van Hove singularities[6] and are the result of this one-dimensional

quantum conduction. Thus, the band gap for the metallic and semiconducting nanotubes is inversely proportional to the tube diameter,[7] resulting in a unique electronic property.[8]

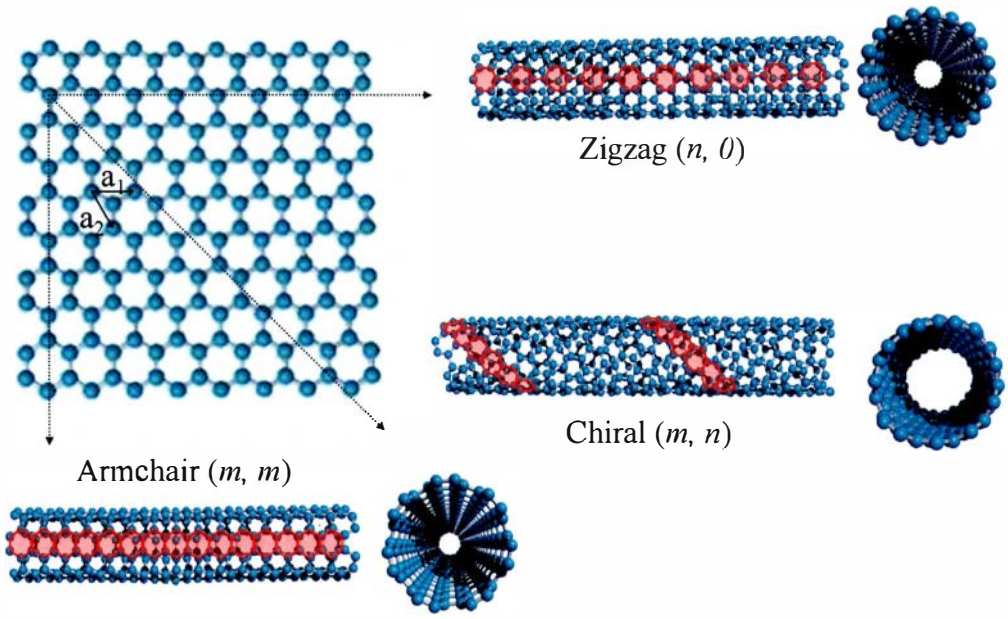

Figure 2 Schematic models of SWNTs when the graphene sheet is wrapped in a certain direction: an "armchair" (*n, n*) nanotube, a "zigzag" (*n, 0*) nanotube, and a chiral (*n, m*) nanotube.

1.1.3 Mechanical Strength of Carbon Nanotube

The sp^2 carbon-carbon bond in the basal plane of graphene is the strongest of all chemical bonds, resulting in the high Young's modulus of graphene (1,086 GPa).[9, 10] A theoretical prediction was verified by an experimental result of 1.06 TPa.[11] Thus, CNT is the stiffest of all known materials. In addition, the flexibility of nanotubes enable them to accommodate extreme deformation without fracturing, and in my cases, they are able to recover apparently from such deformations. These remarkable mechanical properties will lead to many important applications. More specifically, they are a strong candidate for incorporating into numerous structural biomaterials such as bone and scaffold.

1.1.4 Optical Activity of Carbon Nanotube

CNTs have the sharp intensities in the density of states of the tubes (Fig. 3) that are known as van Hove singularities and thus they exhibit high optical activity, such as strong Raman line,[12, 13] bright photoluminescent signal[14-19] and strong absorption peak[20].

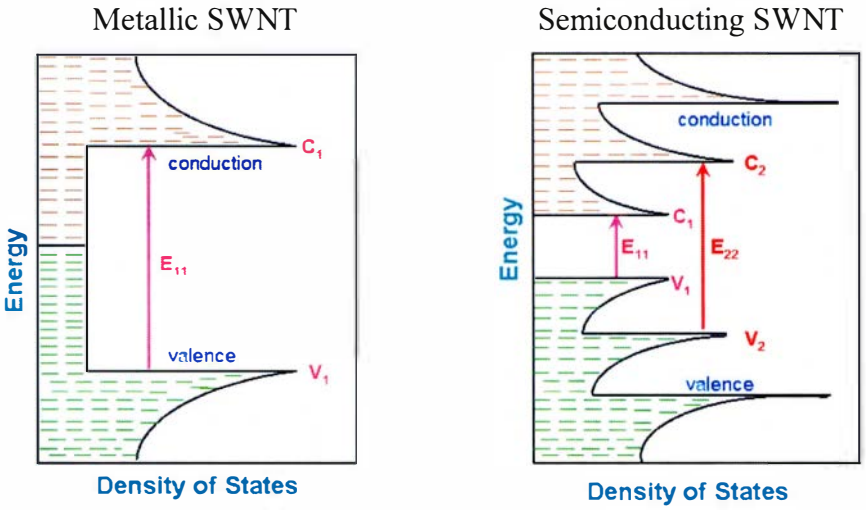

Figure 3 Typical densities of states as a function of energy for metallic and semiconducting SWNTs, where $v_1 \rightarrow c_1$ indicates the first van Hove optical transition (E_{11}) whereas $v_2 \rightarrow c_2$ corresponds to the second van Hove optical transition (E_{22}). From Ref. 21.

1.1.5 The Necessity of Biofunctionalizing Carbon Nanotubes

The potential applications of CNTs in bio or medical fields have been the hottest topic in nanoscience because they have comparable size to that of DNA, and they are optically active, electrically conductive and mechanically strong. Therefore, CNTs hold great promise in medical diagnostic kits, biosensors, and membranes for bio-separators. For example, they could be incorporated in a biosensor both as immobilization matrices and as electron mediator.[22] High conductivity and high accessible surface area of CNTs make them a promising material for bio devices.[23] However, CNTs are intrinsically bundled due to the high van der Waals forces of attraction between adjacent tubes. Therefore, various methods, such as chemical functionalization of the tubes[24-26] and utilization of organic[27, 28] have been examined to disperse (or disentangle) the bundles into isolated tubes so that they could be used in bio or medical fields. Alternatively, DNA has been selected as dispersing agent due to the following reasons: DNA molecules are effective for dispersing and sorting SWNTs,[29, 30] and they are able to wrap around the sidewall of CNTs due to van der Waals attraction between DNA and nanotube, DNA-wrapped CNTs are soluble in an aqueous system and finally CNT/DNA hybrid shows great potential for application in bioengineering and nanotechnology (*e.g.*, biosensor, biomarker and intracellular transporters etc).[31-33]

1.1.6 The Safety Issue of Carbon Nanotube

CNTs are changing their working place from laboratory to their commercial products due to their widespread promising applications. However, the long-term topic on whether "carbon nanotubes are intrinsically toxic or not" remains controversial.[34-37] However, no one could find out which properties (size, shape, surface properties, the entrapped impurities) are influential factors for the evolved toxic behaviors. Their needle-like shape and high durability was suggested to cause asbestos-like pathogenicity.[35] In addition, the deleterious effects of CNTs on human mesothelial cells were reported to associate with their diameter-dependent piercing of the cell membrane. It is reported that the larger the entrapped of impurities, the more severe occurrence of immunological toxicity and the alopecia on the skin.[38] Noticeably, extremely pure carbon nanotubes (below 20 ppm of entrapped metal particles) showed an excellent biocompatibility. The surface engineering of CNTs via a protein coating was one of options to design the safe CNTs.[39] Thus, it is summarized that the controlled preparation of short (less than 15 μm), highly pure and surface-modified CNTs is the critical precondition for their safe and industrial end-use in a various applications.

1.2 References

1. M. S. Dresselhaus, G. Dresselhaus and P. C. Eklund, *Science of Fullerenes and Carbon Nanotubes*, Academic Press, San Diego (1996).
2. A. Jorio, M. S. Dresselhaus, G. Dresselhaus M. Endo, *Carbon Nanotubes: Advanced Topics in the Synthesis, Structure, Properties and Applications*, Springer, (2008).
3. P. J. F. Harris, *Carbon Nanotubes and Related Structures-New materials for the twenty-first century*, Cambridge University Press, New York (1999).
4. A. Oberlin, M. Endo, T. Koyama, *J. Crystal Growth* **32**, 335 (1976).
5. R. Saito, M. S. Dresselhaus, G. Dresselhaus, *Physical Properties of Carbon Nanotubes*, Imperial College Press, London (1998).
6. X. Sun, C.H. Kiang, M. Endo, K. Takeuchi, T. Furuta, M.S. Dresselhaus, *Phys. Rev. B* **54**, 1 (1996).
7. A. M. Rao, E. Richter, S. Bandow, B. Chase, P. C. Eklund, K. A. Williams, S. Fang, K. R. Subbaswamy, M. Menon, A. Thess, R. E. Smalley, G. Dresselhaus, M. S. Dresselhaus, *Science* **275**, 187 (1997).
8. H. Kataura, Y. Kumazawa, Y. Maniwa, I. Umezu, S. Suzuki, Y. Ohtsuka, Y. Achiba, *Synth. Met.* **103**, 2555-2558 (1999).
9. C. Lee, X. Wei, J. W. Kysar, J. Hone, *Science* **321**, 385 (2008)
10. A. A. Balandin, S. Ghosh, W. Z. Bao, I. Calizo, D. Teweldebrhan, F. Miao, C. N. Lau, *Nano Lett.* **8**, 902 (2008).
11. J. P. Salvetat, G. A. D. Briggs, J. M. Bonard, R. R. Bacsa, A. J. Kulik, T. Stockli, N/ A. Burnham, L. Forro, *Phys. Rev. Lett.* **82**, 944 (1999).
12. M. S. Dresselhaus, G. Dresselhaus, A. Jorio, A. G. Souza, M. A. Pimenta, R. Saito, *Accounts of Chemical Research* **35**, 1071 (2002).
13. M. S. Dresselhaus, G. Dresselhaus, R. Saito, A. Jorio, *Physics Reports* **409**, 47–99 (2005).
14. M. J. O'Connell, S. M. Bachilo, C. B. Huffman, V. C. Moore, M. S. Strano, E. H. Haroz, K. L. Rialon, J. Boul, W. H. Noon, C. Kittrell, J. Ma, R. H. Hauge, R. B. Weisman, R. E. Smalley, *Science* **297**, 593 (2002).
15. S. M. Bachilo, M. S. Strano, C. Kittrell, R. H. Hauge, R. E. Smalley, R. B. Weisman, *Science* **298**, 2361 (2002).
16. S. Lebedkin, F. Hennrich, T. Skipa, M. M. Kappes, *J. Phys. Chem. B* **107**, 1949

(2003).

17. Y. Miyauchi, S. Chiashi, Y. Murakami, Y. Hayashida, S. Maruyama, *Chem. Phys. Lett.* **387**, 198 (2004).
18. T. Okazaki, T. Saito, K. Matsuura, S. Ohshima, M. Yumura, Y. Oyama, R. Saito, S. Iijima, *Chem. Phys. Lett.* **420**, 286 (2006).
19. D. A. Heller, E. S. Jeng, T-K. Yeung, B. M. Martinez, A. E. Moll, J. B. Gastala, M. S. Strano, *Science* **311**, 508 (2006).
20. X. Liu, T. Pichler, M. Knupfer, M. S. Golden, J. Fink, H. Kataura, Y. Achiba, *Phys. Rev. B* **66**, 45411 (2002).
21. http://en.wikipedia.org/wiki/Optical_properties_of_carbon_nanotubes
22. P. He, Y. Xu, Y. Fang, *Microchimica Acta* **152**, 175 (2006)
23. E. Katz, I. Willner, *ChemPhysChem* **5**, 1084 (2004).
24. D. E. Hill, Y. Lin, A. M. Rao, L. F. Allard, Y. P. Sun, *Macromolecules* **35**, 9466 (2002).
25. B. Z. Tang, H. Xu, *Macromolecules* **32**, 2569 (1999).
26. M. J. O'Connell, P. Boul, L. M. Ericson, C. Huffman, Y. H. Wang, E. Haroz, C. Kuper, J. Tour, K. D. Ausman, R. E. Smalley, *Chem. Phys. Lett.* **342**, 265 (2001).
27. H. J. Barraza, F. Pompeo, E. A. O'Rear, D. E. Resasco, *Nano Lett.* **2**, 797 (2002).
28. A. B. Dalton, S. Collins, E. Munoz, J. M. Razal, V. H. Ebron, J. P. Ferraris, J. N. Coleman, B. G. Kim, R. H. Baughman, *Nature* **423**, 703 (2003).
29. M. Zheng, A. Jagota, E. D. Semke, B. A. Diner, R. S. McLean, S. R. Lustig, R. E. Richardson, N. G. Tassi, *Nat. Mater.* **2**, 338 (2003).
30. M. Zheng, A. Jagota, M. S. Strano, A. P. Santos, P. Barone, S.G. Chou, B. A. Diner, M. S. Dresselhaus, R. S. Mclean, G. B. Onoa, G. G. Samsonidze, E. D. Semke, M. Usrey, D. J. Walls, *Science* **302**, 1545 (2003).
31. D. A. Heller, S. Baik, T. E. Eurell, M. S. Strano, *Adv. Mater.* **17**, 2793 (2005).
32. Z. Liu, W. Cai, L. He, N. Nakayama, K. Chen, X. Sun, X. Chen, H. Dai, *Nature Nanotech.* **2**, 47 (2007).
33. N. W. S. Kam, M. O'Connell, J. A. Wisdom, H. Dai, *Proc. Natl. Acad. Sci.* **102**, 11600 (2005).
34. A. Takagi, A. Hirose, T. Nishimura, N. Fukumori, A. Ogata, N. Ohashi, S. Kitajima, J. Kanno, *J. Toxicol. Sci.* **33**, 105 (2008).
35. C. A. Poland, R. Duffin, I. Kinloch, A. Maynard, W. A. H. Wallace, A. Seaton, V. Stone, S. Brown, W. Macnee, K. Donaldson, *Nat. Nanotechnol.* **3**, 423 (2008).

36. L. Ma-Hock, S. Treumann, V. Strauss, S. Brill, F. Luizi, M. Mertler, K. Wiench, A. O. Gamer, B van Ravenzwaay, R. Landsiedel, *Toxicol. Sci.* **112**, 468 (2009).
37. D. W. Porter, A. F. Hubbs, R. R. Mercer, N. Wu, M. G. Wolfarth, K. Sriram, S. Leonard, L. Battelli, D. Schwegler-Berry, S. Friend, M. Andrew, B. T. Chen, S. Tsuruoka, M. Endo, V. Castronova, *Toxicol.* **269**, 136 (2010).
38. C. Ge, J. Du, L. Zhao, L. Wang, Y. Liu, D. Li, Y. Yang, R. Zhou, Y. Zhao, Z. Chai, C. Chen, *Proc. Natl. Acad. Sci.* **108**, 16968 (2011).

CHAPTER 2

General Methods

Chapter 2 General Methods

2.1 Preparation of Carbon Nanotubes

Up to now, various synthetic methods for producing CNTs have been reported (e.g., arc discharge, laser vaporization and catalytic CVD).[1] The dominant recent trend is to synthesize CNTs using a CVD method because this technique is very powerful tool for the large-scale production of both SWNTs and MWNTs.[2] By simultaneously feeding hydrocarbons and nanoscale catalytic particles in the gas phase into reaction chamber, CNTs have been synthesized in a large-scale.[3] Growth of SWNTs,[4] DWNTs[5] and MWNTs[6] in reactor has been proposed to involve the catalytic deposition of hydrocarbons over the surface of nano-sized metal particles and a continuous output by the particle of well-organized tubule of hexagonal sp^2-carbon. Here I describe the detailed experimental conditions for growing DWNTs and MWNTs with a strong emphasis on their textures.

2.1.1 Synthesis of Pure Double Walled Carbon Nanotubes

The synthesis of DWNTs was carried by a CCVD method utilizing a conditioning catalyst (Mo/Al_2O_3) at one end of the furnace and the nanotube catalyst (Fe/MgO) in the middle part of the furnace. Subsequently, a methane and argon (1:1) mixture was fed into the reactor typically for 10 min at 875 °C.[5] Within our synthesis conditions, the optimized condition for obtaining high-purity DWNTs is a reaction temperature of 875 °C and the utilization of the conditioning catalyst, when using methane as the carbon feedstock and iron as the tube catalyst. This result implies that molybdenum might function as a moderator for enhancing the production of active carbon species within this limited reaction temperature range. Therefore, the important factors affecting the preferential growth of DWNTs over MWNTs are to keep the size of the metal particles below 3 nm, while the most important factor for the selective growth of DWNTs over SWNTs is to increase the amount of active carbon species. For the same size of metal particles, only the increased carbon solubility introduced by the Mo catalytic particles will make the solvated metal particles preferentially precipitate the carbon into DWNTs. In other words, the metal particles containing a higher amount of dissolved carbon will be more favorable for the formation of DWNTs over SWNTs. From this argument, it is expected that the inner shell and outer shell both grow simultaneously.

In order to obtain high quality DWNTs, a purification process was applied to synthesize these products. Firstly an oxidation process (500 °C, 20 min) were carried

out to reduce of the amount of the chemically active SWNTs. Secondly a hydrochloric acid (18 %, 100 °C, 10 h) treatment was carried out in order to remove magnesium oxide and iron catalysts, followed by air oxidation at 500 °C for 10min in order to remove carbonaceous impurities. A detailed high-resolution TEM observation confirmed the high yield of DWNTs (above 95 %) in bundles (Fig. 1 (a, b)). In addition, we observed that our tubes consist of two relatively round, small and homogeneous-sized (below 2nm in the outer shell) two concentric individual tubules (Fig. 1 (c)). These co-axial tubes are packed in a hexagonal array (Fig. 1 (c)). Furthermore, DWNTs exhibited relatively homogeneous and small-sized inner tubes of mainly ca. 0.9nm diameter and outer diameters of ca. 1.5 nm (see diameter distribution in Fig. 1 (d)).[5, 7] Magnetic susceptibility studies confirmed the high DWNT sample purity through their diamagnetic behavior.

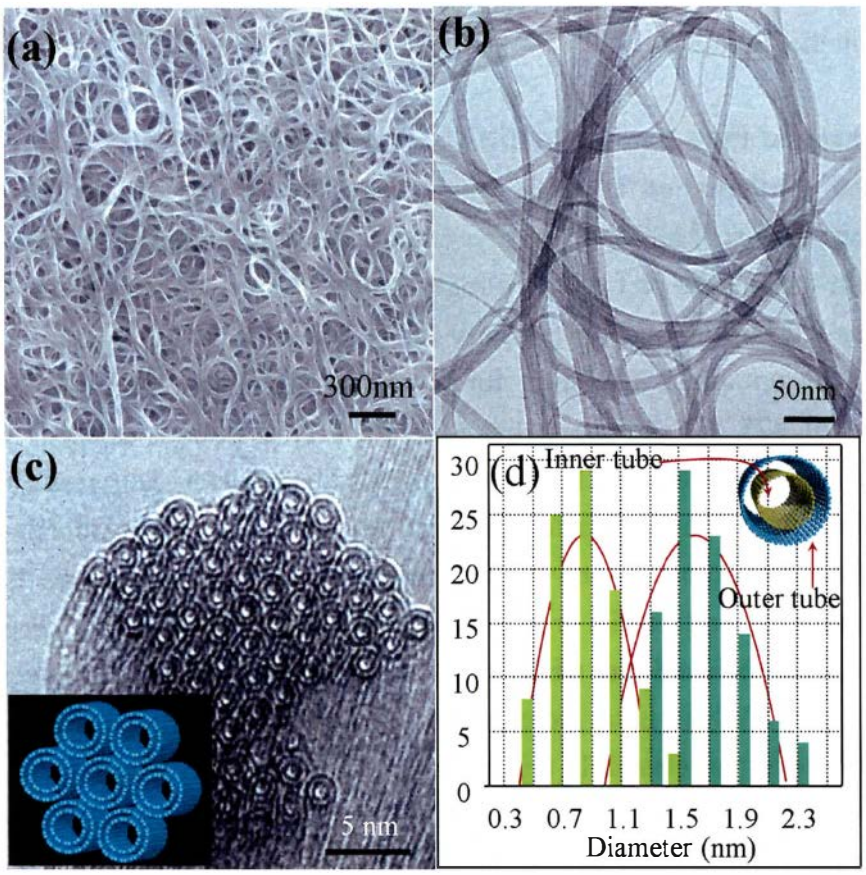

Figure 1 (a) SEM and (b) low-resolution TEM images indicate a bundled structure, (c) cross-sectional high resolution TEM image of a bundle of DWNT (inset is its schematic model, two concentric shells were regularly packed in a hexagonal array), (d) diameter distribution of a CCVD method-derived DWNTs based on a detailed high resolution TEM observation. Note that their inner diameter of ca. 0.9 nm and outer diameter of 1.5 nm were below 2nm.

2.1.2 Multi-Walled Carbon Nanotubes

Catalysts for growing CNTs were prepared by the following procedures. After dissolving a specified amount of $Fe(NO_3)_3 9H_2O$ and $(NH_4)_6Mo_7O_2 4H_2O$ in ethanol, the mixed Fe-Mo solution was introduced into a suspension of MgO powder, followed by sonication for 1hr. In this experiment, the weight ratio of Fe/Mo/MgO was 1/1/40. After drying, the material was baked in a vacuum at 150 °C for 24 hrs and then ground with a mortar pestle. The ground catalyst powder was introduced into the center of the reactor. Finally, by passing the mixed gases (argon: methane = 1:1) into the reactor at 875 °C for 15 minutes, we were able to synthesize MWNTs. For getting high purity tubes,[8] we applied a two-step purification process: high-temperature oxidation to remove both chemically active SWNTs and amorphous carbon deposited on the outer-shell of CNTs (500 °C for 30 minutes) and hydrochloric acid treatment (100 °C for 8 hrs) to dissolve the entrapped metallic particles and MgO.

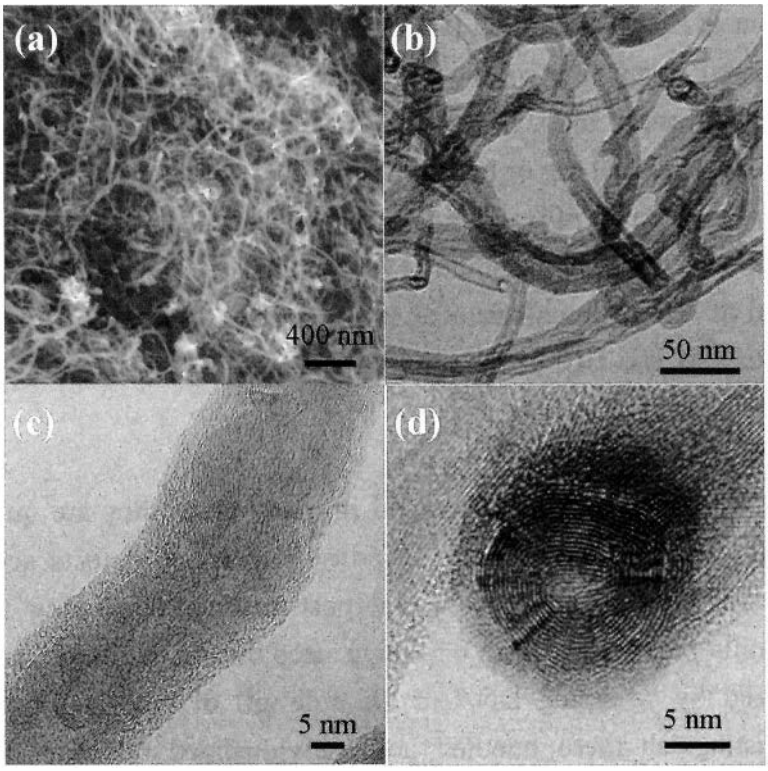

Figure 2 (a) SEM and (b-d) TEM images of CVD-grown MWNTs showing their lengths and morphologies.

Relatively long but distorted (not straight) nanotubes were severely entangled to form aggregates (Fig. 2 (a, b)). Catalytically grown CNTs have been considered to be structurally defective due to their low formation temperature (< 1000 °C) as compared to arc-discharge grown nanotubes (ca. 4000 K). From low-resolution TEM images (see

Fig. 2 (b)), the pristine tubes appeared always curled and bent, exhibiting diameters ranging from 20 to 30 nm. In general, pristine tubes were coated with less crystalline carbon materials, and in some cases partially aligned carbon materials were observed attached to the inner nanotube layers (Fig. 2 (c)). Interestingly, these tubes possess relatively round cross-sections (see Fig. 2 (d)).

In addition, three different types of MWNTs were prepared by aerosol-assisted chemical vapor deposition. The pure MWNTs were synthesized by the thermal decomposition of a mixture of 2.5 wt % ferrocene and toluene at 825 °C in an argon atmosphere for 30 min.[9,10] Nitrogen-doped MWNTs were obtained by the decomposition of a solution containing 2.5 wt % ferrocene and benzylamine.[11] Finally, highly crystalline MWNTs containing hydroxyl groups were produced by using a solution of 2.5 wt % ferrocene, 1 wt % ethanol, and toluene.[12]

2.2 Preparation of Single Stranded DNA

I prepared an aqueous solution of ssDNA using herring sperm DNA (degraded free acid, Nacalai Tesque Inc.). In order to obtain shortened DNA segments with 200 base pairs, we dissolved 10 mg of herring sperm DNA in 10 ml of distilled water under mild sonication (Kubota UP50H, 75 %) for 5 min, and then added 1 ml of 1 N sodium hydroxide solution and placed the solution for 5 min. The DNA solution was neutralized by adding 1 ml of 1 N hydrochloric acid and then the DNA solution was stabilized by adding 200 μl of 1 M Tris-HCl buffer solution (pH 8).

2.3 Characterization tools

CNTs are nano-sized materials and in many cases they are quite different in diameter distribution, diameter length, chirality, purity and defects according to the synthetic method, purification process and post-treatment including the dispersion. CNTs are naturally present in a form of a large sized bundle. However, nanotubes could be individualized by wrapping DNA to the sidewall of tubes helically. Thus, it is essential to distinguish these bundled and individualized tubes to determine their fundamental properties. Here I described most common characterization tools used in my thesis.

2.3.1 Scanning Electron Microscopy

A SEM is an essential tool to get information about the macromorphology of the as-grown tubes and the dispersion state of tubes. In my thesis, I used field-emission scanning electron microscopy (FE-SEM, JSM6335Fs). However, it is not possible to get

information about the diameter and the crystallinity of CNTs from SEM images because of its low resolution.

2.3.2 Transmission Electron Microscopy

A TEM is widely used to characterize CNTs. Historically, TEM was used to see the growth of CNTs from the metal particles[2] and to characterize their atomic structures.[13] The most interesting feature from detailed electron diffraction patterns of individual MWNT was the variation in the helicities of constituent concentric layers. In my thesis, TEM images were obtained using double CS corrector (CEOS GmbH) equipped JEM-2100F (80 kV, JEOL). I used TEM images to evaluate the diameter, crystallinity of tubes, the dispersion state of tubes and the interaction between the sidewall of tubes and DNA.

2.3.3 Raman Spectroscopy

Raman spectroscopy is a rapid, nondestructive optical tool to characterize materials.[14] The incoming light interacts with an electron that makes a real transition to a higher energy, where the electron interacts with a phonon (via electron-phonon coupling) before making a transition back to the electronic ground state. The energy of the inelastically scattered light is measured with respect to the laser energy (in cm^{-1}), and by convention, the stronger signal from the loss side (Stokes) is counted as positive. In the case of CNTs where the density of states is strongly peaked, resonance Raman scattering dominates over non-resonant contributions. Hence, resonance Raman scattering from nanotubes gives information of the vibrational mode from the Raman shift, as well as of the optical transition energy since it is close to the energy of the laser. Thus, Raman has been used to get fundamental information of CNTs such as diameter, electronic structure, purity, crystallinity, metallicity and chirality.[15, 16]

In my thesis, Raman spectra at 785 nm excitations were obtained using a Renishaw setup fitted with a macroscopic sampling kit. We also obtained Raman spectra using 532 nm and 633 nm laser excitations produced by a Kaiser HoloLab5000 system.

In general, there are four distinctive peaks in the Raman spectrum of CNTs: the low-frequency radial breathing mode (RBM) and the higher frequency, D, G and G' modes.[15, 16] Among them, a characteristic Raman line of the tubular structure is RBM, in which all atoms move in phase perpendicular to the tube axis changing the radius of the nanotube. The frequency of RBM enables us to identify the chirality as well as the diameter. The RBM mode is also useful for monitoring the surrounding conditions of the nanotubes.

2.3.4 Photoluminescence

Since the discovery of band gap photoluminescence (PL) from isolated SWNTs,[17, 18] PL maps have been widely utilized for determining the relative (*n, m*) distribution of semiconducting SWNTs.[19-21] The spectra assignment provided a large body of precise optical transition energies for a significant range of tube diameters and chiralities. In addition, the high sensitivity of PL in SWNT systems is very useful in sensing applications.[22]

2.3.5 UV-vis Absorption Spectroscopy

Optical absorption spectroscopy has been used to determine the mean diameter and diameter distribution of the CNTs.[23] In other words, this tool has the ability to probes the joint density of electronic states of CNTs.[23] The absorption intensity is proportional to the amount of CNTs dissolved in the solution and furthermore, provides information for the resonant peaks originating from van Hove singularities at visible region. According to Beer-Lambert's law ($A = log\ I_0/I = \varepsilon\ C\ l$), the absorbance A is expressed in terms of extinction coefficient ε, the concentration of nanotubes C and the light path l.

2.3.6 Theoretical Simulation

The large enhancement in computer performance allows us to simulate carbon nanostructure with high accuracy and reliability. The semi-empirical method PM6 was originally designed to study the biomolecules.[24] This tool is very easy to repeat trial and error experiment by changing composition and model system. In my thesis, I selected the PM6 method to model CNTs and nucleobases as well as to calculate binding-energy between them, in order to support the experimental result. A pure SWNT model was prepared by terminating both ends of the SWNT with hydrogen atoms. Subsequently, by placing nucleobases on the sidewall of SWNT, and after optimizing the atomic structures in order to minimize the total energy of the system, the binding energies (E) were obtained by subtracting the energy of the isolated nucleobases (E_{NB}) and of the SWNTs (E_{CNT}) from the energy of the combined system ($E_{CNT\text{-}NB}$).

2. 4 References

1. A. Jorio, M. S. Dresselhaus, G. Dresselhaus, *Carbon Nanotubes: Advanced Topics in the Synthesis, Structure, Properties and Applications*, Springer (2008).
2. A. Oberlin, M. Endo and T. Koyama, *J. Crystal Growth* **32**, 335-349 (1976).
3. M. Endo, *Chem. Tech.* 568-576 (1988).
4. P. Nikolaev, M. J. Bronikowski, R. K. Bradley, F. Rohmund, D. T. Colbert, K. A. Smith, R. E. Smalley, *Chem. Phys. Lett.* **313**, 91 (1999).
5. M. Endo, H. Muramatsu, T. Hayashi, Y. A. Kim, M. Terrones, M. S. Dresselhaus, *Nature* **433**, 476 (2005).
6. M. Endo, Y. A. Kim, T. Hayashi, K. Nishimura, T. Matushita, K. Miyashita, M. S. Dresselhaus, *Carbon* **39**, 1287 (2001).
7. Y. A. Kim, H. Muramatsu, T. Hayashi, M. Endo, M. Terrones, M. S. Dresselhaus, *Chem. Vapor Dep.* **12**, 327 (2006).
8. Y. A. Kim, M. Kojima, H. Muramatsu, D. Shimamoto, T. Hayashi, M. Endo, M. Terrones, M.S. Dresselhaus, *J. Raman Spectro.* **39**, 1183 (2008).
9. R. Kamalakaran, M. Terrones, T. Seeger, Ph. Kohler-Redlich, M. Ruhle, Y. A. Kim, T. Hayashi, M. Endo, *Appl. Phys. Lett.* **77**, 3385 (2000).
10. M. Mayne, N. Grobert, M. Terrones, R. Kamalakaran, M. Rhle, H. W. Kroto, D. R. M. Walton, *Chem. Phys. Lett.* **338**, 101 (2001).
11. M. Terrones, P. M. Ajayan, F. Banhart, X. Blase, D. L. Carroll, J. C. Charlier, R. Czerw, B. Foley, N. Grobert, R. Kamalakaran, P. Kohler-Redlich, M. Rühle, T. Seeger, H. Terrones, *Appl. Phys. A* **74**, 355 (2002).
12. A. R. Botello-Mendez, J. Campos-Delgado, A. Morelos-Gmez, J. M. Romo-Herrera, A. G. Rodrguez, H. Navarro, M. A. Vidal, H. Terrones, M. Terrones, *Chem. Phys. Lett.* **453**, 55 (2008).
13. S. Iijima, *Nature* **354**, 56 (1991).
14. R. L. McCreery, *Raman Spectroscopy for Chemical Analysis*, Wiley InterScience, Vol. 157 (2000).
15. M. S. Dresselhaus, G. Dresselhaus, A. Jorio, A. G. Souza, M. A. Pimenta, R. Saito, *Accounts of Chemical Research* **35**, 1071 (2002).
16. M. S. Dresselhaus, G. Dresselhaus, R. Saito, A. Jorio, *Physics Reports* **409**, 47–99 (2005).
17. M. J. O'Connell, S. M. Bachilo, C. B. Huffman, V. C. Moore, M. S. Strano, E. H.

Haroz, K. L. Rialon, J. Boul, W. H. Noon, C. Kittrell, J. Ma, R. H. Hauge, R. B. Weisman, R. E. Smalley, *Science* **297**, 593 (2002).

18. S. M. Bachilo, M. S. Strano, C. Kittrell, R. H. Hauge, R. E. Smalley, R. B. Weisman, *Science* **298**, 2361 (2002).
19. S. Lebedkin, F. Hennrich, T. Skipa, M. M. Kappes, *J. Phys. Chem. B* **107**, 1949 (2003).
20. Y. Miyauchi, S. Chiashi, Y. Murakami, Y. Hayashida, S. Maruyama, *Chem. Phys. Lett.* **387**, 198 (2004).
21. T. Okazaki, T. Saito, K. Matsuura, S. Ohshima, M. Yumura, Y. Oyama, R. Saito, S. Iijima, *Chem. Phys. Lett.* **420**, 286 (2006).
22. D. A. Heller, E. S. Jeng, T-K. Yeung, B. M. Martinez, A. E. Moll, J. B. Gastala, M. S. Strano, *Science* **311**, 508 (2006).
23. X. Liu, T. Pichler, M. Knupfer, M. S. Golden, J. Fink, H. Kataura, Y. Achiba, *Phys. Rev. B* **66**, 45411 (2002).
24. J. J. P. Stewart, *J. Mol. Modeling* **13**, 1173 (2007).

CHAPTER 3

Defect-enhanced Dispersion of Carbon Nanotubes in DNA Solutions

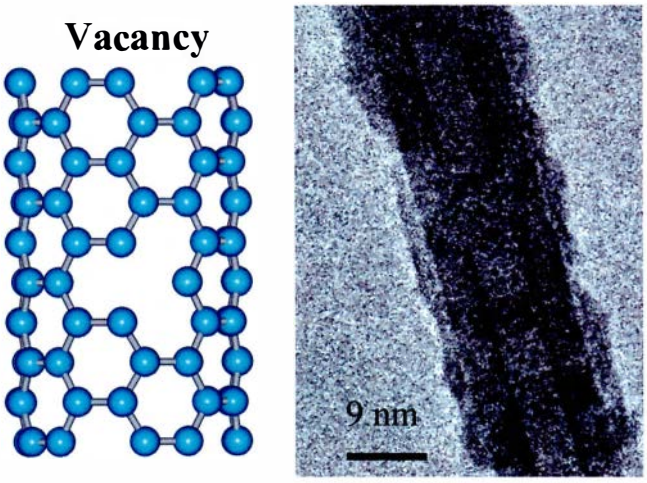

Chapter 3 Defect-enhanced Dispersion of Carbon Nanotubes in DNA Solutions

3.1 Introduction

Since DNA, a well-known biopolymer, has been proven to be effective for dispersing and sorting CNTs,[1-3] intensive studies have been carried out in order to obtain both theoretical and experimental understanding of the DNA-nanotube interaction.[4-11] The ultrasonication process has been applied to dispersing a strongly bundled aggregate of CNTs in a nanotube suspension containing DNA in order to overcome the attractive van der Waals forces between adjacent tubes. The strong hydrodynamic shear forces generated by the ultrasonication process create a space within the bundled nanotubes, which allows the DNA molecules to impinge and become adsorbed on the outer surface of the nanotubes through a hydrophobic interaction,[7] thereby leading to a stable nanotube emulsion through the formation of DNA-nanotube hybrid structures. Until now, ssDNA has been proven to be more effective for dispersing nanotubes than dsDNA,[2] and the combination of the short complementary oligonucleotides $d(GT)_3$ and $d(AC)_3$ exhibited an even superior dispersing ability.[10] Moreover, theoretical studies have assumed that the shape of CNTs constitutes a perfect cylinder.[7] However, the catalytic growth of CNTs in the reaction chamber inevitably involves the formation of defects (*e.g.*, vacancies, nonhexagonal ring, and foreign atoms),[12] which modify the electronic structure and surface properties of the tubes[13, 14] and are expected to ultimately alter the interaction between nanotubes and DNA. In order to be able to reproducibly assemble nanotube-DNA hybrid structures as bio-medical devices, it is essential to consider the effects of defects within CNTs.

In this chapter, the role of defects on the sidewall of CNTs was studied by directly comparing the dispersibility of defective and crystalline thin (small outer diameter) MWNTs in aqueous DNA solutions. We found that the dispersibility of nanotubes depended strongly on the density of the defects on the sidewall. More specifically, crystalline tubes thermally treated at 2300 °C exhibited dispersibility twice as low as that of as-grown tubes in aqueous DNA solutions. Theoretical calculations are here shown to support the conclusion that defect sites exhibit high reactivity toward the adsorption of DNA.

3.2 Experimental Section

3.2.1 Carbon Nanotubes

Thin MWNTs were synthesized using the methods described in the relevant literature.[15] In order to obtain high-purity tubes, we applied a two-step purification

process: high-temperature oxidation to remove both chemically active SWNTs and amorphous carbon deposited on the surface of the CNTs (400 °C for 30 minutes), followed by treatment with hydrochloric acid (100 °C for 8 hrs) to dissolve any entrapped metallic particles and supporting materials. Then, we thermally treated the tubes at various temperatures in the range of 1500-2800 °C using a graphite furnace in an argon atmosphere in order to anneal any structural defects within the tubes.

3.2.2 The Dispersion of Carbon Nanotubes in DNA Solution

I prepared an aqueous solution of ssDNA using herring sperm DNA as described in section 2.2. 1 mg of thin MWNTs was dispersed in each ssDNA solution (we dissolved 1, 3, 5, 8, 10, 20, 50 mg of DNA in 10 ml of distilled water) under sonication for 1hr at 4 °C. Subsequently, these suspensions (containing CNTs) were placed in a centrifuge (20,000 g) for 1 hr in order to remove the insoluble materials. Finally, we have obtained well-dispersed MWNT emulsions. The same dispersion method was done in as-grown defective thin MWNTs.

3.2.3 Characterizations

I used Raman spectroscopy (Hololab-Series 5000, excitation laser 532 nm), FE-SEM (JSM6335Fs), and TEM (JEOL2010FEF) for studying the as-grown and the thermally treated tubes, as well as the DNA-nanotube hybrid structures. Using UV/Vis absorption spectroscopy (Solidspec-3700, Shimazu), we evaluated the degree of dispersion for the prepared nanotube emulsions.

3.3 Results and Discussion

There are three reasons for selecting thin MWNTs[15] rather than SWNTs for this study: (1) Thin MWNTs exhibit a strongly bundled structure like SWNTs because of their small diameter below 10 nm, (2) they are structurally stable up to 2800 °C, while SWNTs and DWNTs are easily transformed into graphitic material at high temperatures,[16, 17] and (3) their diameter is too large (above 2 nm) for the manifestation of detailed quantum effects associated with 1D dispersion relations. As a general metric for comparing the structural integrity of SWNTs or DWNTs, the intensity of the D-band, which is explained by double resonance theory,[18, 19] is suitable for evaluating the quality of SWNTs containing only a small number of defects. However, due to the breakdown of the van Hove singularities, this approach is not applicable to SWNTs or MWNTs containing many defects.

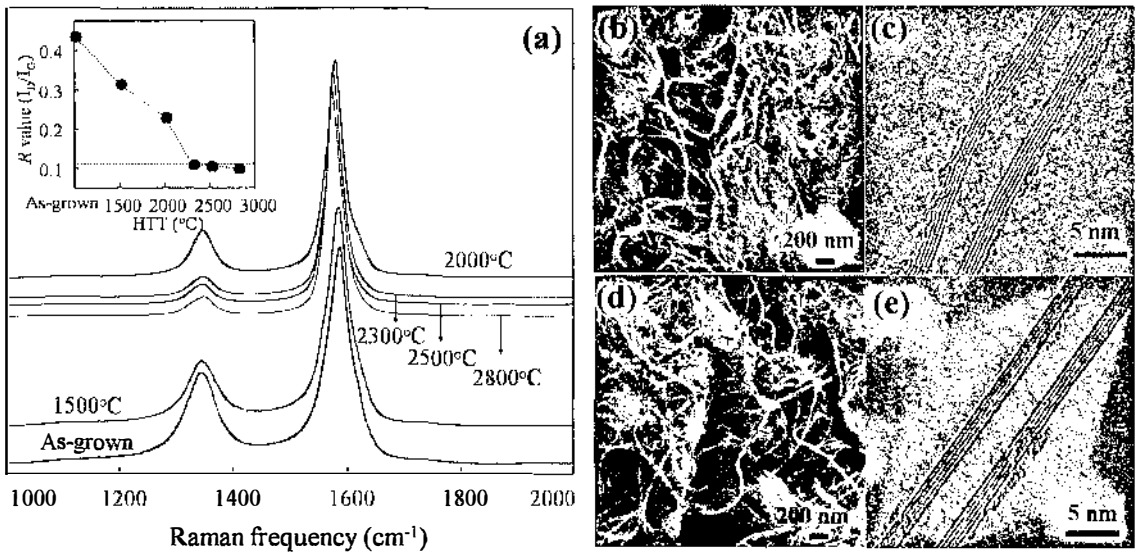

Figure 1 (a) Raman spectra of thin MWNTs thermally treated at different temperatures. The inset represents the variation of the R value (I_D/I_G, the intensity of the D-band divided by the intensity of the G-band) as a function of the annealing temperatures. (b, c) and (d, e) TEM images of as-grown and thermally treated thin MWNTs, respectively.

As a tool for controlling the defect density in as-grown defective thin MWNTs, we chose high-temperature thermal treatment[20, 21] instead of the commonly used chemical treatment. Oxidative chemical treatment can introduce both chemical moieties and defects on the sidewall of the tubes, which might affect the tube-tube interactions as well as their dispersibility. In other words, it is difficult to separate the role of defects within tubes from the effects of chemical treatment in evaluating the dispersibility of tubes in DNA solutions. The effects of high-temperature annealing on the defect density of CNTs are clearly observed as consecutive changes in the Raman spectra (Fig. 1 (a)). Although there are no distinct changes in the G-band located at 1582 cm^{-1} (E_{2g2} graphite mode), the intensities of the D-band (a defect-induced mode) at 1350 cm^{-1} decrease with increasing thermal treatment temperatures, and saturate for samples prepared at 2300 °C in argon. This temperature range is consistent with the region in conventional carbon materials where the mobility of carbon atoms increases abruptly.[22] Therefore, a drastic decrease in the R value (the intensity of the D-band divided by the intensity of the G-band) from 0.42 to 0.1 (see inset in Fig. 1 (a)) indicates the effective removal (or annealing) of defects within CNTs by the high-temperature thermal treatment. In order to visualize the improvement of the structural integrity, we carried out detailed SEM and TEM studies on pristine tubes (Fig. 1 (b, c)) and tubes thermally treated at 2300 °C (Fig. 1 (d, e)). Pristine tubes consisting of undulated fringes and amorphous carbon layers (Fig. 1 (c)) were transformed into crystalline tubes (Fig. 1 (e)) featuring straight

linear fringes lengthwise along the tube. Fortunately, there were no apparent changes in the long, bundled and entangled macro-morphologies of the pristine and the thermally treated tubes caused by the thermal treatment, which is another reason for selecting thin MWNTs as a starting material.

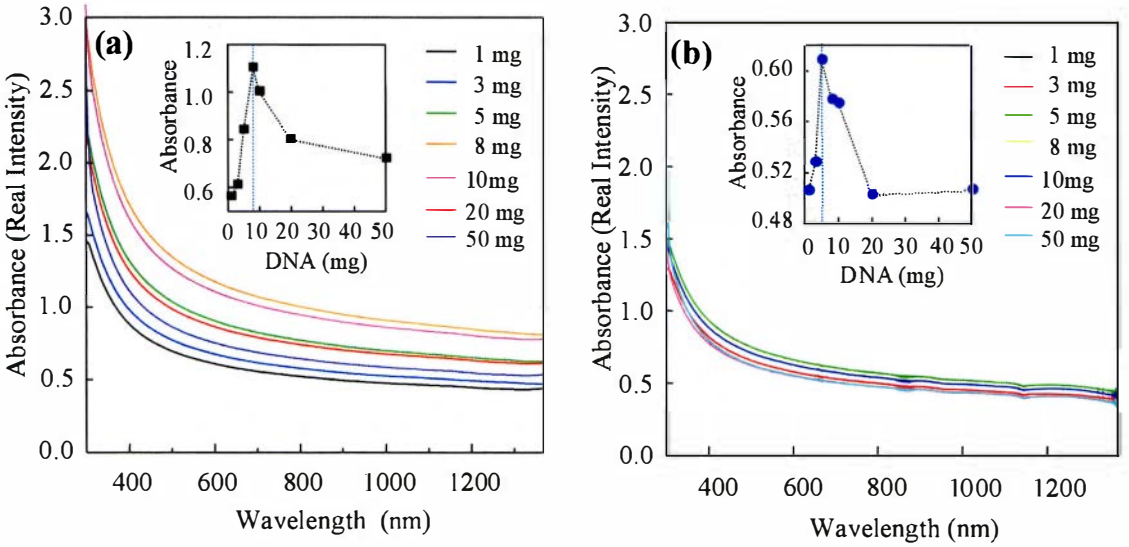

Figure 2 UV-Vis absorption spectra for DNA solutions with dispersed (a) as-grown and (b) thermally treated tubes. The values in the figures indicate the added amount of DNA per mg of tubes. The inset shows the relation between the added amount of DNA and the absorbance at a wavelength of 700 nm.

In order to compare the dispersibility of defective as-grown MWNTs and thin crystalline MWNTs thermally treated at 2300 ℃ in aqueous DNA solutions, I prepared several homogeneously dispersed nanotube solutions as follows: 1mg of thin MWNTs was dispersed in distilled water (10 ml) with 1, 3, 5, 8, 10, 20 and 50 mg of DNA under sonication for 1hr at 4 °C. Subsequently, these suspensions (containing carbon nanotubes) were placed in a centrifuge (20,000 g) for 1 hr in order to remove the insoluble materials, and this process yielded well-dispersed nanotube emulsions resulting from this processing. It is noted that there is no change in the pH of a nanotube emulsion. A detailed study of the insoluble materials, which agglomerated as a black precipitate, revealed that they consist of severely entangled nanotube aggregates. All solutions exhibited a similar opaque black color, and thus it was impossible to evaluate with the naked eye whether there were any differences in the dispersed state of the CNTs.

In order to further explore the distinctive differences in the dispersibility of defective and crystalline nanotubes in aqueous DNA solutions, we measured the

absorption spectra of all samples (Fig. 2). As expected, all solutions showed similar absorption behaviour in accordance with theoretical studies which have demonstrated that large-sized tubes with diameters above 5 nm do not exhibit van Hove singularities.[23] Therefore, the measured intensity of the absorbance at a wavelength of 700 nm is directly proportional to the amount of dispersed nanotubes within the solution. The observed linear relation of the absorbance from DNA solutions in the range from 1 to 8 mg (see inset in Fig. 2 (a)) indicates a consecutive increase in the amount of dispersed carbon nanotubes in water. When the amount of added DNA exceeds 10 mg, the consecutive decrease in the dispersibility of the tubes is possibly due to the self-aggregation ability of DNA (i.e., hydrogen bonding) in distilled water. We found that 8 mg of DNA showed the highest dispersibility against as-grown nanotubes in distilled water. On the other hand, the thermally treated tubes exhibited very similar dispersion behaviour, which was a function of the added amount of DNA. However, the actual intensity of the absorbance (see inset in Fig. 2 (b)) was approximately two times lower than that in the case of as-grown tubes, even though there were no distinct changes in the bundled features except for the defect density. From these results, it could be concluded that defects at the sidewall of tubes act as reactive sites for binding with DNA.

In addition, in order to characterize DNA-nanotube hybrid structures, we carried out detailed TEM observations on DNA-dispersed nanotube samples. A low-resolution TEM image (Fig. 3 (a)) revealed that amorphous DNA was attached on the outer surface of CNTs in a random manner, where it was not discernible whether DNA was wrapped or simply attached. However, by taking a high-resolution TEM image, we found that DNA was helically wrapped around the sidewall of CNTs in an irregular pattern (Fig. 3 (b)). Although it is well known that hydrophobic interactions are the driving force behind the attraction between DNA and nanotubes,[2, 3] it is now assumed on the basis of this TEM image that defects are another factor governing their interaction.

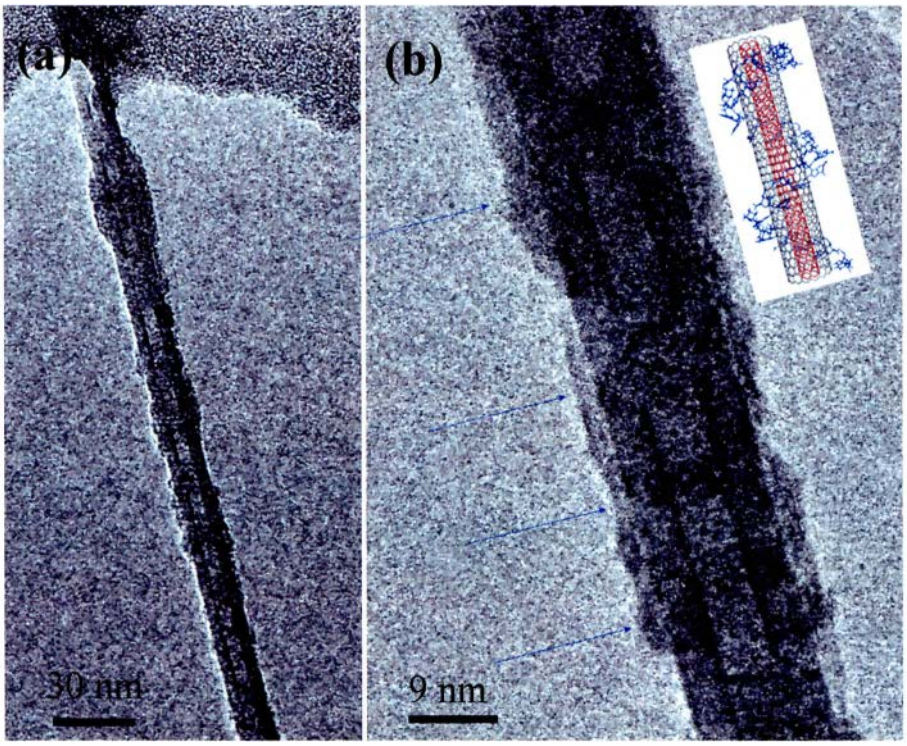

Figure 3 (a, b) TEM images at different resolutions showing linear thin MWNTs wrapped in ssDNA. The inset shows a schematic model of ssDNA coated MWNTs. Note that DNA is wrapped helically in an irregular pattern.

Finally, we carried out energy calculations on four types of nucleobases placed near a perfect (*5, 5*) tube, the same tube with a Stone-Wales defect, and with a vacancy, in order to verify the experimentally observed high dispersibility of defective tubes in aqueous DNA solutions. First, we have prepared a perfect (*5, 5*) tube model with both ends terminated by hydrogen atoms, and added either a Stone-Wales or a vacancy defect to the tube. A nucleobases model was prepared as well, and the binding energies were obtained. We used the PM3 method to optimize and calculate the energies. Then, by placing nucleobases on the sidewall of perfect and defective model tubes (Fig. 4), and by optimizing the structure to minimize the energy of the system, the binding energies (E) were obtained by subtracting the energy of the isolated nucleobases (E_{NB}) and of the nanotubes (E_{CNT}) from the energy of the combined system ($E_{CNT\text{-}NB}$) (Table 1). Generally, perfect tubes exhibited lower binding energies which are almost zero, showing a weak interaction between the tube and nucleobases. Defective tubes, with one exception, had definitely higher binding energies showing that the defect sites tend to attract nucleobases. From this result, we can say that defects in nanotubes act as specific active sites for binding with DNA, thus promoting the dispersibility of carbon nanotubes in aqueous DNA solutions.

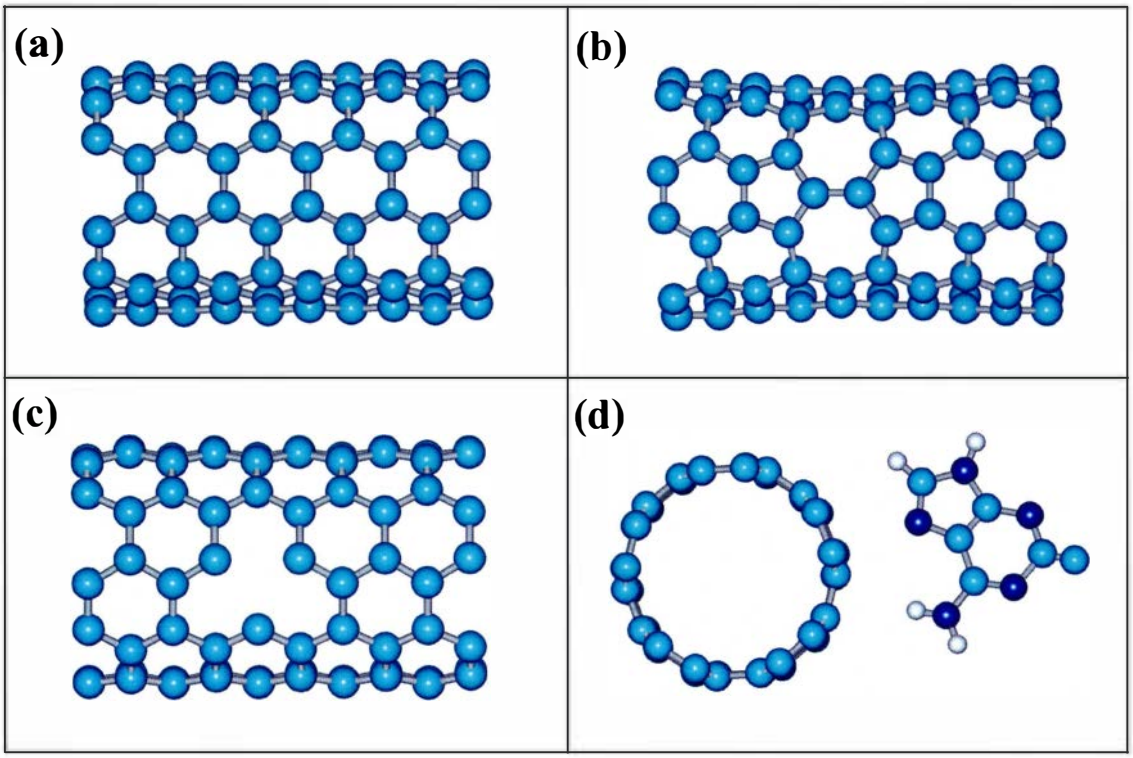

Figure 4 Model nanotubes with (a) perfect, (b) Stone-Wales, and (c) vacancy structure and (d) a typical side-view indicating the interaction of the nanotube sidewall with adenine.

Table 1 Theoretically calculated binding energy (E (eV)) for perfect, Stone-Wales and vacancy (*5, 5*) tubes with various nucleobases.

Nucleobases	Perfect CNT	Stone-Wales CNT	Vacancy CNT
Adenine	- 0.0498	- 0.0758	- 2.1681
Cytosine	- 0.0472	- 0.1017	- 1.9993
Guanine	- 0.0461	- 0.1565	- 2.3992
Thymine	- 0.0228	- 0.0501	- 0.06569

3.4 Conclusion

I revealed the strong influence of defects on the dispersibility of nanotubes in preparing stable nanotube/DNA suspensions under strong sonication and subsequent centrifugation. The low dispersibility of tubes thermally treated at 2300 °C can be explained by the reduction of the density of defects on the sidewall of as-grown tubes caused by the high-temperature thermal treatment in argon. We found that the highest

dispersibility was reached at 8 mg of DNA per 1 mg of thin MWNTs in distilled water (10 ml), as well as that DNA was helically wrapped around the sidewall of the tubes in a random manner. Based on DFT calculations, it was concluded that defects are effective for dispersing nanotubes in aqueous DNA solutions. Our study indicates the importance of nanotube quality in the reproducible fabrication of nanotube/DNA devices.

3.5 References

1. N. Nakashima, S. Okuzono, H. Murakami, T. Nakai, K. Yoshikawa, *Chem. Lett.* **32**, 456 (2003).
2. M, Zheng, A. Jagota, E. D. Semke, B. A. Diner, R. S. McLean, S. R. Lustig, R. E. Richardson, N. G. Tassi, *Nat. Mater.* **2**, 338 (2003).
3. M. Zheng, A. Jagota, M. S. Strano, A. P. Santos, P. Barone, S. G. Chou, B. A. Diner, M. S. Dresselhaus, R. S. Mclean, G. B. Onoa, G. G. Samsonidze, E. D. Semke, M. Usrey, D. J. Walls, *Science* **302**, 1545 (2003).
4. M. S. Strano, M. Zheng, A. Jagota, G. B. Onoa, D. A. Heller, P. W. Barone, M. L. Usrey, *Nano Lett.* **4**, 543 (2004).
5. M. Zheng, B.A. Diner, *J. Am. Chem. Soc.* **126**, 15490 (2004).
6. C. Fantini, A. Jorio, A. P. Santos,V. S. T. Peressinotto, M.A. Pimenta, *Chem. Phys. Lett.* **439**, 138 (2007).
7. X. Zhao, J. K. Johnson, *J. Am. Chem. Soc.* **129**, 10438 (2007).
8. S. Meng, P. Maragakis, C. Papaloukas, E. Kaxiras, *Nano Lett.* **7**, 45 (2007).
9. Y. Chen, H. Liu, T. Ye, J. Kim, C. Mao, *J. Am. Chem. Soc.* **129**, 8696 (2007).
10. S. R. Vogel, M. M. Kappes, F. Hennrich, C. Richert, *Chem. Eur. J.* **13**, 1815 (2007).
11. D. Das, A. K. Sood, P. K. Maiti, M. Das, R. Varadarajan, C. N. R. Rao, *Chem. Phys. Lett.* **453**, 266 (2008).
12. T. W. Ebbesen, T. Takada, *Carbon* **33**, 973 (1995).
13. J.-C. Charlier, T. W. Ebbesen, Ph. Lambin, *Phys. Rev. B* **53**, 11108 (1996).
14. J.-C. Charlier, *Acc. Chem. Res.* **35**, 1063 (2002).
15. H. J. Jeong, K. K. Kim, S. Y. Jeong, M. H. Park, C. W. Yang, Y. H. Lee, *J. Phys. Chem. B* **108**, 17695 (2004).
16. S. L. Fang, A. M. Rao, P. C. Eklund, P. Nikolaev, A. G. Rinzler, R. E. Smalley, *J. Mater. Research* **13**, 2405 (1998).
17. Y. A. Kim, H. Muramatsu, T. Hayashi, M. Endo, M. Terrones, M. S. Dresselhaus, *Chem. Phys. Lett.* **398**, 87 (2004).
18. C. Thomsen, S. Reich, *Phys. Rev. Lett.* **85**, 5214 (2000).
19. R. Saito, A. Jorio, A. G. Souza Filho, G. Dresselhaus, M. S. Dresselhaus, M.A. Pimenta, *Phys. Rev. Lett.* **88**, 027401 (2002).
20. Y. A. Kim, K. Osada, T. Hayashi, M. Endo, M. S. Dresselhaus, *Chem. Phys. Lett.* **380**, 319 (2003).

21. Y. A. Kim, T. Hayashi, M. Endo, Y. Kaburagi, T. Tsukada, J. Shan, K. Osato, and S. Tsuruoka, Carbon 2005, 43, 2243-2250.
22. D. B. Fischbach, In Chemistry and Physics of Carbon, Vol. 7 (Ed: P. L. Walker), Marcel Dekker, New York, 1971, pp. 1-97.
23. R. Saito, M. S. Dresselhaus, and G. Dresselhaus, Physical Properties of Carbon Nanotubes, Imperial College Press, New York, 1998.

CHAPTER 4

Unusually High Dispersion of Nitrogen-Doped Carbon Nanotubes in DNA Solution

The Role of Pyridinic Nitrogen Atoms in the CNT Sidewall

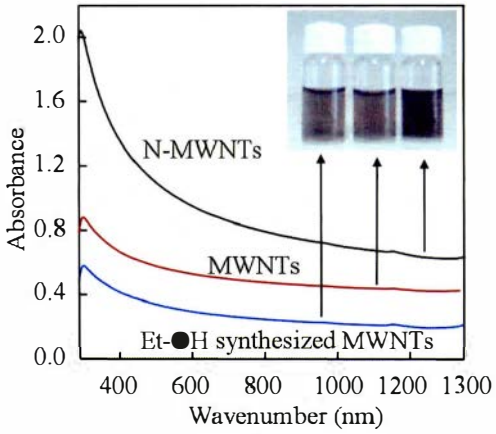

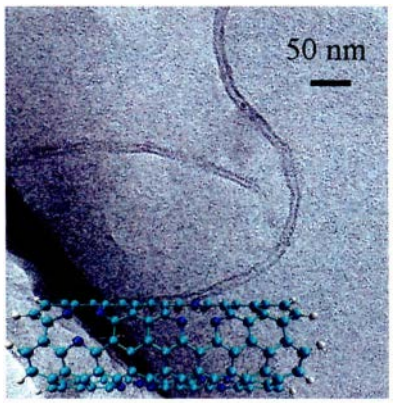

Chapter 4 Unusually High Dispersion of Nitrogen-Doped Carbon Nanotubes in DNA Solution

4.1 Introduction

CNTs can be viewed as graphene that has been rolled into a cylinder with a nanoscale diameter.[1] The excellent mechanical and electrical properties of CNTs and their flexibility make them potentially useful in a wide variety of applications.[2, 3] At present, several hundreds tons of CNTs are commercially produced each year. However, most of these CNTs are in a strongly bundled state due to strong van der Waals interactions established between adjacent CNTs. For this reason, improving the processability of CNTs via dispersion (i.e., individualization) is of great importance in order to fully exploit their intrinsic physical and chemical properties at the molecular level. The uniform dispersion of individual CNTs without a marked change in either their length or crystallinity remains a critical challenge in CNT processing. In fact, the conversion rate from noncovalently bundled CNTs to individual CNTs, when using strong sonication and subsequent ultracentrifugation, is quite low. Among many types of surfactants, DNA, a flexible amphiphilic biopolymer, has been found to be well-suited for dispersing and sorting CNTs.[4-7] Theoretical and experimental studies have found that the van der Waals interactions between the nucleobase backbone of DNA and the hydrophobic CNT sidewall is the main driving force behind the dispersion of CNTs in DNA solution, where DNA is helically wrapped around the CNT sidewall.[8-17] Possible applications of such a hybrid DNA/CNT system have been examined, including biosensors,[18, 19] DNA transporters,[20] and field-effect transistors[21]; in these applications, the reproducibility of the hybrid DNA/CNT structure is essential. From the viewpoint of tube crystallinity, intrinsic structural defects in CNTs have been reported to provide an additional driving force behind the dispersion of CNTs in DNA solution.[22] In other words, the surface properties of the CNT sidewall govern the DNA/CNT interaction. Functional groups covalently attached to the sidewall of CNTs are sometimes by-products of oxidative purification and could also be intentionally introduced in order to extend the sidewall reactivity[23-25]. However, the role of functional groups in the dispersibility of strongly bundled CNTs still remains an open issue.

In this chapter, I investigate the role of sidewall functional groups in dispersing three different types of the strongly bundled MWNTs containing different types of functional groups (e.g. nitrogenated (N) and hydroxyl groups (OH)) in DNA solutions. We note that N doped MWNTs exhibited the highest dispersibility in DNA solution, higher than MWNTs not intentionally doped. Using theoretical calculations, this

experimental result was explained by the presence of pyridinic-like nitrogen situated next to carbon vacancies within N-doped MWNTs, thus contributing to increased binding forces, and a small HOMO-LUMO gap established between the nucleobases and the sidewall of N-doped MWNTs.

4.2 Experimental Section

4.2.1 Nanotube Synthesis

Three different types of MWNTs were synthesized by aerosol-assisted chemical vapor deposition. The pure MWNTs were synthesized by the thermal decomposition of a mixture of 2.5 wt % ferrocene and toluene at 825 °C in an argon atmosphere for 30 min.[26, 27] N-doped MWNTs were obtained by the decomposition of a solution containing 2.5 wt % ferrocene and benzylamine.[28] Finally, highly crystalline MWNTs with hydroxyl groups were produced by using a solution of 2.5 wt % ferrocene, 1 wt % ethanol, and toluene.[29] The three different types of CNTs tested in this work were used without any chemical modification. The basic morphological features of the three types of MWNTs are summarized in Table 1.

Table 1 Morphological feature and atomic compositions of the three types of MWNTs.

Sample	Morphology [a]		R value I_D/I_G [b]	Atomic composition (%) [c]			
	Diameter (nm)	Length (μm)		C	O	N [d]	Fe
Pure MWNTs	40	300	0.30	97.2	1.47	-	0.17
N-MWNTs	35	200	0.36	96.3	1.61	1.92	0.17
OH-MWNTs	35	200	0.27	96.1	3.72	-	0.19

[a] Diameter and length were obtained from SEM images. [b] R is the integrated intensity of the D band divided by the integrated intensity of the G band from Raman spectra (λ = 532 nm). [c] The atomic composition was obtained by XPS. [d] The amount of pyridinic and quaternary nitrogen were found to be 67.2 and 32.8 %

4.2.2 The Dispersion of Carbon Nanotubes in DNA Solution

I prepared an aqueous solution of ssDNA using herring sperm DNA as described in section 2.2. Then, 10 mg of MWNT sample (pure, N-dopes, or OH-decorated) was dispersed in DNA stock solution under sonication for 1 h at 4 °C. The resultant MWNT suspensions were placed in an ultracentrifuge (15,000 × g) for 1

hr in order to remove insoluble material; well-dispersed MWNT emulsions were thus obtained. The molecular weights of ssDNA before and after sonication are over 20 kb and around 200 bp, respectively. We found a saturated fragmentation of the DNA under our sonication condition. Indeed, agarose gel electrophoresis of the ssDNA sample showed no additional DNA fragmentation.

4.2.3 Determination of the Amount of Adsorbed DNA in Carbon Nanotubes

With the help of a Qubit fluorometer (Invitrogen), the amount of adsorbed DNA in the MWNT suspension was measured as follows. First, 5 ml of MWNT suspension was filtered (0.22 μm membrane) in order to remove free DNA. The remaining materials were redispersed in 5 ml of distilled water using a vortex and then the MWNT suspension was diluted by adding 50 ml of distilled water. Second, we made the working solution by diluting the ssDNA reagent 1:200 in the ssDNA buffer. Next, we added each of samples to the assay containing the working solution and mixed them together by vortexing them for 2-3 seconds and we incubated all the tubes at room temperature for 2 minutes. After calibration using two standard samples, we have recorded the values by inserting the three tubes containing MWNT suspensions into the Qubit fluorometer.

4.2.4 Optical and Structural Characterizations

Using UV-Vis absorption spectroscopy (Solidspec-3700, Shimadzu), we evaluated the degree of dispersion that was achieved for these three emulsions. We have confirmed the reproducibility of the dispersion state of the MWNT suspensions by carrying out the same experimental procedure 3 times. In order to calculate the amount of MWNT with respect to the amount of DNA, solid-state DNA/MWNT samples that were prepared by freeze-drying the suspensions were then heated to 700 ℃ in air on a thermogravimetric analyzer (PerkinElmer, USA). The morphology and the texture of the DNA/MWNT samples were then observed by field-emission scanning electron microscopy (FE-SEM; JSM6335Fs) and transmission electron microscopy (TEM; JEM-2100F, JEOL).

4.2.5 Theoretical Simulation

Models of CNTs with different functionalities were prepared and optimized using the HyperChem Professional 7.01 program package.[30] Semi-empirical molecular orbital theory31 was used to calculate the binding energy between the four types of nucleobases and the three types of MWNTs.

4.3 Results and Discussion

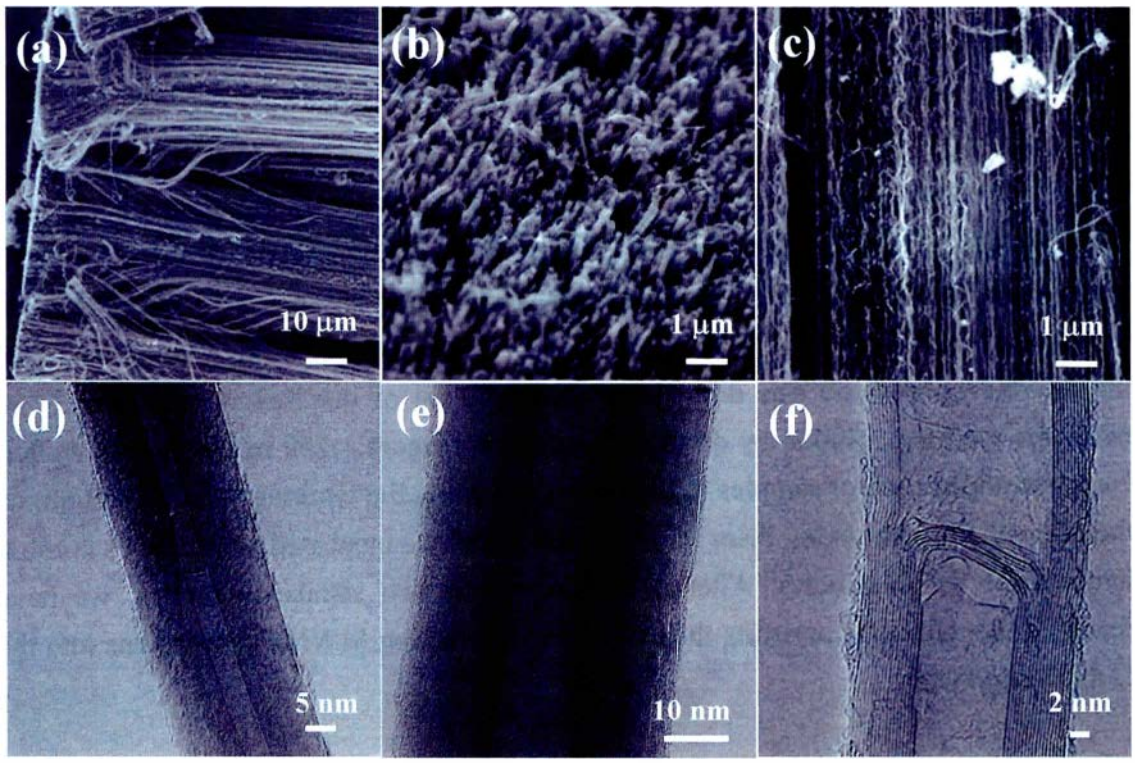

Figure 1 (a-c) Typical SEM images of vertically aligned MWNTs at different angles and representative TEM images of (d) pure, (e) OH-decorated, and (f) N-doped MWNTs.

Pure, N-doped, and OH-decorated MWNT samples were grown by aerosol-assisted chemical vapor deposition.[26-29] All the as-prepared samples consisted of MWNT bundles (Fig. 1 (a)), in which the CNTs were aligned along the tube length direction (Fig. 1 (c)); after scratching the bundles from the walls of the quartz reactor, we noted that in some cases the tube ends were opened (Fig. 1 (b)). No large differences were observed in the degree of crystallinity and the diameter distribution between the three samples (Fig. 1 (d-f)), except that for the N-doped and OH-decorated MWNTs the tubular structures were compartmentalized. These as-produced MWNTs were selected in order to examine the effect of the sidewall functional groups for the following reasons: (1) Even though post treatments (*e.g.*, strong acids and oxygen plasma) could be used to introduce functional groups to the CNTs, such treatments result in the partial disintegration of the bundled structure and the shortening of the tubes;[23] (2) Two factors that affect the adsorption of DNA on the sidewalls of CNTs are the overall coverage of DNA (which relates to the CNT diameter) and the crystallinity of the CNTs (which

relates to the relative number of defects). Experimentally, it is not possible to control both the adsorption of DNA and the crystallinity of the CNTs when using any post treatment. It is noteworthy that pristine and doped chemical vapor deposition-grown MWNTs were selected because they exhibited similar bundled structures and degrees of crystallinity, but had different functional groups on their surface.

I prepared DNA-dispersed MWNT suspensions by subjecting DNA solutions containing the three MWNT samples to strong sonication, followed by centrifugation. All three MWNT suspensions prepared in this way were opaque (Fig. 2 (a), top-left inset) and thus it was not possible to observe any differences by the naked eye. Upon mild centrifugation, we observed a visual difference between the supernatant obtained from the three MWNT suspensions: the N-doped MWNT suspension was more opaque than the pure and OH-MWNT suspensions (Fig. 2 (a), top-right inset). With regard to morphology, we observed that the CNTs were randomly and individually dispersed with the aid of DNA (Fig. 2 (b, c)), which was thickly coated along the sidewall of individual tubes (inset in Fig. 2 (c)), as observed by SEM and TEM. These results indicate a strong interaction between DNA and the sidewall of N-doped tubes. In addition, the absence of structural degradation of the tubes in the dispersion process by a strong sonication was confirmed using Raman studies (see Fig. 3). In order to examine the dispersibility of the three MWNTs in DNA solution quantitatively, UV-Vis absorption spectra were acquired for the three MWNT suspensions (Fig. 2 (a)), because the relative absorbance is proportional to the dispersed amount of CNTs in suspension according to the Lambert-Beer law. When compared with pure and OH-MWNTs, N-doped MWNTs exhibited a 2-fold higher absorbance. However, it is suggested that the presence of bundles in the solution causes an increase in the absorbance background. However, in the case of MWNTs, the bundling is less common for the weaker van der Waals forces caused by the presence of imperfect MWNTs. In addition, I verified the presence of individualized MWNTs using TEM and SEM observations. Therefore, the increase in the absorbance is not coming from the bundled tubes, but rather from the higher amount of the individually dispersed MWNTs in DNA solution.

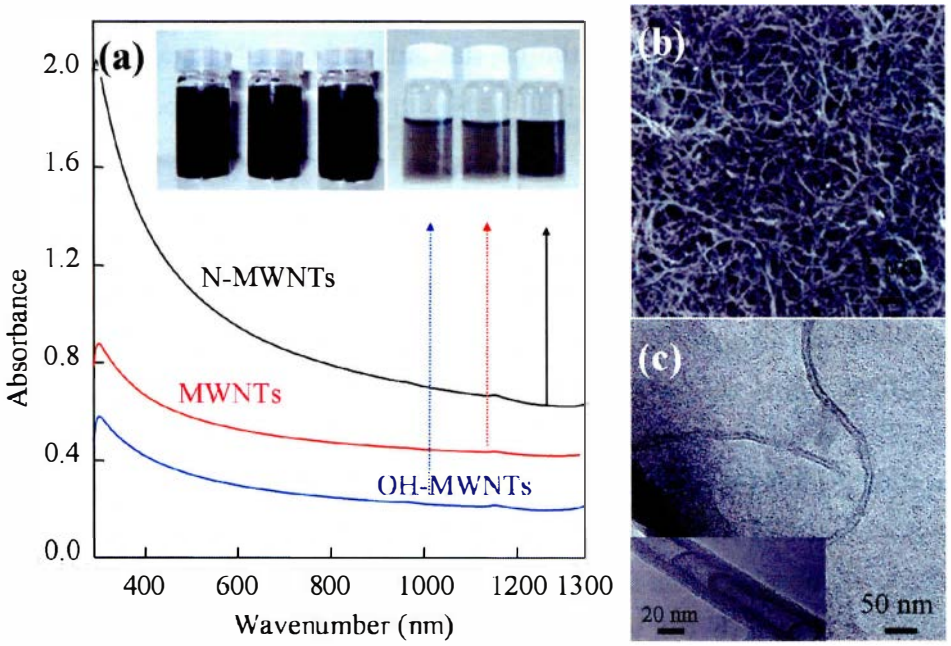

Figure 2 (a) UV absorption spectra of DNA-dispersed pure, OH-decorated, and N-doped MWNT suspensions (insets: photographs of DNA-dispersed MWNT suspensions under sonication and after centrifugation). (b) SEM and (c) TEM images of DNA-adsorbed N-doped MWNTs (inset: high resolution TEM image indicates that the sidewall is fully covered with DNA).

In addition, by using a Qubit fluorometer, we measured the ratio of adsorbed DNA to MWNT in the suspensions by removing any free DNA. The amount of the adsorbed ssDNA on CNTs was found to be 10.1 μg/ml for pure MWNTs, 10.3 μg/ml for OH-MWNTs and 12.0 μg/ml for N-doped MWNTs, respectively. This result is also consistent with the higher dispersion of N-doped MWNTs in a DNA solution.

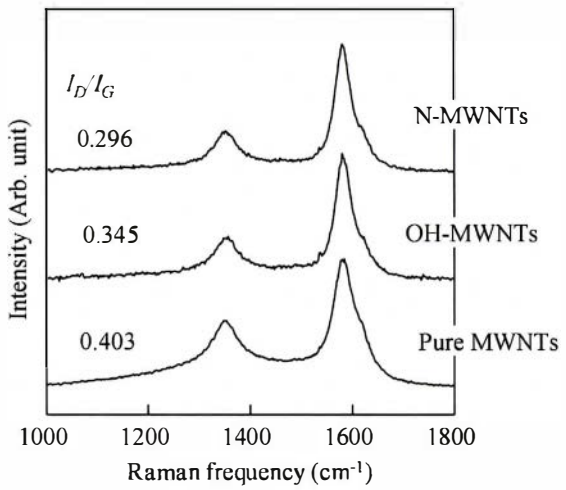

Figure 3 Raman spectra of DNA-dispersed MWNT samples using a 532-nm laser line.

In addition, in order to measure the dispersed amount of MWNTs in suspension, TGA was carried out on freeze-dried DNA/MWNTs in air (Fig. 4). Here we observe that the DNA molecules begin to show an abrupt weight loss in the temperature range of 200–300 °C, and their yield at 700 °C was found to be about 59 %. Both pure MWNT/DNA and OH-MWNT/DNA samples exhibited very similar behaviors and their yields were both 33 %. In contrast, the yield of the DNA/N-MWNT sample was 20 %. However, the pure MWNT sample was completely burned out. Thus, the amount of CNTs could be calculated by subtracting the weight loss of the pure DNA from the weight loss of the DNA-wrapped nanotube sample. Such a marked difference in the yield of DNA/MWNTs and DNA/OH-MWNTs from that of DNA/N-MWNTs could be attributed to the larger amount of the dispersed N-MWNTs in DNA solution. Nitrogen atoms in CNTs are known to function as anchoring sites for growing metal particles.[32-35] Furthermore, N-doped MWNTs have been used in a metal-free electrode that has higher electrocatalytic activity, longer-term operation stability, and a greater tolerance to the crossover effect than a platinum electrode for oxygen reduction in an alkaline fuel cell.[36] Moreover, nitrogen atoms are known to improve the biocompatibility of CNTs[37] and a small amount of nitrogen doping (substitutional type) in CNTs could induce metallic behavior.[38]

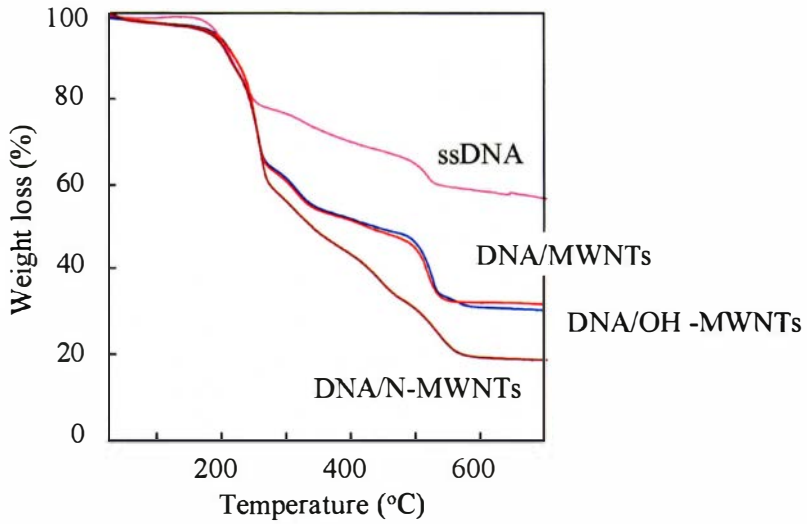

Figure 4 Thermogravimetric profiles, measured in air, of DNA, pure MWNT/DNA, OH-MWNTs/DNA, and N-MWNTs/DNA samples.

Such an enhanced performance of N-MWNTs could be explained by the configuration of the nitrogen atom. To show such effects, we analyzed the bonding

nature of carbon and nitrogen atoms in N-MWNTs by XPS (Fig. 5). In all cases we observed a strong but asymmetric C 1s spectrum. A strong peak at 285.5 eV can be assigned to sp^2-bonded carbon atoms while a broad peak at 287 eV can be assigned to O–C bonds (Fig. 5 (a)). Interestingly, the small, broad peak at 287 eV is here explained by randomly incorporated nitrogen atoms and a net change in the C–N binding energy.[39] In the N 1s XPS spectrum (Fig. 5 (b)), we found two configurations of nitrogen atoms in N-MWNTs: a strong peak at 400.7 eV (N_Q) from substitutional quaternary nitrogen and a relatively weak peak at 398.6 eV (N_P) from pyridinic nitrogen. The amount of pyridinic- and quaternary-type nitrogen was found to be 32.8 and 67.2 %, respectively. When considering the chemical reactivity of the two types of nitrogen atoms, the pyridinic nitrogen atoms exhibit higher activity than the substitutional nitrogen atoms because they are positioned next to atomic vacancies (see Fig. 5 (c)). From these results, the electron-accepting pyridinic-type nitrogen atoms in CNTs are expected to increase the dispersibility of the CNTs in DNA solution. In this context, theoretical calculations have indicated that van der Waals interactions in N-doped MWNTs are significantly weaker and therefore these doped tubes are more easily dispersable.[40, 41]

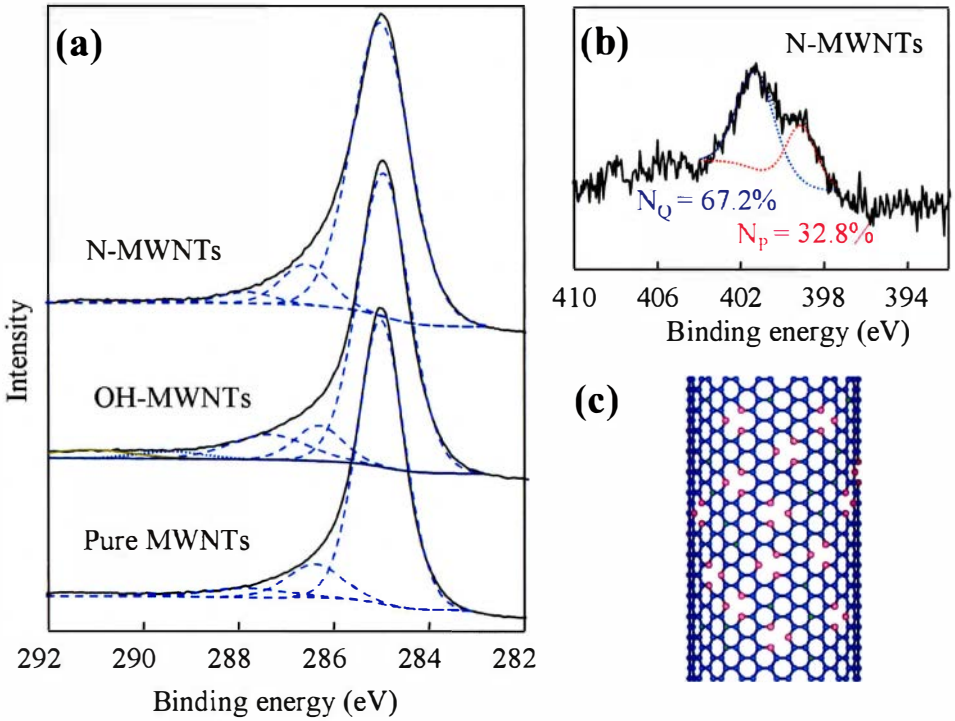

Figure 5 (a) C 1s XPS spectra of pure, OH-decorated and N-doped MWNTs. (b) N 1s XPS spectrum of N-doped MWNTs and (c) a schematic model of N-doped CNTs containing two types of nitrogen atoms.

In order to verify this experimentally observed high dispersibility of N-MWNTs in aqueous DNA solution, binding-energy calculations on DNA/CNT were carried out by placing four types of nucleobases on pure (*5, 5*) SWNTs, and on OH-, pyridinic and quaternary N-doped SWNTs. A pure (*5, 5*) SWNT model was prepared by terminating both ends of the SWNT with hydrogen atoms. The OH-decorated SWNT model was constructed by covalently attaching OH to the sidewall of the (*5, 5*) SWNT, and pyridinic and quaternary nitrogen atoms were incorporated into the SWNT sidewall (Fig. 6 (a-d)). We used the PM6 method to optimize and calculate the energies.[31, 40] Subsequently, by placing nucleobases on the sidewall of pure, OH-, pyridinic and quaternary N-doped SWNTs (Fig. 6 (e)), and after optimizing the atomic structures in order to minimize the total energy of the system, the binding energies (E) (Table 2) were obtained by subtracting the energy of the isolated nucleobases (E_{NB}) and of the SWNTs (E_{CNT}) from the energy of the combined system ($E_{CNT\text{-}NB}$). The binding energy between the nucleobases and the pure SWNT model was quite low, with interactions having magnitudes G > T > C ≈ A (weak interactions) for the various nucleobases. However, greatly enhanced binding energies were observed for the pyridinic and quaternary N-doped SWNTs, and the order of the binding energies then changed to C > T > G > A (strong interactions). The lowest binding energy for the pure SWNTs and the nucleobases can be explained by the fact that the net change in the dipole moment is small. However, the largest binding energy for N-doped SWNTs is due to a large change in the dipole moment.

I found that the order of the HOMO-LUMO gap for the three models followed exactly the same order as the binding energies. Notably, the value of the HOMO-LUMO gap for the pyridinic N-doped SWNT was extremely small (0.126 eV). When calculating the chemical reactivity of the different types of SWNTs towards nucleobases from the energy gap observed between the LUMO of the nucleobases, and the HOMO of the SWNTs (where nucleobases are acceptors and SWNTs are donors), the ease of the surface adsorption of nucleobases onto the pyridinic N-doped SWNT was found to be the highest. According to these theoretical calculations, adenine, when adsorbed on the SWNT induces a small change in the dipole moment, thus resulting in a weak interaction with the CNT sidewall. In contrast, DNA which contains a large fraction of cytosine is expected to improve the dispersibility of CNTs.

Table 2 Theoretically calculated binding energy, dipole moment, and HOMO-LUMO gap for pure, OH-decorated, and N-doped (*5, 5*) SWNT with various nucleobases.

Sample I.D.		Adenine	Cytosine	Guanine	Thymine
SWNT	Binding energy [a]	-0.0874	-0.0969	-0.2382	-0.1698
	Dipole moment	0.158	0.180	0.114	0.002
	HOMO-LUMO gap	7.033	7.125	6.959	6.899
OH-SWNT	Binding energy [a]	-0.6099	-0.8222	-0.9204	-0.8699
	Dipole moment	0.093	2.967	3.244	4.184
	HOMO-LUMO gap	6.716	6.809	6.642	6.582
N-SWNT	Binding energy [a]	-1.3221	-2.7018	-2.0682	-2.4275
	Dipole moment	0.922	6.811	2.309	1.699
	HOMO-LUMO gap	0.026	0.067	0.100	0.160

[a] Binding energies (E) were obtained by subtracting the energy of the isolated nucleobase (E_{NB}) and of the CNT (E_{CNT}) from the energy of the combined system (E_{CNT}-N_B).

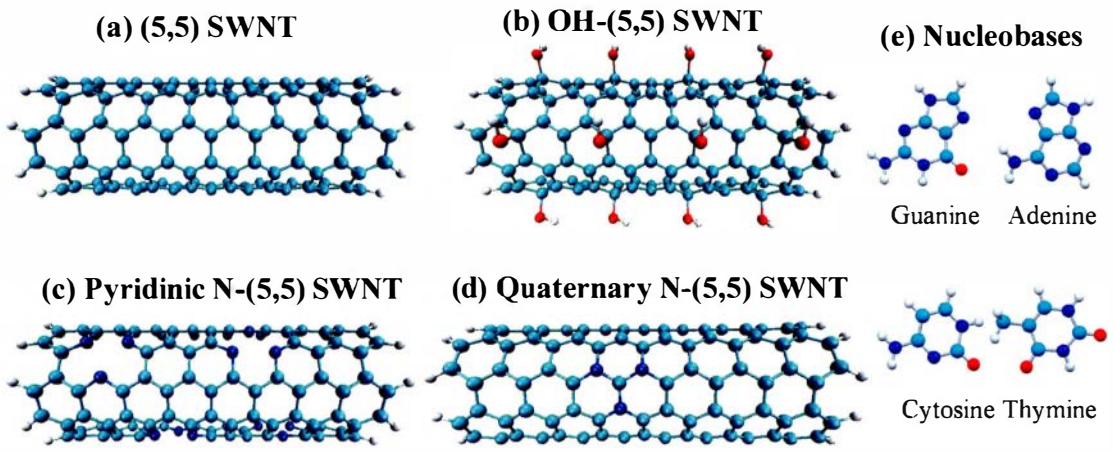

Figure 6 Models of (a) pure, (b) OH-decorated, (c) pyridinic and (d) quaternary N-doped (5, 5) SWNTs, and (e) the four types of nucleobases.

4.4 Conclusion

Here, I presented both experimental and theoretical evidence demonstrating that the dispersibility of MWNTs in DNA solution strongly depends on the type of functional group that is attached to the CNT sidewall. The particularly high dispersion of N-doped MWNTs in DNA solutions, when compared with that of pure and

OH-decorated MWNTs, is explained by the presence of nitrogenated sites (substitutional and pyridinic) present on the CNT sidewall. DNA molecules could readily adsorb onto the hydrophobic surface of the pure CNT via π-π stacking interactions. Based on our theoretical calculations, the pyridinic nitrogen next to carbon vacancies in N-doped MWNTs was found to be a major contributor to the large binding energy, as well as to the small HOMO-LUMO gap between the nucleobases and the sidewall of N-doped MWNTs. The calculations also revealed that DNA which contains a large fraction of cytosine could significantly improve the dispersibility of both SWNTs and MWNTs.

4.5 References

1. M. S. Dresselhaus, G. Dresselhaus, P.C. Eklund, *Science of Fullerenes and Carbon Nanotubes*, Academic Press, New York, 1996.
2. R. H. Baughman, A. A. Zakhidov, W. A. de Heer, W. A. *Science* **297**, 787 (2002).
3. A. Jorio, M. S. Dresselhaus, G. Dresselhaus, *Carbon Nanotubes: Advanced Topics in the Synthesis, Structure, Properties and Applications*, Springer, New York, 2008.
4. N. Nakashima, S. Okuzono, H. Murakami, T. Nakai, K. Yoshikawa, *Chem. Lett.* **32**, 456 (2003).
5. M. Zheng, A. Jagota, E. D. Semke, B. A. Diner, R. S. McLean, S. R. Lustig, R. E. Richardson, N. G. Tassi, *Nat. Mater.* **2**, 338 (2003).
6. M. Zheng, A. Jagota, M. S. Strano, A. P. Santos, P. Barone, S. G. Chou, B. A. Diner, M. S. Dresselhaus, R. S. Mclean, G. B. Onoa, G. G. Samsonidze, E. D. Semke, M. Usrey, D. J. Walls, *Science* **302**, 1545 (2003).
7. J. H. Kim, M. Kataoka, Y. A. Kim, D. Shimamoto, H. Muramatsu, T. Hayashi, M. Endo, M. Terrones, M. S. Dresselhaus, *Appl. Phys. Lett.* **93**, 223107 (2008).
8. M. S. Strano, M. Zheng, A. Jagota, G. B. Onoa, D. A. Heller, P. W. Barone, M. L. Usrey, *Nano Lett.* **4**, 543 (2004).
9. M. Zheng, B. A. Diner, *J. Am. Chem. Soc.* **126**, 15490 (2004).
10. C. Fantini, A. Jorio, A. P. Santos, V. S. T. Peressinotto, M. A. Pimenta, *Chem. Phys. Lett.* **439**, 138 (2007).
11. X. Zhao, J. K. Johnson, *J. Am. Chem. Soc.* **129**, 10438 (2007).
12. S. Meng, P. Maragakis, C. Papaloukas, E. Kaxiras, *Nano Lett.* **7**, 45 (2007).
13. Y. Chen, H. Liu, T. Ye, J. Kim, C. Mao, *J. Am. Chem. Soc.* **129**, 8696 (2007).
14. S. R. Vogel, M. M. Kappes, F. Hennrich, C. Richert, *Chem. Eur. J.* **13**, 1815 (2007).
15. D. Das, A. K. Sood, P. K. Maiti, M. Das, R. Varadarajan, C. N. R. Rao, *Chem. Phys. Lett.* **453**, 266 (2008).
16. M. L. Carot, R. M. Torresi, C. D. Garcia, M. J. Esplandiu, C. E. Giacomelli, *J. Phys. Chem. C* **114**, 4459 (2010).
17. J.H. Kim, M. Kataoka, D. Shimamoto, H. Muramatsu, Y. C. Jung, T. Hayashi, Y. A. Kim, M. Endo, J. S. Park, R. Saito, M. Terrones, M. S. Dresselhaus, *ACS Nano* 4, 1060 (2010).
18. C. Staii, A. T. Johnson, M. Chen, A. Gelperin, *Nano Lett.* **5**, 1774 (2005).
19. H. Gao, Y. Kong, *Annu. Rev. Mater. Res.* **34**, 123 (2004).
20. N. W. S. Kam, Z. Liu, H. Dai, *Angew. Chem. Intl. Ed.* **45**, 577 (2006).

21. Y. Lu, S. Bangsaruntip, X. Wang, L. Zhang, Y. Nishi, H. Dai, *J. Am. Chem. Soc.* **128**, 3518 (2006).
22. J. H. Kim, M. Kataoka, D. Shimamoto, H. Muramatsu, Y. C. Jung, T. Tojo, T. Hayashi, Y. A. Kim, M. Endo, M. Terrones, M. S. Dresselhaus, *ChemPhysChem* **10**, 2414 (2009).
23. J. Liu, A. G. Rinzler, H. Dai, J. H. Hafner, R. K. Bradley, P. J. Boul, A. Lu, T. Iverson, K. Shelimov, C. B. Huffman, F. Rodriguez-Macias, Y. S. Shon, T. R. Lee, D. T. Colbert, R. E. Smalley, *Science* **280**, 1253 (1998).
24. V. Ivanov, A. Fonseca, J. B. Nagy, A. Lucas, P. Lambin, D. Bernaerts, X. B. Zhang, *Carbon* **33**, 1727 (1995).
25. S. S. Wong, E. Joselevich, A. T. Woolley, C. L. Cheung, C. M. Lieber, *Nature* **394**, 52 (1998).
26. R. Kamalakaran, M. Terrones, T. Seeger, Ph. Kohler-Redlich, M. Ruhle, Y. A. Kim, T. Hayashi, M. Endo, *Appl. Phys. Lett.* **77**, 3385 (2000).
27. M. Mayne, N. Grobert, M. Terrones, R. Kamalakaran, M. Rhle, H. W. Kroto, D. R. M. Walton, *Chem. Phys. Lett.* **338**, 101 (2001).
28. M. Terrones, P. M. Ajayan, F. Banhart, X. Blase, D. L. Carroll, J. C. Charlier, R. Czerw, B. Foley, N. Grobert, R. Kamalakaran, P. Kohler-Redlich, M. Rühle, T. Seeger, H. Terrones, *Appl. Phys. A* **74**, 355 (2002).
29. A. R. Botello-Mendez, J. Campos-Delgado, A. Morelos-Gmez, J. M. Romo-Herrera, A. G. Rodrguez, H. Navarro, M. A. Vidal, H. Terrones, M. Terrones, *Chem. Phys. Lett.* **453**, 55 (2008).
30. O. Ivanciuc, *Chem. Inf. Comput. Sci.* **36**, 612 (1996).
31. J. J. P. Stewart, *J. Mol. Model.* **13**, 1173 (2007).
32. K. Jiang, L. S. Schadler, R. W. Siegel, X. J. Zhang, H. F. Zhang, M. Terrones, *J. Mater. Chem.* **14**, 37 (2004).
33. K. Jiang, A. Eitan, L. S. Schadler, P. M. Ajayan, R. W. Siegel, N. Grobert, M. Mayne, M. Reyes-Reyes, H. Terrones, M. Terrones, *Nano Lett.* **3**, 275 (2003).
34. A. Zamudio, A. L. Elias, J. A. Rodriguez-Manzo, F. Lopez-Urias, G. Rodriguez-Gattorno, F. Lupo, M. Ruhle, D. J. Smith, H. Terrones, D. Diaz, M. Terrones, *Small* **2**, 346 (2005).
35. X. Lepro, Y. Vega-Cantu, F. J. Rodriguez-Macias, Y. Bando, D. Golberg, M. Terrones, *Nano Lett.* **7**, 2220 (2007).
36. K. Gong, F. Du, Z. Xia, M. Durstock, L. Dai, *Science* **323**, 760 (2009).
37. J. L. Carrero-Sanchez, A. L. Elias, R. Mancilla, G. Arellin, H. Terrones, J. P. Laclette, M. Terrones, *Nano Lett.* **6**, 1609 (2006).

38. D. Golberg, P. S. Dorozhkin, Y. Bando, Z. C. Dong, C. C. Tang, Y. Uemura, N. Grobert, M. Reyes-Reyes, H. Terrones, M. Terrones, *Appl. Phys. A-Mater.* **76**, 499 (2003).
39. P. Ayala, A. Grulneis, T. Gemming, D. Grimm, C. Kramberger, M. H. Rulmmeli, Jr. F. L. Freire, H. Kuzmany, R. Pfeiffer, A. Barreiro, B. Bulchner, T. Pichler, *J. Phys. Chem. C* **111**, 2879 (2007).
40. B. G. Sumpter, J. S. Huang, V. Meunier, J. M. Romo-Herrera, E. Cruz-Silva, H. Terrones, M. Terrones, *Int. J. Quantum Chem.* **109**, 97 (2009).
41. B. G. Sumpter, V. Meunier, J. M. Romo-Herrera, E. Cruz-Silva, D. A. Cullen, H. Terrones, D. J. Smith, M. Terrones, *ACS Nano* **1**, 369 (2007).

CHAPTER 5

Raman and Fluorescence Spectroscopic Studies of a DNA-Dispersed Double Walled Carbon Nanotube Solution

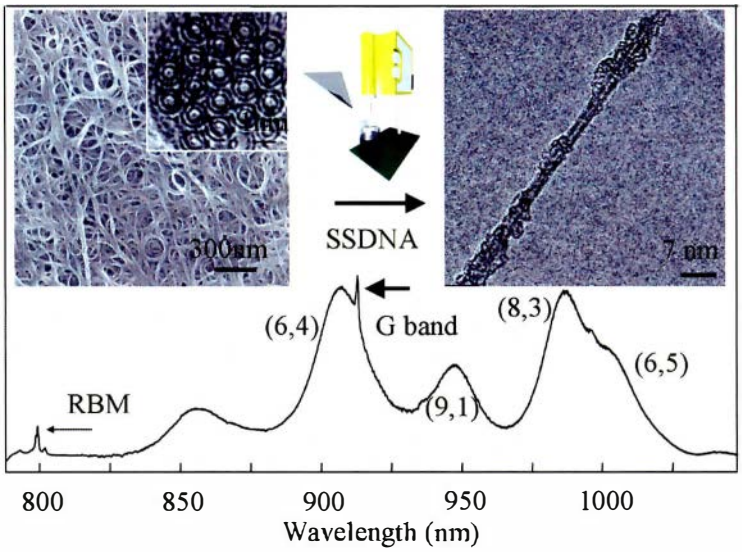

Chapter 5 Raman and Fluorescence Spectroscopic Studies of a DNA-Dispersed Double Walled Carbon Nanotube Solution

5.1 Introduction

DWNTs have attracted a great deal of attention[1] because their intrinsic coaxial structures make them mechanically, thermally and structurally more stable than SWNTs.[2] Geometrically, the buffer-like function of the outer tubes in DWNTs allows the inner tubes to exhibit exciting transport and structural properties[3-6] that make them promising in the fabrication of field-effect transistors,[7-10] stable field emitters[11] and lithium ion batteries[12]. In addition, selective functionalization of the outer tubes makes DWNTs useful for anchoring semiconducting quantum dots[13] as well as for use as an effective multifunctional filler in producing tough, conductive transparent polymer films,[14] while the inner tubes with diameters below 0.9 nm preserve their excitonic transitions.[15] Up to now, the vibrational properties of the inner tubes in the solid form of a DWNT sample have been systematically studied using Raman spectroscopy as a characterization tool,[16-22] where strong Raman lines associated with the inner tubes have been used as a fingerprint for identifying the growth of the inner tubes in the hollow core of large diameter SWNT hosts.

On the other hand, optical studies on a density gradient-enriched DWNT solution[23] suggested that the luminescence originates not from the inner tube of the DWNT but from impurity SWNTs by referring to the absence of luminescence in peapod-grown DWNTs,[24] even though several studies reported bright and stable luminescence from the inner tubes in a SDBS-dispersed DWNT solution.[25-29] In this context, our group has confirmed the bright luminescence coming from the inner tube from peapod-grown DWNTs without the presence of any impurity SWNTs, in a DWNT sample that was prepared by thermally treating a peapod sample above 1700 °C in an argon atmosphere.[30] On this basis, it is expected that DWNTs will someday replace SWNTs in biomarkers[31] and optoelectronics[32] due to their strong and stable luminescence.

Therefore, when considering the promising application of DWNTs as stable luminescent biomarkers, a long-time stable and homogeneously dispersed DWNT solution with a high biocompatibility should be prepared. In this sense, we have selected ssDNA as the dispersing agent because DNA is well known to be effective for dispersing and sorting SWNTs[33-36] and the interaction of DNA with SWNTs has been studied both theoretically and experimentally.[37-44]

In this account, it is very important to understand the interaction between DNA and the outer tubes in a DWNT solution, where the inner tubes are structurally shielded by outer tubes, and where a possible charge transfer occurs from the outer tubes to the inner tubes, thereby affecting the luminescence from the inner tubes. I have thus prepared DNA-dispersed DWNT solutions at different dispersion states, and then carried out detailed Raman and luminescence spectroscopic studies on a DNA-dispersed DWNT aqueous solution in comparison to a corresponding SDBS-dispersed DWNT solution using three different laser lines (532, 633 and 785 nm). I observed intensified luminescence signals and as well as preserved RBMs in the Raman spectra coming from the inner tubes in both individually dispersed DWNT solutions, though the RBMs coming from the outer tubes were severely depressed after DNA wrapping, regardless of the outer tube metallicity.

5.2 Experimental Section

5.2.1 Preparation of Double Walled Carbon Nanotubes

Highly pure (ca. 99 %), highly crystalline DWNTs (absence of the D-band in their Raman spectra) were used in this study, in which nanotubes with an outer diameter of ca. 1.6 nm were packed in hexagonal arrays within the bundles.[45]

5.2.2 Dispersion of Double Walled Carbon Nanotubes

Then we prepared a homogeneously dispersed DWNT aqueous solution using ssDNA, as described in our previous study.[46] The prepared highly pure DWNTs (ca. 3 mg) were individually dispersed (or isolated) in an aqueous solution (10 ml) with the help of ssDNA wrapping under strong sonication (KUBOTA UP50H, ca. 470 W/cm^2) for 1 hr at 4 °C, and subsequent ultracentrifugation (Optima Max-XP, Beckman Coulter, 240,000 g). Their supernatant (70 %), rich with isolated nanotubes, was characterized in solution by transferring these solutions to a quartz cuvette.

5.2.3 Characterizations

Raman spectra at 785 nm excitations were obtained using a Renishaw setup fitted with a macroscopic sampling kit. We also obtained Raman spectra using 532 nm and 633 nm laser excitations produced by a Kaiser HoloLab5000 system. In order to confirm the individually dispersed DWNTs in the DNA solution, we measured their UV-Vis absorption spectra (SolidSpec-3700, Shimazu) and photoluminescence maps (NIR-PL system, Shimazu). Finally, we used TEM (JEOL2010FEF) for studying the dispersed state of the DWNTs.

5.3 Results and Discussion

Figure 1 shows Raman/fluorescence spectra taken with laser excitation of 785 nm for pristine DWNTs, and DNA-dispersed DWNT solutions at different dispersion states. From the Raman spectra of pristine DWNTs, we could see a strong G-band (E_{2g2} mode) at around 1592 cm^{-1}, while below 500 cm^{-1}, several RBMs (which correspond to a coherent vibration of the carbon atoms normal to the tube axis) could be seen along with the second order symmetry-allowed G'-band at around 2600 cm^{-1}.[47] However, by sonicating DWNTs in a DNA aqueous solution, several strong luminescence peaks start to appear, indicating that individually dispersed DWNTs are generated through the interaction with DNA, because we are not able to see bright luminescence from the bundled sample due to the presence of entrapped metallic (M) tubes which quench the luminescence.[48] Moreover, by concentrating individually isolated DWNTs in a DNA solution through the removal of thin bundled DWNTs using ultracentrifugation, we found that the intensity of the luminescence peaks becomes very strong and comparable to the intensity of the G-band in the supernatant sample.

Since the RBMs of SWNTs are well known to provide information on the chirality and diameter,[49-51] the low-frequency Raman spectra is magnified (see inset in Fig. 1). Because of their intrinsic coaxial geometries, DWNTs are able to have the four configurations (i.e., S@S, S@M, M@S and M@M, where S@M denotes a semiconducting (S) inner tube within a metallic (M) outer tube). Thus, by using a theoretical Kataura plot based on the extended tight binding exciton model for SWNTs, [52] we could assign the inner tubes with diameters of ca. 0.8 nm that are in resonance with 785 nm laser excitation to be S tubes, while the outer tubes with diameters of ca. 1.56 nm were identified to be M tubes. It is noteworthy that the RBM signals are arising from an ensemble of different DWNTs, and not from an individual DWNT. The intensity of the peak at 267 cm^{-1} decreases through a debundling process and finally disappears in individually isolated DWNTs. On the other hand, the frequencies and intensities of the RBM associated with the semiconducting inner tubes are constant regardless of the dispersion state of the DWNTs. However, the depressed intensity of the RBM at 160 cm^{-1} associated with the metallic outer tube is quite different from the behavior of the peak at 267 cm^{-1} because the outer tubes are in contact with DNA and their electronic structure is modified by charge transfer from the negatively charged DNA.

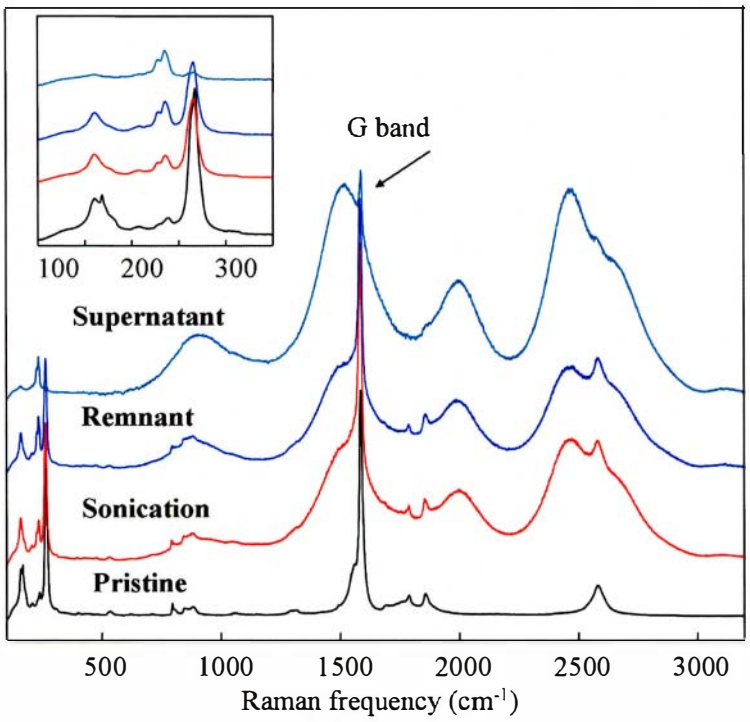

Figure 1 Raman/fluorescence spectra taken with laser excitation of 785 nm for pristine DWNTs, and for DNA-dispersed DWNT solutions at different dispersion states (sonicated, remnant and supernatant). The inset shows the magnified low-frequency Raman spectra for the corresponding samples.

In order to understand the effect of DNA (which is known to helically wrap around CNTs)[34, 35] on the RBMs and luminescence peaks in detail, we have compared Raman/luminescence spectra taken with the laser excitation of 785 nm for SDBS- and DNA-dispersed DWNT solutions (Fig. 2). The strong luminescent peaks in the SDBS-dispersed DWNT solution could be assigned to the *(6,4)*, *(9,1)*, *(8,3)*, *(6,5)* and *(7,5)* nanotubes.[53] Noticeably, the luminescence spectra of DNA-dispersed DWNT solution (Fig. 2) are red-shifted compared to the SDBS-dispersed DWNT solution. This shift should be explained by environmental dielectric screening effects,[54-58] since the accessibility of water to the surface of DWNTs in DNA-dispersed DWNTs is expected to be greater than for SDBS-dispersed DWNTs, thereby allowing water molecules to interact strongly with the outer tubes. In addition, a strong luminescence peak from the *(8,3)* tube is observed from the SDBS-dispersed DWNTs solution, while the *(6,4)* tube shows the strongest peak in the DNA-dispersed DWNT solution. This result suggests differences in DNA- and SDBS-dispersed DWNTs species due to their intrinsically different interactions with their wrapping molecules. This assumption is clearly verified in the drastic change of the RBMs for both solutions (see inset in Fig. 2). The RBM

intensity associated with the outer tube in the DNA-dispersed DWNT solution is highly depressed, whereas the corresponding RBM in the SDBS-dispersed DWNT solution maintains its intensity comparable to a pristine DWNT. This RBM depression can be explained by direct charge transfer from DNA to the outer tubes, thus filling states below the resonant van Hove singularity of the metallic outer tube of the DWNT, as previously demonstrated in the detailed Raman study carried out on individual semiconducting and metallic SWNTs.[59] Moreover, we observed an upshifted RBM frequency (ca. 4 cm^{-1}) associated with outer tubes, indicating that the circumferentially generated concentrated stress due to the presence of the helically wrapped DNA along the outer surface of the DWNT suppresses the coherent RBM vibration of the carbon atoms in a direction normal to the tube axis. However, the absence of a change in the frequency of the RBMs associated with the inner tubes suggests the absence of stress transfer from the outer to the inner tubes, as evidenced by the fluorescence study of polyvinlypyrrolidone-dispersed DWNTs.[29] This result also supports the protective function of the outer tubes in DWNTs.

However, the depressed RBM intensity at 265 cm^{-1} in the DNA-dispersed solution is unexpected, because the protective effect of the outer tubes maintains the intensity of their RBMs which appear at around 240 cm^{-1}. Using the inverse relationship between the RBM frequency (ω) and the tube diameter (d) ($\omega = 218.3/d + 15.9$),[60] we are able to assign the two RBMs at 265 and 150 cm^{-1} as due to a semiconducting inner tube having a diameter of 0.88 nm and a metallic outer tube having a diameter of 1.63 nm (S@M DWNT), as confirmed by a resonance Raman study on isolated DWNTs.[61] Very recently, two separate Raman studies[62, 63] showed a severely modified electronic structure for metallic SWNTs due to the presence of helically wrapped DNA, where water molecules activated a transition from metallic to a p-type semiconducting behavior in a SWNT. Therefore, in the case of the S@M DWNT configuration, strong charge transfer between the outer tube and the DNA wrapping is thought to be one of the reasons for the substantial depression of the RBM at 265 cm^{-1}.

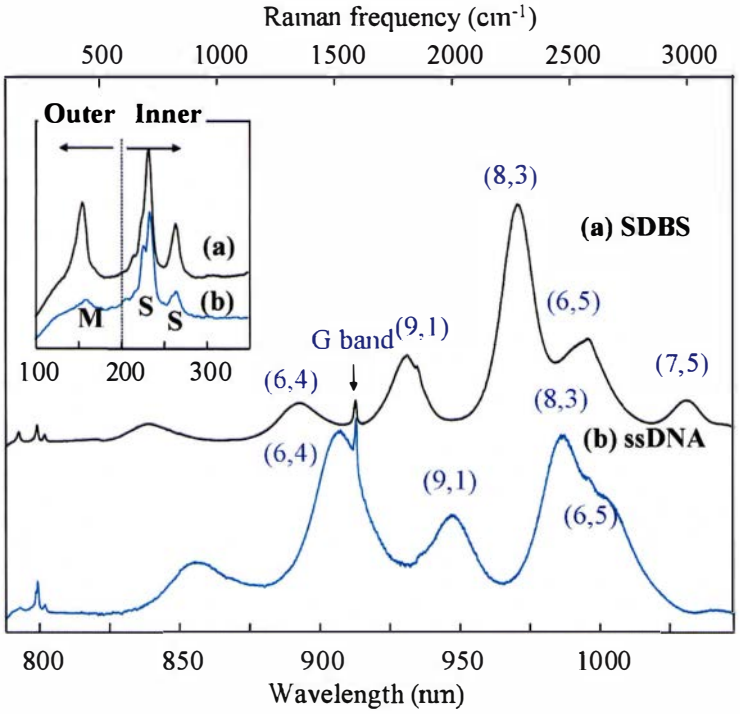

Figure 2 Comparative Raman/fluorescence spectra taken with laser excitation of 785 nm for SDBS- and DNA-dispersed DWNT supernatants. The inset shows the magnified low frequency Raman spectra, where M indicates metallic and S indicates semiconducting tubes.

Furthermore, in order to confirm the individually isolated state of the DWNTs in the supernatant, we have carried out PL, UV-Vis absorption spectra and TEM observations. The appearance of three strong PL peaks (corresponding to the inner tubes with chiralites *(8,3)*, *(7,5)* and *(10,2)*) in the PL map (Fig. 3 (a)) indicates the presence of individually isolated DWNTs in the DNA solution. In addition, DWNTs dispersed in a DNA solution exhibited well-resolved and sharp optical absorption peaks due to their excitonic transitions between van Hove singularities (Fig. 3 (b)), thus indicating that individual nanotubes were isolated. The observed redshifted E_{11} emission (ca. 45 meV) (Fig. 3 (a)) and UV absorption peaks (Fig. 3 (b)) as compared to the SDBS-dispersed DWNT solution are ascribed to their different environmental dielectric screening effects.[54-58] In order to confirm these effects, an SDS solution (1 wt%) was steadily added to the DNA-dispersed DWNT solution and then sonicated for 10 minutes. Interestingly, we then observed a blue shift in the DNA and SDS dispersed DWNT solution. Such a blueshift can be explained by the increased coverage of the DWNTs by surfactants resulting from the combination of long and helical DNA and particle-like SDS molecules on the outer surface of the outer tubes, which give rises to a decreased

dielectric constant. Visually, we have verified the individually dispersed DWNTs in low resolution TEM (Fig. 3 (c)). Interestingly, typical high resolution TEM (Fig. 3 (d)) revealed that DNA is helically wrapped along the outer surface of DWNT in an irregular pattern, and bare nanotube surfaces are partially present and allow water molecules to interact with the outer tube, which is closely related with the redshift of the E_{11} emission (Fig. 3 (a)) and absorption peaks (Fig. 3 (b)).

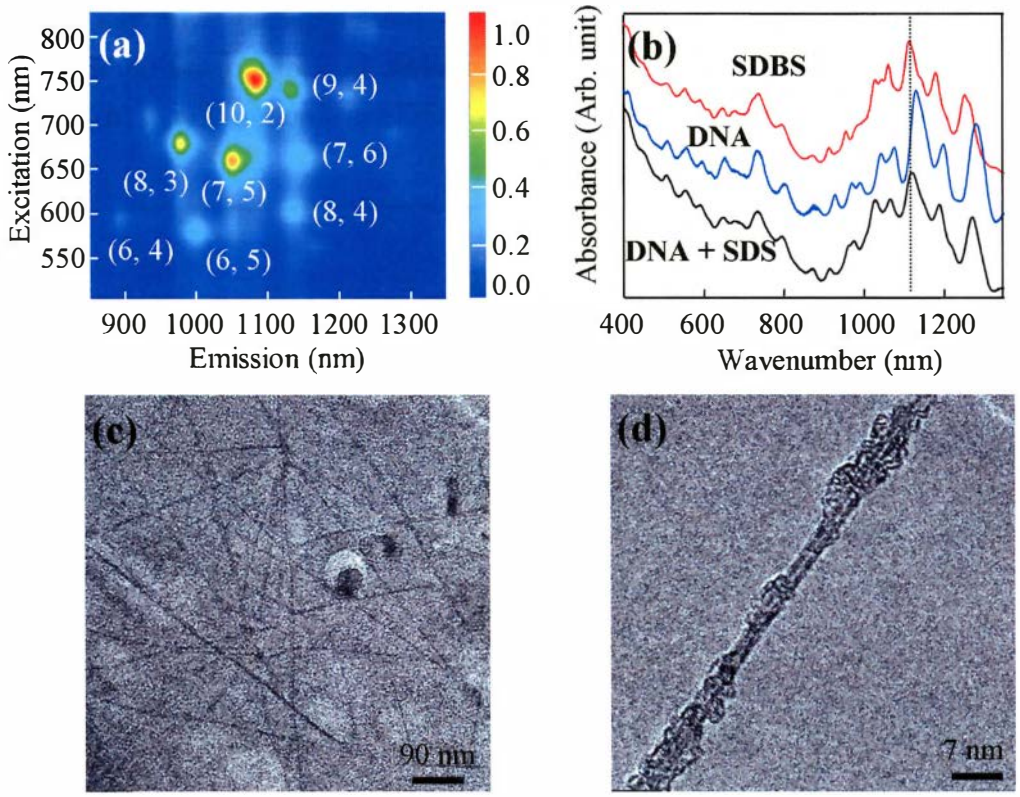

Figure 3 (a) PL map and (b) UV-visible absorption spectra of DNA-dispersed DWNT solution at pH = 8.0, (c, d) their corresponding TEM images. Note that DWNTs are individualized with the help of helically wrapped DNA. The color represents the PL intensity on a linear scale.

We also have measured Raman spectra using a laser excitation of 633 nm for pristine DWNTs, DNA-dispersed DWNT solutions at different dispersion states (Fig. 4 (a)). Here we could see a broad peak coming from the O-H stretching transitions of water molecules[64] at around 3300 cm^{-1} from the individually isolated DWNT solution. In order to see Raman changes in greater detail, we have magnified the RBMs below 400 cm^{-1}, the G-band and the G'-band (Fig. 4 (b-d)), respectively. According to the calculated diameter from the sharp RBMs (Fig. 4 (b)), we are able to assign two possible configurations (i.e., dominantly S@S and partially M@S). We could see a

severely depressed RBM intensity (which is associated with the semiconducting outer tube) at 150 cm^{-1} in the supernatant. Concurrently, the RBM associated with the metallic inner tube at 220 cm^{-1} is also depressed, while the RBM for (semiconducting inner tube) at 258 cm^{-1} retains its intensity and the RBM for semiconducting inner tube at 280 cm^{-1} is significantly intensified. These facts tell us that metallic inner tubes could be affected through charge transfer from DNA-wrapped outer tubes. When looking at the G band (Fig. 4 (c)), the broad and asymmetric BWF line[65] in the pristine DWNT sample is strongly depressed and shifted to a low frequency with the increasing dispersion state of the DWNTs in the DNA solution. In addition, the width of the G' band is decreased for the individually isolated DWNTs in solution (Fig. 4 (d)).

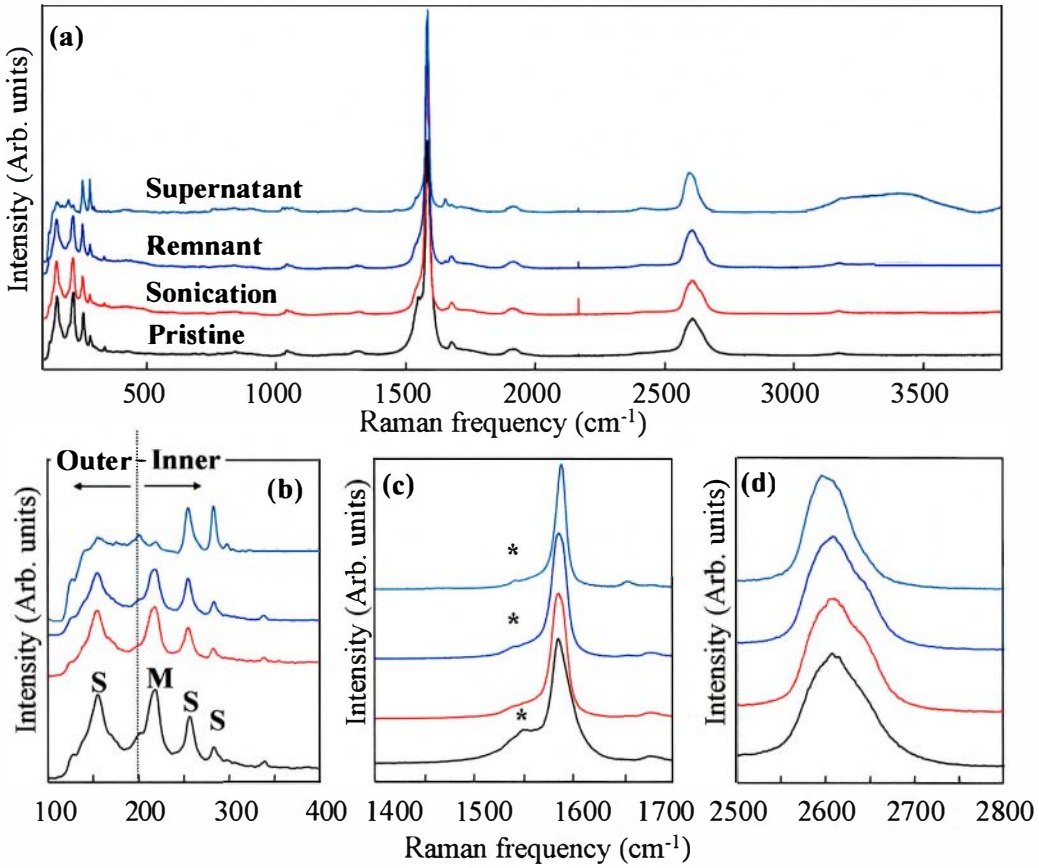

Figure 4 (a) Wide-range Raman spectra taken with laser excitation of 633 nm for pristine DWNTs, and for DNA-dispersed DWNT solutions at different dispersion states (sonicated, remnant and supernatant), and their corresponding (b) radial breathing mode (where S indicates semiconducting and M indicates metallic tubes), (c) G-band (asterisk indicates the BWF line associated with metallic outer tubes) and (d) the G'-band Raman spectra, respectively.

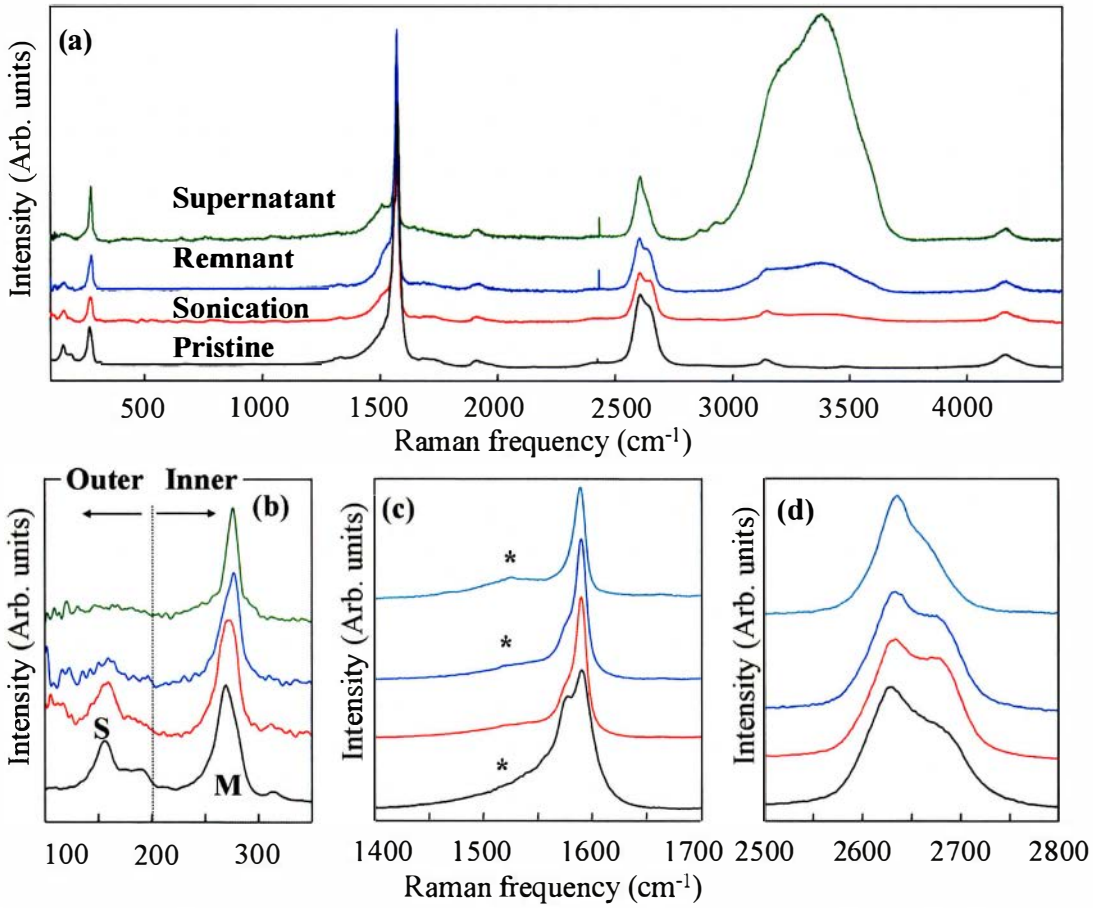

Figure 5 (a) Wide-range Raman spectra taken with laser excitation of 532 nm for pristine DWNT, and DNA-dispersed DWNT solutions at different dispersion states (sonicated, remnant and supernatant), and their corresponding (b) radial breathing mode (where S indicates semiconducting and M indicates metallic tubes), (c) the G-band (asterisk indicates the BWF line associated with metallic inner tubes) and (d) the G'-band Raman spectra, respectively.

Finally, we have measured Raman spectra using the 532 nm laser excitation for pristine DWNTs and DNA-dispersed DWNT solutions at different dispersion states (Fig. 5 (a)). With increasing the dispersion state of the DWNTs in DNA solution, the OH-stretching transitions from water molecules become intense consecutively. From the low-frequency Raman spectra (Fig. 5 (b)), we can easily assign the RBM at 265 cm^{-1} to a metallic inner tube and the RBM at 158 cm^{-1} to a semiconducting outer tube (in a M@S configuration). The RBM intensity at 158 cm^{-1} decreases continuously with increasing dispersion state of the tubes, and finally disappears in the individually isolated DWNT solution. The G-band consists of two Lorentzian peaks at 1592 and 1572 cm^{-1} and a broad metallic tail at 1519 cm^{-1} because both the inner and outer tubes are resonant with the laser excitation of 532 nm. By increasing the dispersion state of

the DWNTs in the DNA solution, we could see a consecutive decrease in the G-band coming from the semiconducting outer tubes at 1570 cm^{-1} (Fig. 5 (c)). Therefore, we could assign the strong G band at 1592 cm^{-1} to the metallic inner tubes with the clear observation of the broad and asymmetric BWF line at around 1525 cm^{-1} in the supernatant. As shown in Fig. 5 (d), the G'-band of pristine DWNTs consists of two Lorentzian peaks. Two previous studies have assigned the Raman line at ca. 2630 cm^{-1} to the inner tubes and the Raman line at 2677 cm^{-1} to the outer tubes by analyzing the Raman spectra in peapod-derived DWNTs.[66, 67] In addition, a recent study showed that the presence of defects in SWNTs was a reason for the evolution of the low frequency component of the G' band.[68] For individual isolated DWNTs in the DNA solution, our results show that the outer tube-induced Raman line at 2677 cm^{-1} becomes highly depressed and correlated with the disappearance of the RBM.

5.4 Conclusions

Here I report, for the first time, detailed Raman/luminescence spectroscopic studies on ssDNA-dispersed DWNT solutions at different dispersion states, in comparison with an SDBS-dispersed DWNT solution using three different laser lines, in order to understand the interactions between DNA and the outer tubes, and the effect of these different DWNT environments on the vibrational and luminescence behaviors. By increasing the dispersion state of the DWNTs in an aqueous DNA solution, the luminescence peaks were intensified and shifted to longer wavelengths, indicating that DWNTs are individually dispersed in an aqueous DNA solution, which is strongly supported by the strong PL map and the sharp absorption spectra as well as high-resolution TEM observations. Noticeably, we observed cases of completely depressed RBM intensities associated with the outer tubes (regardless of their metallicity) for three configurations of DWNTs (S@M, S@S and M@S). This result strongly supports the interpretation that the evolved luminescence and sharp absorption peaks (Fig. 3 (a, b)) solely come from the semiconducting inner tubes of the DWNTs, not from impurity SWNTs. In addition, the metallic inner tubes are partially affected by the DNA-wrapped outer tubes. Conclusively, the circumferentially wrapped DNA on the outer tubes of individually isolated DWNTs in an aqueous solution gives rise to strong charge transfer to the semiconducting and metallic outer tubes as well as generating physical strain in the outer tubes. Therefore, we envisage that DNA-dispersed DWNTs are highly promising for producing strong and stable luminescence signals as well as for high yield optoelectronics applications.

5. 5 References

1. R. Pfeiffer, T. Pichler, Y. A. Kim, H. Kuzmany, In *Carbon Nanotubes: Advanced Topics in the Synthesis, Structure, Properties and Applications* (Edited by A. Jorio, M. S. Dresselhaus, G. Dresselhaus, G.) Springer, New York, 2008, pp. 495-530.
2. Y. A. Kim, H. Muramatsu, T. Hayashi, M. Endo, M. Terrones, M. S. Dresselhaus, *Chem. Phys. Lett.* **398**, 87 (2004).
3. R. Pfeiffer, H. Kuzmany, C. Kramberger, C. Schaman, T. Pichler, H. Kataura, Y. Achiba, J. Kürti, V. Zólyomi, *Phys. Rev. Lett.* **90**, 225501 (2003).
4. E. Herández, V. Meunier, B. W. Smith, R. Rurali, H. Terrones, M. Buongiorno Nardelli, M. Terrones, D. E. Luzzi, J.-C. Charlier, *Nano Lett.* **3**, 1037 (2003).
5. L. Kavan, L. Dunsch, H. Kataura, *Carbon* **42**, 1011 (2004).
6. A. G. Souza Filho, V. Meunier, M. Terrones, B. G. Sumpter, E. B. Barros, F. Villalpando-Paez, J. Mendes Filho, Y. A. Kim, H. Muramatsu, T. Hayashi, M. Endo, M. S. Dresselhaus, *Nano Lett.* **7**, 2383 (2007).
7. T. Shimada, T. Sugai, Y. Ohno, S. Kishimoto, T. Mizutani, H. Yoshida, T. Okazaki, H. Shinohara, *Appl. Phys. Lett.* **84**, 2412 (2004).
8. S. Yuan, Q. Zhang, D. Shimamoto, H. Muramatsu, T. Hayashi, Y. A. Kim, M. Endo, *Appl. Phys. Lett.* **91**, 143118 (2007).
9. K. H. Liu, W. L. Wang, Z. Xu, X. D. Bai, E. G. Wang, Y. G.; Yao, J. Zhang, Z. F. Liu, *J. Am. Chem. Soc.* **131**, 62 (2009).
10. S. Yuan, Q. Zhang, Y. You, Z.-X. Shen, D. Shimamoto, M. Endo, *Nano Lett.* **9**, 383 (2009).
11. B. Ha, D. H. Shin, J. Park, C. J. Lee, *J. Phys. Chem. C* **112**, 430 (2009).
12. Y. A. Kim, M. Kojima, H. Muramatsu, S. Umemoto, T. Watanabe, K. Yoshida, K. Sato, T. Ikeda, T. Hayashi, M. Endo, M. Terrones, M. S. Dresselhaus, *Small* **2**, 667 (2006).
13. Y. A. Kim, H. Muramatsu, K. C. Park, D. Shimamoto, Y. C. Jung, J. H. Kim, T. Hayashi, Y. Saito, M. Endo, M. Terrones, M. S. Dresselhaus, *Appl. Phys. Lett.* **93**, 051901 (2008).
14. Y. C. Jung, D. Shimamoto, H. Muramatsu, Y. A. Kim, T. Hayashi, M. Terrones, M. Endo, *Adv. Mater.* **20**, 4509 (2008).
15. T. Hayashi, D. Shimamoto, Y. A. Kim, H. Muramatsu, F. Okino, H. Touhara, T. Shimada, Y. Miyauchi, S. Maruyama, M. Terrones, M. S. Dresselhaus, M. Endo, *ACS Nano* **2**, 485 (2008).

16. S. Bandow, M. Takizawa, K. Hirahara, M. Yudasaka, S. Iijima, *Chem. Phys. Lett.* **337**, 48 (2001).
17. R. Pfeiffer, F. Simon, H. Kuzmany, V. N. Popov, *Phys. Rev. B* **72**, 161404 (2005).
18. S. Bandow, T. Hiraoka, T. Yumura, K. Hirahara, H. Shinohara, S. Iijima, *Chem. Phys. Lett.* **384**, 320 (2004).
19. C. Kramberger, A. Waske, K. Biedermann, T. Pichler, T. Gemming, B. Buchner, H. Kataura, *Chem. Phys. Lett.* **407**, 254 (2005).
20. R. Pfeiffer, M. Holzweber, H. Peterlik, H. Kuzmany, Z. Liu, K. Suenaga, H. Kataura, *Nano Lett.* **7**, 2428 (2007).
21. V. Zolyomi, F. Simon, A. Rusznyak, R. Pfeiffer, H. Peterlik, H. Kuzmany, J. Kurt, *Phys. Rev. B* **75**, 195419 (2007).
22. H. Kuzmany, W. Plank, R. Pfeiffer, F. Simon, *J. Raman Spectroscopy* **39**, 134 (2008).
23. A. A. Green M. C. Hersam, *Nature Nanotech.* **4**, 64 (2009).
24. T. Okazaki, S. Bandow, G. Tamura, Y. Fujita, K. Iakoubovskii, S. Kazaoui, N. Minami, T. Saito, K. Suenaga, S. Iijima, *Phys. Rev. B* **74**, 153404 (2006).
25. N. Kishi, S. Kikuchi, P. Ramesh, T. Sugai, Y. Watanabe, H. Shinohara, *J. Phys. Chem. B* **110**, 24816 (2006).
26. T. Hertel, A. Hagen, V. Talalaev, K. Arnold, F. Hennrich, M. Kappes, S. Rosenthal, J. McBride, H. Ulbricht, E. Flahaut, *Nano Lett.* **5**, 511 (2005).
27. K. Iakoubovskii, N. Minami, S. Kazaoui, T. Ueno, Y. Miyata, K. Yanagi, H. Kataura, S. Ohshima, T. Saito, *J. Phys. Chem. B* **110**, 17420 (2006).
28. K. Iakoubovskii, N. Minami, T. Ueno, S. Kazaoui, H. Kataura, *J. Phys. Chem. C* **112**, 11194 (2008).
29. D. Shimamoto, H. Muramatsu, T. Hayashi, Y. A. Kim, M. Endo, J. S. Park, R. Saito, M. Terrones, M. S. Dresselhaus, *Appl. Phys. Lett.* **94**, 083016 (2009).
30. H. Muramatsu, T. Hayashi, Y. A. Kim, D. Shimamoto, M. Endo, V. Meunier, B. G. Sumpter, M. Terrones, M. S. Dresselhaus, *Small* **5**, 2678 (2009).
31. D. A. Heller, S. Baik, T. E. Eurell, M. S. Strano, *Adv. Mater.* **17**, 2793 (2005).
32. M. E. Itkis, F. Boronndics, A. Yu, R. C. Haddon, *Science* **312**, 413 (2006).
33. N. Nakashima, S. Okuzono, H. Murakami, T. Nakai, K. Yoshikawa, *Chem. Lett.* **32**, 456 (2003).
34. M. Zheng, A. Jagota, E. D. Semke, B. A. Diner, R. S. McLean, S. R. Lustig, R. E. Richardson, N. G. Tassi, *Nat. Mater.* **2**, 338 (2003).

35. M. Zheng, A. Jagota, M. S. Strano, A. P. Santos, P. Barone, S. G. Chou, B. A. Diner, M. S. Dresselhaus, R. S. Mclean, G. B. Onoa, G. G. Samsonidze, E. D. Semke, M. Usrey, D. J. Walls, *Science* **302**, 1545 (2003).
36. X. Tu, S. Manohar, A. Jagota, M. Zheng, *Nature* **460**, 250 (2009).
37. M. S. Strano, M. Zheng, A. Jagota, G. B. Onoa, D. A. Heller, P. W. Barone, M. L. Usrey, *Nano Lett.* **4**, 543 (2004).
38. M. Zheng, B. A. Diner, *J. Am. Chem. Soc.* **126**, 15490 (2004).
39. C. Fantini, A. Jorio, A. P. Santos, V. S. T. Peressinotto, M. A. Pimenta, *Chem. Phys. Lett.* **439**, 138 (2007).
40. X. Zhao, J. K. Johnson, *J. Am. Chem. Soc.* **129**, 10438 (2007).
41. S. Meng, P. Maragakis, C. Papaloukas, E. Kaxiras, *Nano Lett.* **7**, 45 (2007).
42. Y. Chen, H. Liu, T. Ye, J. Kim, C. Mao, *J. Am. Chem. Soc.* **129**, 8696 (2007).
43. C. Fantini, A. Jorio, A. P. Santos, V. S. T. Peressinotto, M. A. Pimenta, *Chem. Phys. Let.* **439**, 138 (2007).
44. C. Fantini, J. Cassimiro, V. S. T. Peressinotto, F. Plentz, A. G. Souza Filho, C. A. Furtado, A. P. Santos, *Chem. Phys. Lett.* **473**, 96 (2009).
45. M. Endo, H. Muramatsu, T. Hayashi, Y. A. Kim, M. Terrones, M. S. Dresselhaus, *Nature* **433**, 476 (2005).
46. J. H. Kim, M. Kataoka, Y. A. Kim, D. Shimamoto, H. Muramatsu, T. Hayashi, M. Endo, M. Terrones, M. S. Dresselhaus, *Appl. Phys. Lett.* **93**, 223107 (2008).
47. A. M. Rao, E. Richter, S. Bandow, B. Chase, P. C. Eklund, K. W. Williams, M. Menon, K. R. Subbaswamy, A. Thess, R. E. Smalley, G. Dresselhaus, M. S. Dresselhaus, *Science* **275**, 187 (1997).
48. M. J. O'Connell, S. M. Bachilo, C. B. Huffman, V. C. Moore, M. S. Strano, E. H. Haroz, K. L. Rialon, P. J. Boul, W. H. Noon, C. Kittrell, J. Ma, R. H. Hauge, R. B. Weisman, R. E. Smalley, *Science* **297**, 593 (2002).
49. D. A. Heller, P. W. Barone, J. P. Swanson, R. M. Mayrhofer, M. S. Strano, *J. Phys. Chem. B* **108**, 6905 (2004).
50. P. T. Araujo, C. Fantini, M. M. Lucchese, M. S. Dresselhaus, A. Jorio, *Appl. Phys. Lett.* **95**, 261902 (2009).
51. A. Jorio, A. P. Santos, H. B. Ribeiro, C. Fantini, M. Souza, J. P. M. Vieira, C. A. Furtado, J. Jiang, R. Saito, L. Balzano, D. E. Resasco, M. A. Pimenta, *Phys. Rev. B* **72**, 075207 (2005).
52. J. Jiang, R. Saito, G. G. Samsonidze, A. Jorio, S. G. Chou, G. Dresselhaus, M. S. Dresselhaus, *Phys. Rev. B* **75**, 035407 (2007).

53. S. M. Bachilo, M. S. Strano, C. Kittrell, R. H. Hauge, R. E. Smalley, R. B. Weisman, *Science* **298**, 2361 (2002).
54. J. Lefebvre. J. M. Fraser, Y. Homma, P. Finnie, *Appl. Phys. A: Mater. Sci. Process.* **78**, 1107 (2004).
55. P. Finnie, Y. Homma, J. Lefebvre, *Phys. Rev. Lett.* **94**, 247401 (2005).
56. Y. Ohno, S. Iwasaki, Y. Murakami, S. Kishimoto, S. Maruyama, T. Mizutani, *Phys. Rev. B* **73**, 235427 (2006).
57. K. Arnold, S. Lebedkin, O. Kowski, F. Hennrich, M. M. Kappes, *Nano Lett.* **4**, 2349 (2004).
58. Y. Miyauchi, R. Saito, K. Sato, Y. Ohno, S. Iwasaki, T. Mizutani, J. Jiang, S. Maruyama, *Chem. Phys. Lett.* **442**, 394 (2007).
59. M. Kalbac, H. Farhat, L. Kavan, J. Kong, K. Sasaki, R. Saito, M. S. Dresselhaus, *ACS Nano* **3**, 2320 (2009).
60. M. Endo, Y. A. Kim, T. Hayashi, H. Muramatsu, M. Terrones, R. Saito, F. Villalpando-Paez, S. G. Chou, M. S. Dresselhaus, *Small* **2**, 1031 (2006).
61. F. Villalpando-Paez, H. Son, D. Nezich, Y. P. Hsieh, J. Kong, Y. A. Kim, D. Shimamoto, H. Muramatsu, T. Hayashi, M. Endo, M. Terrones, M. S. Dresselhaus, *Nano Lett.* **8**, 3879 (2008).
62. M. Shoda, S. Bandow, Y. Maruyama, S. Iijima, *J. Phys. Chem. C* **113**, 6033 (2009).
63. M. Cha, S. Jung, M.-H. Cha, G. Kim, J. Ihm, J. Lee, *Nano Lett.* **9**, 1345 (2009).
64. D. Eisenberg, W. Kauzmann, *The Structure and Properties of Water*, Oxford, Oxford University Press, 2005.
65. A. M. Rao, P. C. Eklund, S. Bandow, A. Thess, R. E. Smalley, *Nature* **388**, 257 (1997).
66. M. Kalbac, L. Kavan, M. Zukalova, L. Dunsch, *Carbon* **42**, 2915 (2004).
67. P. Pfeiffer, H. Kuzmany, F. Simon, S. N. Bokova, E. Obraztsova, *Phys. Rev. B* **71**, 155409) 2005).
68. I. O. Maciel N. Anderson, M. A. Pimenta, A. Hartschuh, H. H. Qian, M. Terrones, H. Terrones, J. Campos-Delgado, A. M. Rao, L. Novotny, A. Jorio, *Nat. Mater.* **7**, 878 (2008).

CHAPTER 6

Optically and Biologically Active Mussel Protein-Coated Double Walled Carbon Nanotube

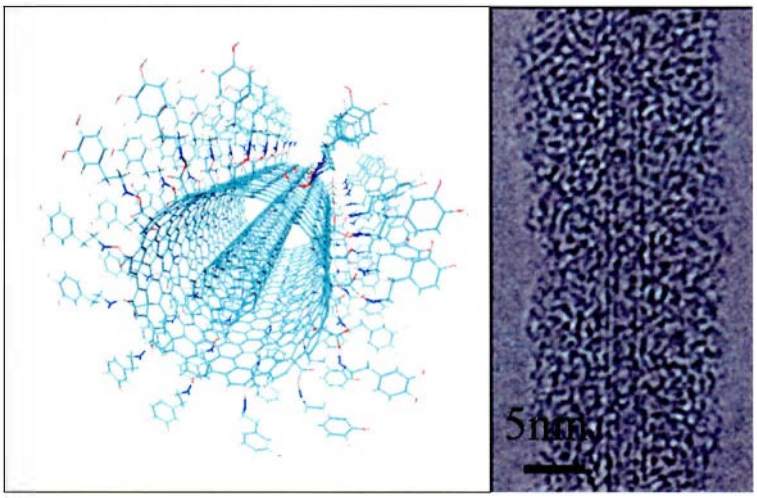

Chapter 6 Optically and Biologically Active Mussel Protein-Coated Double Walled Carbon Nanotube

6.1 Introduction

CNTs have been suggested as a promising tool for bioapplications because of their one-dimensional characteristics.[1-6] However, CNTs are intrinsically hydrophobic and exhibit a low degree of biocompatibility. Thus, in order to fully exploit their excellent physical and chemical properties at a molecular level, various types of proteins have been examined for use as the individualization (or dispersion) agent for fabricating protein-nanotube conjugation. [6-10]

Among the various types of proteins, the mussel protein is selected as a biofunctionalization and individualization agent for CNTs in our study for the following reasons: (1) The mussel protein has a high ability to adhere to organic and inorganic materials in a wet condition,[11] The 3, 4-dihydroxy-L-phenylalanine (DOPA) is exceptionally rich in mussel foot proteins (i.e., mytilus galloprovincialis foot protein (Mgfp)-3 and Mgfp-5) and plays a key role in the adhesion of this protein to surfaces. [12-14] Thus, the mussel protein chemistry appears to be an efficient approach for modifying substrates by forming DOPA layers. The capability of adhering to both organic and inorganic surfaces[15-17] allows mussel protein to be utilized in moisture-resistant adhesives and coatings.[18-21] (2) It is insoluble in water (or waterproof) after solidification. (3) It exhibits a high degree of biocompatibility with no immunogenecity (or inflammation). (4) Water could be used as the solvent. (5) Specific bioactive peptides which genetically have the ability of mimicking the extracellular matrix protein for cell growth could be incorporated into the mussel protein. (6) Finally, the mussel protein remains structurally and thermally stable after undergoing ultrasonication process that is essential to individualize (or biofunctionalize) nanotubes in an aqueous solutions.

Very recently, using mussel-inspired surface chemistry, CNTs were reported to form a high-strength fiber[22] as well as serve as an efficient scaffold for bone tissue engineering,[23] and graphene oxide was successfully reduced and functionalized simultaneously.[24] In addition, CNTs functionalized with mussel protein exhibited a low cytotoxic effect on bone osteoblast cells.[23] Thus, in order to fully exploit the quantum confinement effects in CNTs (e.g., strong optical activity)[4, 5] as well as the versatile chemistry of mussel protein in biological applications, it is essential to evaluate the dispersing ability of mussel protein with regard to strongly bundled CNTs in an aqueous system, as well as to understand the interaction between the mussel protein and the

nanotubes.

In order to achieve such targets, DWNTs, rather than MWNTs or SWNTs, were selected in this study to better utilize the outer tube chemistry as well as the optical signals coming from the inner tubes.[25-28] There are no quantum confinement effects in large-diameter MWNTs, and SWNTs experienced an optical suppression when chemical moieties were covalently anchored at high concentration.[29-31] Moreover, carboxyl groups via a hydroxyl peroxide treatment were heavily attached to the outer tubes in DWNTs because they possess a high ability to react with the amines in mussel protein. The carboxyl group-decorated SWNTs eliminate the possibility that photoluminescent signals could arise from impurity SWNTs.[31, 32] In this chapter, a homogeneously dispersed stable DWNT suspension, prepared by sonicating a DWNT sample in a mussel protein solution, was characterized using TEM, FT-IR, XPS, Raman, UV-absorption spectra and photoluminescence. The individualization of the tubes in an aqueous medium was identified by the sharp absorption peaks and bright PL signals that were observed. Noticeably, TEM images showed that individual tubes were homogenously coated by mussel protein (ca. 5 nm).

6.2 Experimental Section

6.2.1 The Decoration of Hydroxyl Groups on the Double Walled Carbon Nanotubes

The high-purity DWNT sample (5 mg) was treated in H_2O_2 (20 ml, 30 wt%) under a bath-type sonication for 1 hr and this was followed by a horn-type sonication for 2 hrs. Then, the filtered sample was washed with distilled water several times and dried in a vacuum drier.

6.2.2 The Preparation of the Mussel Protein-Dispersed Double Walled Carbon Nanotube Suspension

High-purity mussel protein (80 %, MAPTrix®) was kindly provided by the Kollodis Biosciences Incorporation. The OH decorated DWNT sample (1 mg) was dispersed in heavy water (D_2O) with the help of mussel protein (10 mg) and SDBS (0.5 wt%) under strong sonication (UP50H, ca. 600 W/cm^2) for 1 hr at 4 °C and the subsequent ultracentrifugation (Optima Max-XP, Beckman Coulter, 240,000 g). Subsequently, their supernatant (70 %), rich with isolated nanotubes, was used in our optical studies.

6.2.3 Characterizations

I have used HRTEM (JEM-2010FEF, JEOL) to see the dispersion state of tubes as well as of the coated mussel protein on the sidewalls of the DWNTs. The functional groups of the OH-decorated and mussel protein coated DWNT samples were characterized by FT-IR spectroscopy (IR Prestige-21, Shimadzu) and XPS (ESCA-3400, Kratos Analytical) using a MgK_{α} X-ray source with a 10 mA emission current and a 10 kV accelerating voltage. UV absorption spectra, PL maps and fluorescent spectra for DWNT suspensions were obtained using a UV-Vis-NIR spectrophotometer (Shimadzu soildspec-3700), a Shimadzu NIR-PL system and a 785 nm-excited Raman system (Renishaw). We have measured the electrical conductivity of mussel protein-dispersed DWNT film using a four probe method.

6.3 Results and Discussion

My approach to prepare optically and biologically active nanotubes consists of dispersing catalytically grown high-purity and small-diameter DWNTs individually in an aqueous solution through the formation of covalent bonds between the carboxyl groups on the sidewall of the outer tube and the amine groups of DOPA (Fig. 1 (a)). Thus, highly pure (ca. 95 %), highly crystalline (shown by the absence of a D-band intensity in the Raman spectra) and strongly bundled DWNTs (Fig. 1 (c)) were prepared by a catalytic CVD process, followed by an oxidative purification process.[34, 35] It is noteworthy that DWNTs with an inner diameter of ca. 0.7 nm and an outer diameter of ca. 1.6 nm were closely packed in hexagonal arrays within the bundles (inset in Fig. 1 (c)). Moreover, DWNTs are intrinsically insoluble in water because of the hydrophobic nature of their sidewalls. However, the individualized DWNTs containing chemical moieties are critically needed in order to exploit their intrinsic quantum confinement effect. As a first step to extend the development of the outer tube chemistry of DWNTs, our DWNT sample used in this work was first treated in hydroxyl peroxide in order to create carboxyl groups on the sidewalls of the outer tubes covalently.[36, 37]

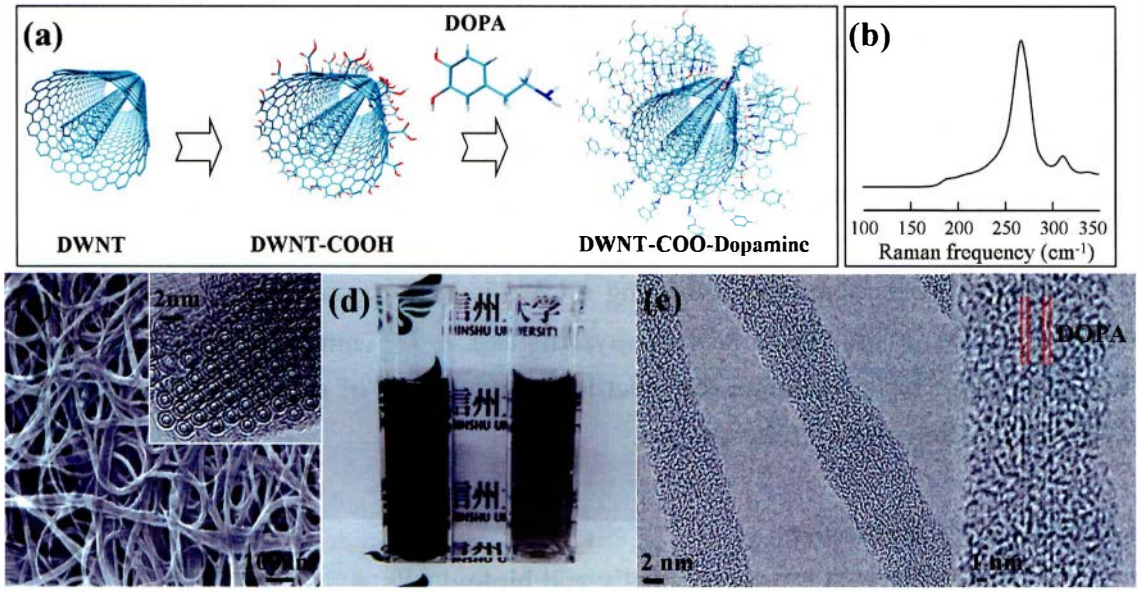

Figure 1 (a) A schematic illustration of the formation of covalent bonds between the carboxyl groups on the outer tube of the DWNT and the amine groups on dopamine. (b) Low frequency Raman spectra of the pristine and OH-decorated DWNT samples using a 532-nm laser line. (c) SEM image of the strongly bundled DWNT sample (inset is a cross sectional TEM image of hexagonally packed DWNTs). (d) (Left) the sonicated opaque DWNT suspension and (right) the following ultracentrifugated semitransparent DWNT suspension. (e) TEM image indicating that mussel protein coats the sidewall of DWNTs homogeneously and completely (inset is a TEM image showing that two coaxial tubes can be clearly seen).

The effective introduction of functional groups on the outer tubes within DWNTs was verified by the strongly depressed radial breathing mode coming from the outer tubes (Fig. 1 (b)). An additional merit of the hydroxyl peroxide treatment is that this treatment eliminates the possibility that optical signals will come from SWNT impurities because the covalently introduced chemical moieties on the sidewall of the SWNTs severely suppress their optical emissions.[29-31] Therefore, by dispersing the OH-attached DWNT sample (1 mg) using mussel protein (10 mg) in distilled water under strong sonication, we have prepared an opaque (black) DWNT suspension (left in Fig. 1 (d)). A subsequent ultracentrifugation allows us to prepare a relatively semitransparent DWNT suspension (right in Fig. 1 (d)), in which the nanotubes are individually dispersed, and bundled tubes are precipitated. The shortening of nanotubes in the sonication-assisted preparation of the nanotube suspension is an avoidable phenomenon. Thus, the length distribution of DWNTs is measured using atomic force microscopy (Fig. 2). The length distribution of DWNTs ranges from 200 nm to 1.8 μm and their average value is ca. 500 nm. Due to their coaxial structure, DWNTs are

expected to be more robust than SWNTs to the hydrodynamic shear forces generated by the ultrasonication process. According to TEM observations (Fig. 1 (e)), we note that two linear and long coaxial tubes were individualized because amorphous-like mussel proteins are coated homogeneously and completely around the sidewalls of each DWNT.

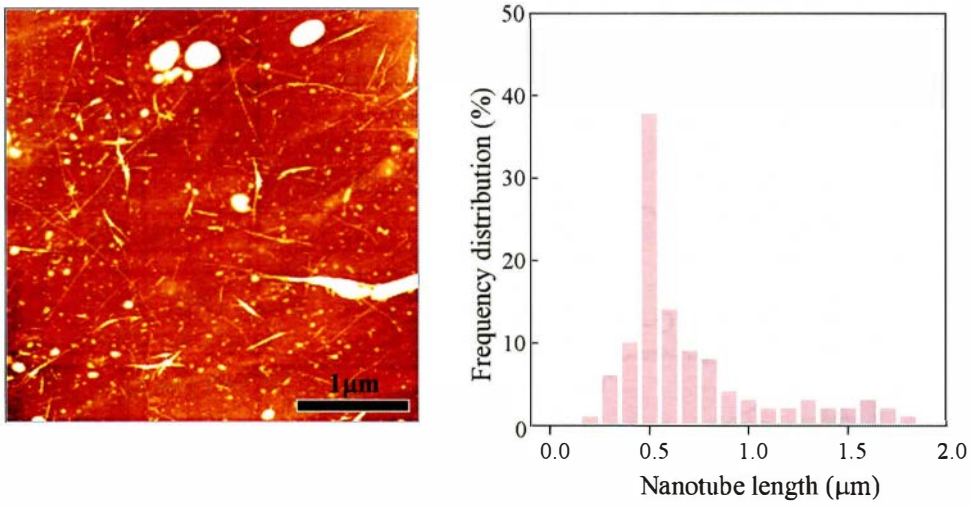

Figure 2 (a) A typical 4 × 4 mm AFM image of mussel protein-dispersed DWNTs and (b) the length distribution of DWNTs.

In order to identify the formation of covalent bonds between mussel protein and the outer tubes of the DWNTs, we recorded FT-IR spectra of the mussel protein, pristine DWNTs, OH-decorated DWNTs, and the mussel protein-coated DWNTs (Fig. 3). Generally, the OH moiety is identified as a broad IR absorption peak in the range of 3400-3600 cm^{-1}.[38, 39] However, the NH_2 signal coming from the stretch mode of the N-H moiety coexists with the OH signal, and the broad and weak IR peak in the range of 3000-3400 cm^{-1} is assigned to OH.[38, 39] Therefore, we were able to identify the presence of NH2 and OH groups in the range of 3000-3600 cm^{-1} for the mussel protein. In addition, a strong IR peak appears at 1644 cm^{-1}, corresponding to the strong bending vibration of the amide I group, whereas the peak located at 1515 cm^{-1} arises from the bending vibration of the amide II group and the stretching vibration of the C-N bond. In addition, an intense but broad peak located at *ca.* 3400 cm^{-1} coming from the hydrogen-bonded OH groups strongly indicates that OH groups are heavily introduced on the sidewalls of the outer tubes (Fig. 3 (b, c)). From the IR spectrum of the mussel protein-coated DWNT sample (Fig. 3 (d)), we found that the two IR peaks coming from the amide I and II bands appeared at a higher wavenumber than those for the pristine

mussel protein and furthermore the intensity of the IR peak coming from the amide II band is largely depressed. Noticeably, no distinctive IR peak is observed above 3000 cm^{-1}. Thus, the observed changes in the IR spectrum could be explained by the spontaneous chemical reaction established between the OH groups on the sidewalls of the tubes and the NH groups of mussel protein.

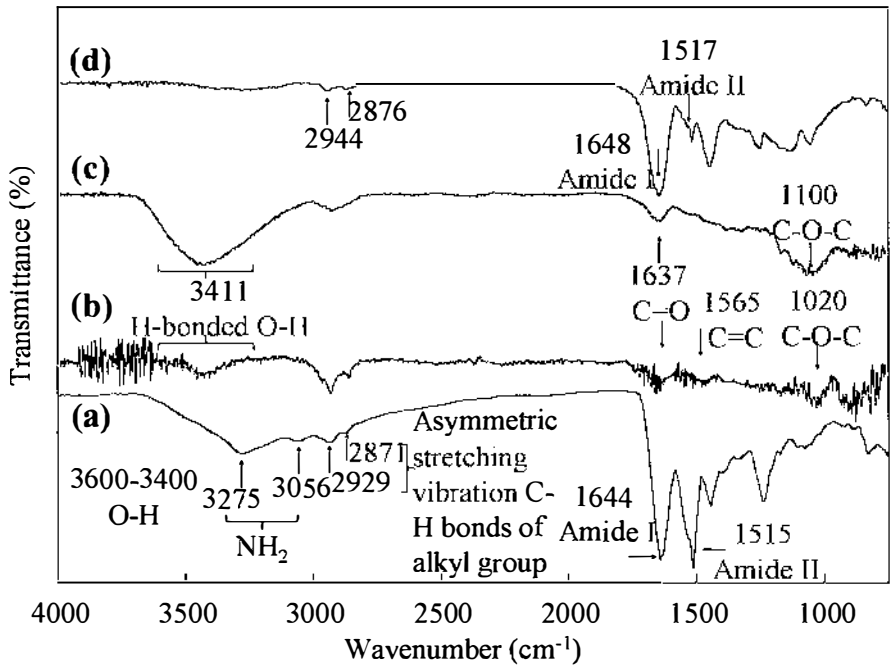

Figure 3 FT-IR spectra of (a) mussel protein, (b) pristine DWNTs, (c) OH-decorated DWNT and (d) mussel protein-coated DWNTs showing amide I and amide II signature.

We also carried out XPS measurements on pristine, OH-decorated and mussel protein-coated DWNT samples in order to track down the relative quantity of functional groups that become attached to the outer walls of the DWNTs (Fig. 4). For the pristine DWNT sample, there is an intense peak at ca. 284.3 eV coming from the sp^2-hybridized carbon atoms and also a broad peak at 285.2 eV coming from the sp^3-hybridized carbon atoms (Fig. 4 (a)).[40, 41] The appearance of oxygen signals from pristine DWNTs (Fig. 4 (b)) could be explained by the oxygen functional groups that are introduced after the oxidative purification process used to remove metallic impurities.[34, 35] The effectiveness of the hydroxyl peroxide treatment is confirmed by the intensified peaks of –COOH, –COO and –C-O- at 290.5, 288.6 and 286.7 eV, respectively, thus indicating that OH groups are anchored to the sidewall of the tubes. The split O 1s peak in the XPS spectrum (Fig. 4 (b)), the largely increased amount of oxygen atoms, the decreased sp^2/sp^3 ratio and the increased O/C ratio (Table 1) confirm the effectiveness of this

reported chemical treatment by introducing OH groups on the sidewalls of the DWNTs. From the mussel protein-coated DWNT sample, the nitrogen signal in the N 1s XPS spectrum (Fig. 4 (c)) originates from the mussel protein because there is no nitrogen atom on either pristine or OH-decorated DWNT samples. When analyzing the C 1s XPS spectrum, we could also observe significantly decreased intensities coming from –COOH and –C-O- groups at 290.5 and 286.7 eV, respectively (Fig. 4 (a)). These results indicate that the OH groups located on the sidewall of DWNTs via a hydroxyl peroxide treatment covalently react with the NH groups of dopamine, thus resulting in a thin-layer coating of mussel protein along the sidewall, as well as in the homogeneous dispersion of tubes in an aqueous solution.

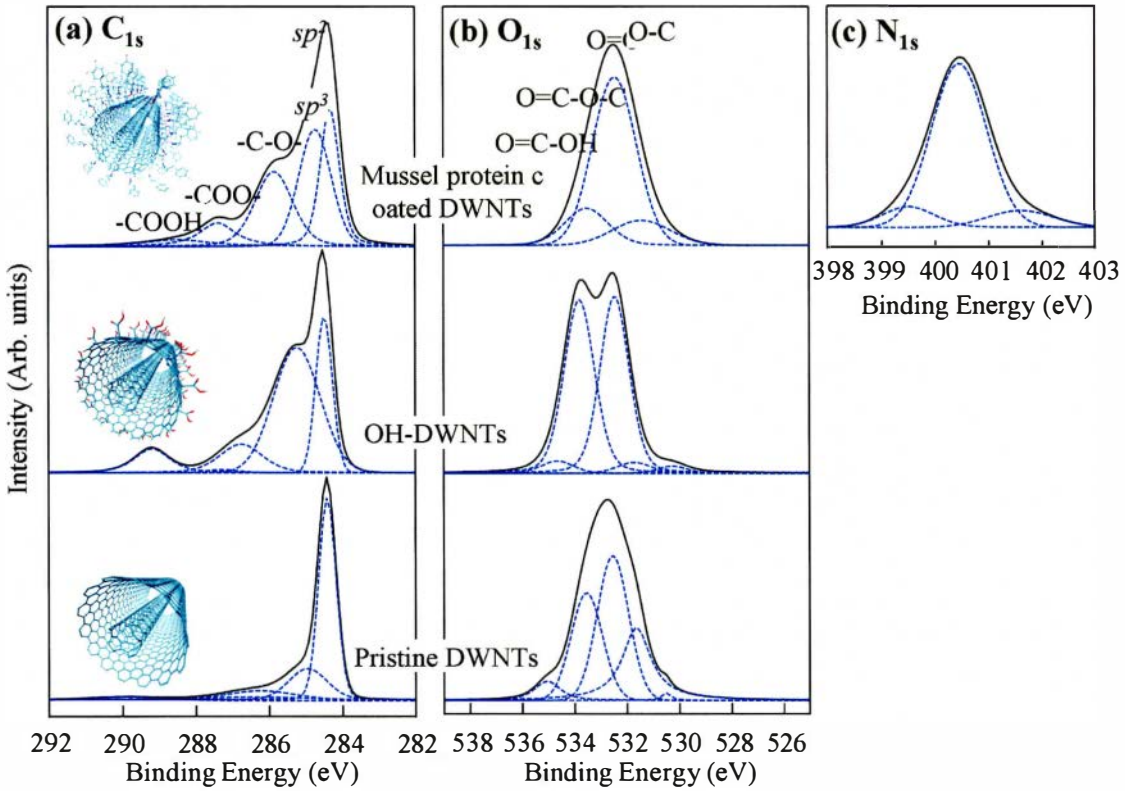

Figure 4 The C 1s (a), O 1s (b) and N 1s (c) XPS spectra of pristine DWNTs, OH-decorated DWNTs and mussel protein-coated DWNTs, occurring in a different range of binding energies.

Table 1 Relative concentration of compositional atoms and oxygen-containing functional groups for pristine, OH-decorated and mussel protein-coated DWNT samples, respectively.

Sample ID	Atomic composition (%)			-C-O- (%)	-COO- (%)	-COOH- (%)	sp^2/sp^3 [a]	O/C atomic ratio
	C	O	N					
Pristine DWNTs	96.48	3.51	-	10.17	4.62	3.78	3.104	0.04
OH-DWNTs	75.76	24.24	-	12.36	0.94	9.54	0.442	0.32
Mussel protein-coated DWNTs	60.18	33.93	5.89	27.04	9.96	3.07	0.784	0.56

[a] sp^2/sp^3 is the integrated intensity of the sp^2-carbon assigned peak at 284.3 eV divided by the integrated intensity of the sp^3-carbon assigned peak at 285.2 eV.

Finally, in order to understand the effect of the thin-layer coated mussel protein on the optical properties of DWNT suspension, we have carried out UV absorption and PL studies on mussel protein-coated DWNT suspensions. It is noteworthy that well-resolved and sharp optical absorption peaks coming from the inner tubes indicate the presence of DWNTs that have been successfully individualized with the aid of the mussel protein (Fig. 5 (a)). The absorption peaks in the region between 900 and 1300 nm (Fig. 5 (a)) result from the overlap of the S_{22} transition for the outer tube and the S_{11} transition for the inner tube. However, the covalent introduction of OH groups on the sidewall of the outer tubes leads to the complete depression of the absorption peaks from the outer tubes.[29-31] Thus, we can be certain that the absorption peaks are arising from the inner tubes within the DWNTs. Moreover, we have measured a two-dimensional PL map from such a suspension (Fig. 5 (b)). The observation of several strong peaks in the PL map indicates that tubes are isolated in an aqueous suspension. We believe that such peaks are coming from the inner tubes of DWNTs, and not from impurity SWNTs, because the covalently introduced OH groups on the SWNTs act as an energy drain. Each peak in the PL map corresponds to an excitation involving the second excitonic transition E_{22} of the semiconducting inner tubes of the DWNTs, and the emission coming from the corresponding first excitonic transition E_{11} of the semiconducting inner tubes of DWNTs. Noticeably, the distinctive redshift in the excitation and emission of mussel protein-coated DWNT suspension as compared with those of SDBS-dispersed DWNT suspension (see white circles in Fig. 5 (b)), should be explained by environmental dielectric screening effects.[42, 43] Furthermore, in order to

examine such a redshift in the PL map, we have compared the luminescence spectra taken with the laser excitation of 785 nm for SDBS- and for mussel protein-dispersed DWNT suspensions (Fig. 5 (c)). Strong luminescent peaks in the SDBS-dispersed DWNT suspension are assigned to the (6, 4), (9, 1), (8, 3), (6, 5) and (7, 5) inner tubes within the DWNTs. We again confirmed that the luminescent spectra of the mussel protein-dispersed DWNT suspension is redshifted by up to 200 cm^{-1} when compared to that of the SDBS-dispersed DWNT suspensions.

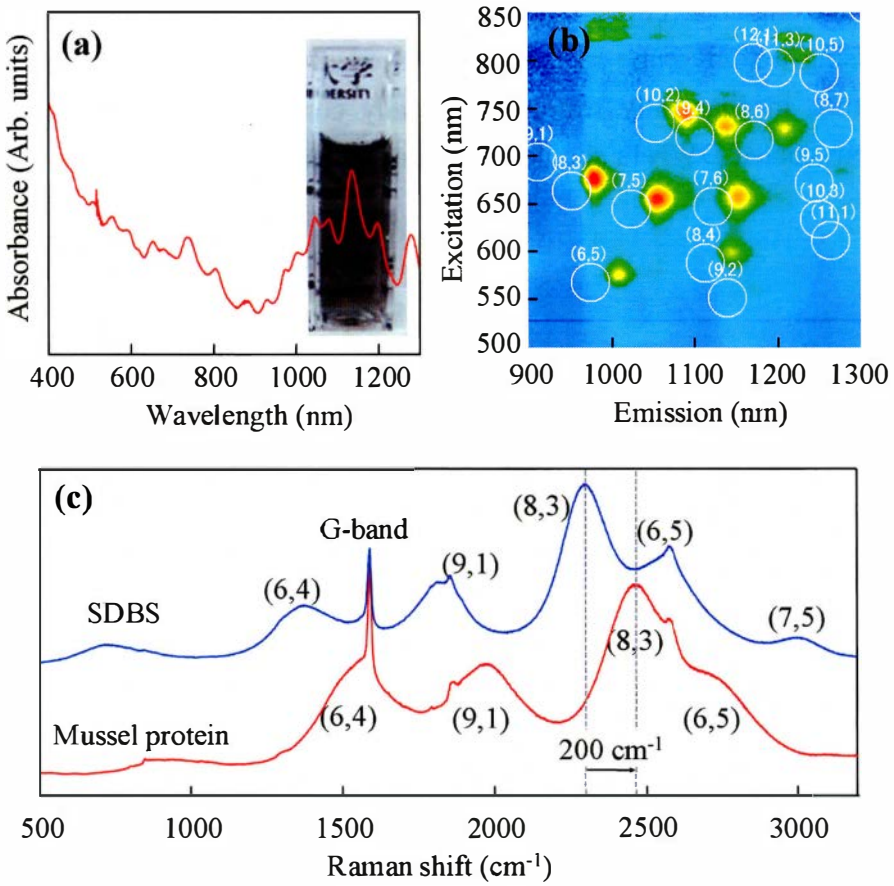

Figure 5 (a) UV-visible absorption spectra and (b) two dimensional photoluminescence maps of mussel protein-coated pristine DWNT and hydroxyl group-decorated DWNT suspensions. (c) Fluorescence spectra taken with laser excitation of 785 nm for SDBS-dispersed and mussel protein-dispersed DWNT suspensions.

6.4 Conclusion

I have shown a method for dispersing the strongly bundled DWNTs through the covalent interaction of the mussel protein with the sidewalls of the tubes. In order to generate a covalent bridge between the DWNTs and the mussel protein, OH groups were introduced onto the sidewall of the outer tubes of the DWNTs via a hydroxyl

peroxide treatment, and then they were reacted with the NH groups of dopamine. Detailed optical studies revealed that the mussel protein coated DWNT suspension exhibited sharp absorption peaks as well as strong luminescent emissions from the inner tubes of the DWNTs, thus indicating that nanotubes were individually present by the formation of a homogeneous thin-layer coating of the mussel protein on the sidewalls of the DWNTs. The DWNT suspension prepared in this study is stable up to five months and this suspension could be easily converted into thin films using a simple casting method or alternatively the suspensions could be converted into a three-dimensional nanofiber web using an electrospinning system. The measured electrical conductivity of thin films using a four probe method corresponded to 5.31×10^3 S/cm. Therefore, optically active, mechanically strong, electrically conductive and biologically active mussel protein-coated DWNTs should find many potential uses in the bio and medical areas.

6.5 References

1. K. Besteman, J. O. Lee, F. G. M. Wiertz, H. A. Heering, C. Dekker, *Nano Lett.* **3**, 727 (2003).
2. N. W. Shi Kam, T. C. Jessop, P. A. Wender, H. Dai, *J. Am. Chem. Soc.* **126**, 6850 (2004).
3. P. Asuri, S. S. Karajanagi, E. Sellitto, D. Y. Kim, R. S. Kane, J. S. Dordick, *Biotechnol. Bioeng.* **95**, 804 (2006).
4. M. S. Dresselhaus, G. Dresselhaus, P. C. Eklund, *Science of Fullerenes and Carbon Nanotubes*, Academic Press, New York, 1996.
5. R. Saito, G. Dresselhaus, M. S. Dresselhaus, *Physical Properties of Carbon Nanotubes*, Imperial College Press, London, 1988.
6. M. Shim, N. W. S. Kam, R. J. Chen, Y. Li, H. Dai, *Nano Lett.* **2**, 285 (2002).
7. S. S. Karajangi, H. Yang, P. Asuri, E. Sellitto, J. S. Dordick, R. S. Kane, *Langmuir* **22**, 1392 (2006).
8. D. Nepal, K. E. Geckeler, *Small* **7**, 1259 (2007).
9. D. Nepal, K. E. Geckeler, *Small* **3**, 406 (2006).
10. Y. Lee, K. E. Geckeler, *Adv. Mater.* **22**, 4076 (2010).
11. J. H. Waite, *Chemtech* **17**, 692 (1987).
12. J. H. Waite, M. L. Tanzer, *Science* **212**, 1038 (1981).
13. H. Zhao, N. B. Robertson, S. A. Jewhurst, J. H. Waite, *J. Biol. Chem.* **281**, 11090 (2006).
14. H. Zhao, J. H. Waite, *J. Biol. Chem.* **281**, 26150 (2006).
15. H. Lee, N. F. Scherer, P. B. Messersmith, *Proc. Natl. Acad. Sci. USA* **102**, 12999 (2006).
16. H. Lee, B. P. Lee, P. B. Messersmith, *Nature* **448**, 338 (2007).
17. H. Lee, S. M. Dellatore, W. M. Miller, P. B. Messersmith, *Science* **318**, 426 (2008).
18. J. L. Dalsin, L. Lin, S. Tosatti, J. Voros, M. Textor, P. B. Messersmith, *Langmuir* **21**, 640 (2005).
19. B. P. Lee, C. Y. Chao, F. N. Nunalee, E. Motan, K. R. Shull, P. B. Messersmith, *Macromolecules* **39**, 1740 (2006).
20. G. Westhood, T. N. Horton, J. J. Wilker, *Macromolecules* **40**, 3960 (2007).
21. J. Wang, M. N. Tahir, M. Kappl, W. Tremel, N. Metz, M. Barz, P. Theato, H. J. Butt, *Adv. Mater.* **20**, 3872 (2008).
22. S. Ryu, Y. Lee, J-W. Hwang, S. Hong, C. Kim, T. G. Park, H. Lee, S. H. Hong, *Adv Mater.* **23**, 1971 (2011).

23. M. Lee, S. H. Ku, J. Ryu, C. B. Park, *J. Mater. Chem.* **20**, 8848 (2010).
24. S. M. Kang, S. Park, D. Kim, S. Y. Park, R. S. Ruoff, H. Lee, *Adv. Funct. Mater.* **21**, 108 (2011).
25. T. Hayashi, D. Shimamoto, Y. A. Kim, H. Muramatsu, F. Okino, H. Touhara, T. Shimada, Y. Miyauchi, S. Maruyama, M. Terrones, M. S. Dresselhaus, M. Endo, *ACS Nano* **2**, 485 (2008).
26. D. Shimamoto, H. Muramatsu, T. Hayashi, Y. A. Kim, M. Endo, J. S. Park, R. Saito, M. Terrones, M. S. Dresselhaus, *Appl. Phys. Lett.* **94**, 083016 (2009).
27. H. Muramatsu, T. Hayashi, Y. A. Kim, D. Shimamoto, M. Endo, V. Meunier, B. G. Sumpter, M. Terrones, M. S. Dresselhaus, *Small* 5, 2678 (2009).
28. J. H. Kim, M. Kataoka, D. Shimamoto, H. Muramatsu, Y. C. Jung, T. Hayashi, Y. A. Kim, M. Endo, J. S. Park, R. Saito, M. Terrones, M. S. Dresselhaus, *ACS Nano* **4**, 1060 (2010).
29. H. Park, J. Zhao, J. P. Lu, *Nano Lett.* **6**, 916 (2006).
30. M. S. Strano, C. A. Dyke, M. L. Usrey, P. W. Barone, M. J. Allen, H. Shan, C. Kittrell, R. H. Hauge, J. M. Tour, R. E. Smalley, *Science* **201**, 1519 (2003).
31. S. H. Lee, Y. C. Jung, Y. A. Kim, H. Muramatsu, K. Teshima, S. Oishi, M. Endo, *Nanotechnology* **20**, 105708 (2009).
32. A. A. Green, M. C. Hersam, *Nature Nanotech.* **4**, 64 (2009).
33. D. A. Tsyboulski, Y. Hou, N. Fakhri, S. Ghosh, R. Zhang, S. M. Bachilo, M. Pasquali, L. Chen, J. Liu, R. B. Weisman, *Nano Lett.* **9**, 3282 (2009).
34. M. Endo, H. Muramatsu, T. Hayashi, Y. A. Kim, M. Terrones, M. S. Dresselhaus, *Nature* **433**, 476 (2005).
35. Y. A. Kim, H. Muramatsu, T. Hayashi, M. Endo, M. Terrones, M. S. Dresselhaus, *Chem. Vap. Deposition* **12**, 327 (2006).
36. Y. Peng, H. Liu, *In. Eng. Chem. Res.* **45**, 6483 (2006).
37. J. T. Han, S. Y. Kim, J. S. Woo, H. J. Jeong, W. Oh, G-W. Lee, *J. Phys. Chem. C* **112**, 15961 (2008).
38. G. Wang, H. Huang, G. Zhang, X. Zhang, B. Fang, L. Wang, *Langmuir* **27**, 1224 (2011).
39. B. Fei, B. Qian, Z. Yang, R. Wang, W.C. Liu, C.L. Mak, J. H. Xin, *Carbon* **46**, 1792 (2008).
40. H. Ago, T. Kugler, F. Cacialli, W. R. Salaneck, M. S. P. Shaffer, A. H. Windle, R. H. Friend, *J. Phys. Chem. B* **103**, 8116 (1999).
41. H. Murphy, P. Papakonstantinou, T. I. T. Okpalugo, *J. Vac. Sci. Technol. B* **24**, 715 (2006).

42. J. Lefebvre, J. M. Fraser, Y. Homma, P. Finnie, *Appl. Phys. A: Mater. Sci. Process.* **78**, 1107 (2004).
43. Y. Ohno, S. Iwasaki, Y. Murakami, S. Kishimoto, S. Maruyama, T. Mizutani, *Phys. Rev. B* **73**, 235427 (2006).

CHAPTER 7

Tough, Conductive PEO Nanofiber Web by Incorporating DNA or DNA-Wrapped Carbon Nanotubes

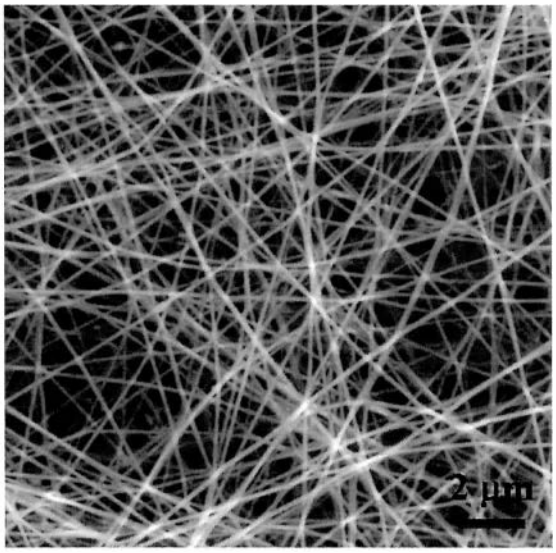

Chapter 7 Tough, Conductive PEO Nanofiber Web by Incorporating DNA or DNA- Wrapped Carbon Nanotubes

7.1 Introduction

The biomolecule-based nanofiber web using electrospinning system is promising in medical applications including scaffold, drug and gene delivery and artificial organ.[1-10] Electrospinning system to fabricate nanofiber web from polymer or protein is very simple and fast.[11] What is more, electrospun fibers exhibited noticeable properties, such as nano-sized diameter, high surface area, the tunable pore sizes, the versatile surface functionality and thin web morphology that useful in the field of biomedicine (e.g., tissue engineering, wound healing and drug delivery system).

In this chapter, I have selected water-soluble polyethylene oxide (PEO) since PEO exhibits high biocompatibility, non-fouling activity that enable to them be used in manufacturing cosmetics and medical tools. However, PEO nanofiber web have showed mechanically weak, and electrically insulating properties which coming from intrinsic nature of polymers properties that limited in versatile nanofiber applications.[12] To solve this problem, we have incorporated DNA or DNA wrapped CNTs. CNTs are small enough in diameter, optically conductive and mechanically strong.[13] However, CNTs are usually present in a strongly bundled structure, thus they have to be dispersed homogeneously. Up to now, the various dispersing agents have been studied in order to disperse individually and modify the sidewall of nanotubes.[14-17] Among them, DNA was identified as a powerful agent for the strongly bundled CNTs because of its ability to wrap around the sidewall of nanotubes.[18-25] DNA is abundant natural resource and easy to handle than protein due to they are stable in heat. They are important material that supplies the information necessary for cells to reproduce. In spite of their high usefulness as a natural biomass, they have been wasted in many industries because of their poor renewability. Here, by utilizing DNA or DNA-wrapped CNTs as reinforcing filler, I demonstrated to fabricate dimensionally thin, mechanically tough, electrically conductive PEO nanofiber web. Then, I characterized their properties using various analytical techniques and will find their application in biomedical fields.

7.2 Experimental Section

7.2.1 Dispersion of Double Walled Carbon Nanotubes

The highly pure and crystalline DWNTs were prepared by a CVD method and followed by an oxidative purification process (see section 2.1). Salmon DNA (300 base, Maruha Nichiro, Japan) is used as staring material. Then, I prepared homogeneously

dispersed (or isolated) DWNT suspensions as follows: 2 mg of high purity DWNT sample were dispersed in double stranded DNA solution (dsDNA, 10 ml) under a strong sonication for 1 hr at 4˚C. Subsequently, we subjected these suspensions (containing CNTs) to an ultracentrifuge (150,000g), and finally we could obtain well dispersed individual DWNTs. The dispersion state of tubes in DNA solution was confirmed using UV-Vis absorption spectra (SolidSpec-3700, Shimazu) and photoluminescence maps (NIR-PL system, Shimazu).

7.2.2 Preparation of PEO and PEO/DNA solution

The PEO (7 wt%, MW = 300,000, Aldrich Co.) was dissolved in distilled water. Also, the 7 wt% of DNA solution and the 7 wt% of DNA-dispersed DWNT solutions were prepared. Then, the 7 wt% of DNA or the 7 wt% of DNA-dispersed DWNT/PEO solution was added to PEO solution at different blending ratios (*e.g.*, PEO/DNA = 100/0, 90/10, 80/20, 70/30, 60/40, 50/50, 40/60, 30/70, 20/80 and 10/90). Then, 1 % and 5 % DNA-dispersed DWNT solutions were added to PEO/DNA solution, respectively.

7.2.3 Nanofiber Formation Using the Electrospinning System

The PEO/DNA solution was transferred into a 5 ml syringe with a capillary tip of 0.5 mm in diameter. Using typical apparatus electrospinning is carried out by applying a voltage of 10-15 kV, flow late of 0.3-0.5 ml/h and tip-to-collector distance of 8-12 cm. The electrospun fibers were collected as thin web by rotating metal drum (about 50 rpm) wrapped with aluminum foil.

7.2.4 Analysis of Electrospun Nanofiber Web

The macromorphology of the nanofiber web was observed by SEM (JSM-7000F, JEOL). The mechanical properties of the specimens were evaluated at room temperature according to the ASTM D638 test method using a tensile tester (RTC Series) for a rectangular specimen. The dimensions of the specimens were 60 (length) ×10 (width) × 0.50 (thickness) mm. The following measurement conditions were used: gauge length = 25 mm; crosshead speed = 10 mm/min; load cell = 2.5 kN. A standard four probe method was used to measure the electrical conductivity of the composite films with the 1M6ex ZAHNER electric analyzer.

7.3 Results and Discussion

I used highly pure and highly crystalline DWNTs that were prepared by a catalytic CVD method (Fig. 1 (a)).[26] Then I prepared a homogeneously dispersed

DWNT suspension using double-stranded DNA (Fig. 1 (b)).[27] I confirmed the individually dispersed state of the tubes using optical tools. The appearance of three strong PL peaks in the PL map (Fig. 1 (c)) indicates the presence of individually isolated DWNTs in the DNA solution. In addition, DWNTs dispersed in a DNA solution exhibited well-resolved and sharp optical absorption peaks due to their excitonic transitions between Van Hove singularities (Fig. 1 (d)), thus indicating that nanotubes were individually dispersed.

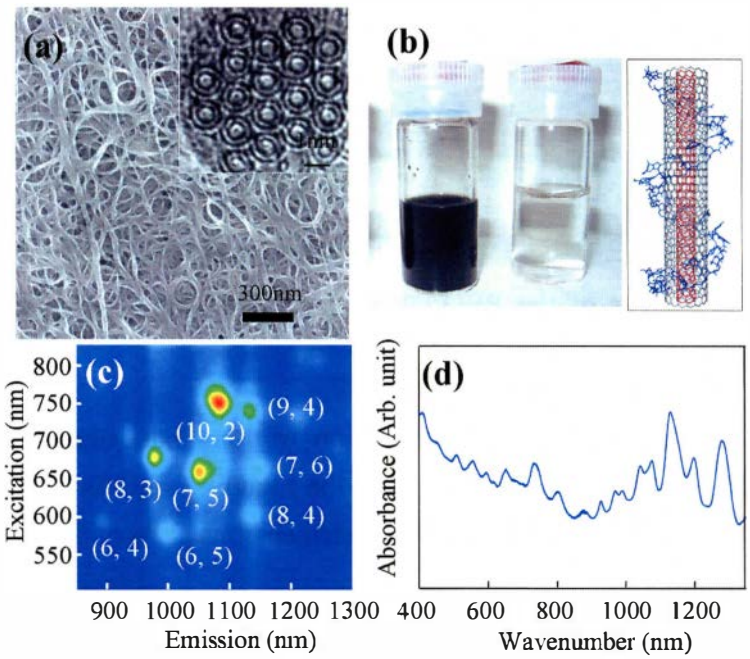

Figure 1 (a) SEM images of catalytically grown DWNTs (inset is a cross sectional TEM images showing a hexagonally packed structure), (b) DNA-dispersed DWNT suspensions (sonication (left) and ultra-centrifugation (right)) and the schematic model of DNA-wrapped DWNT, (c) PL map and (d) UV-visible absorption spectra of DNA-dispersed DWNT suspension at pH 8.0.

Then, I prepared PEO solution for electrospinning by adding DNA or DNA-dispersed DWNT suspensions and examined the spinnability of such PEO/DNA solutions at the different blending ratios. Interestingly, nanosized but long nanofibers are generated from PEO/DNA solutions that have blending ratios of 70/30 and 80/20 (Fig. 2 (a, b)). However, with increasing the fraction of DNA, the morphologies of the electrospun materials are largely changed from fibers to beads (Fig. 2 (c, d)). Such kind of morphological change could be explained by the low spinnability of DNA solution.

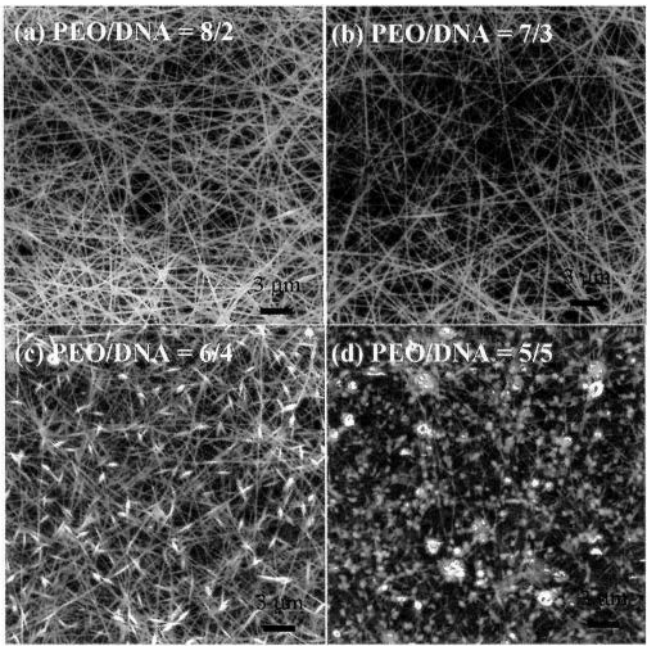

Figure 2 FE-SEM images of the PEO/DNA blend electrospun fiber web at different blending ratios.

In addition, I confirmed the formation of long nanofiber web (Fig. 3) by electrospining the PEO/DNA solutions (when the blending ratio is PEO/DNA = 80/20 and 70/30) containing DNA-dispersed DWNT suspensions (1 % or 5 %).

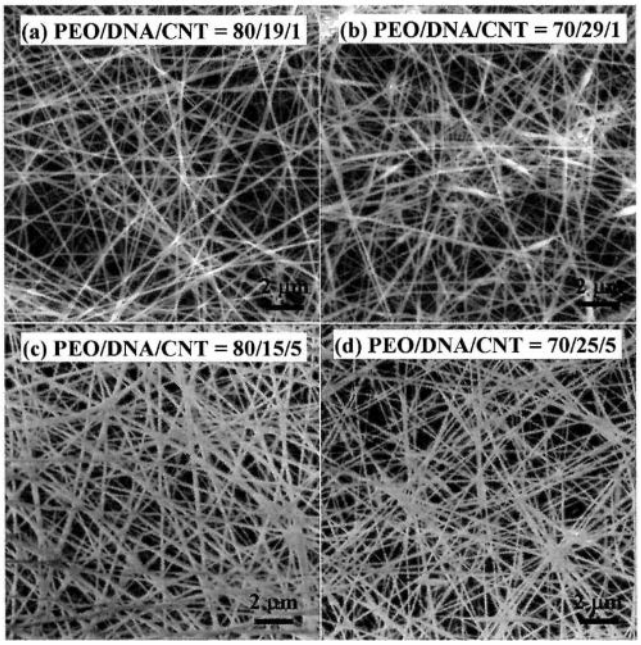

Fig. 3 FE-SEM images of the PEO/DNA/DWNT electrospun fiber web containing 1% (a, b) and 5 % DNA-dispersed DWNTs (c, d), respectively.

The miscibility of PEO and DNA in nanofiber was characterized using the low-resolution TEM observation. The absence of component separation indicates good phase miscibility of PEO/DNA. I found that the diameter of PEO/DNA nanofiber is about 100 nm (Fig. 4 (a)). However, the individually dispersed carbon nanotubes were not observed, because of the small amount of CNTs within PEO nanofiber. Alternatively, I carried out SEM observation of PEO/DNA/CNT nanofiber web after removing PEO and DNA with distilled water several times. Interestingly, I was able to see individually dispersed and very long nanotubes (Fig. 4 (b)).

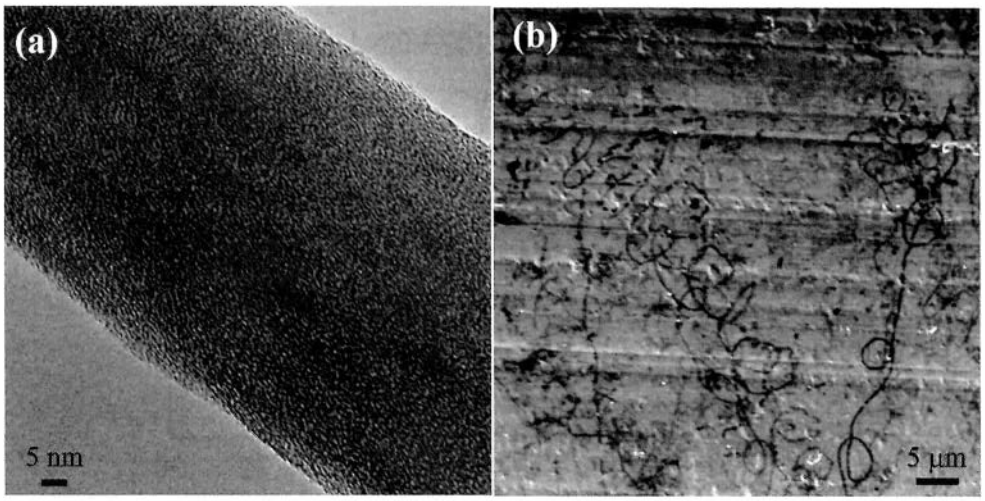

Figure 4 (a) Low-resolution TEM and (b) FE-SEM images of the PEO/DNA/CNT-derived nanofiber.

Finally, in order to confirm the effectiveness of DNA-wrapped DWNTs in PEO nanofiber, the electrical conductivity of the nanofiber webs is measured using the four probe method whereas their mechanical strength were evaluated using a tensile tester. As shown in Table 1, the relatively high electrical conductivity of nanofiber web from PEO/DNA solution indicates that DNA acts as an electrical path in PEO nanofiber. In addition, we have prepared highly conductive PEO nanofibers having 3.72×10^2 S/cm by electrospinning PEO solution containing 5 % of DWNTs that are individually dispersed with the help of DNA. Figure 5 shows the stress-strain curves of the electrospun nanofiber webs, indicating that the addition of DNA or DNA-wrapped CNTs surely improve the tensile properties of PEO-derived nanofiber web. Noticeably, the addition of the DNA-wrapped CNTs allows the PEO nanofiber web to have a 5 times enhanced modulus and a doubled tensile strength, compared to the corresponding values of the pure PEO nanofiber web. Thus, I expect that the individually present

DNA-wrapped CNTs are present within PEO nanofiber along the length direction, where DNA molecules act as a buffer between CNTs and PEO.

Table 1 Electrical Conductivity of PEO/DNA and PEO/DNA/CNT Nanofiber Web

I.D.	PEO/DNA (S/cm)	PEO/DNA/CNT (1%) (S/cm)	PEO/DNA/CNT (5%) (S/cm)
Average	2.54×10^{-4}	7.65×10^{-2}	3.72×10^{2}

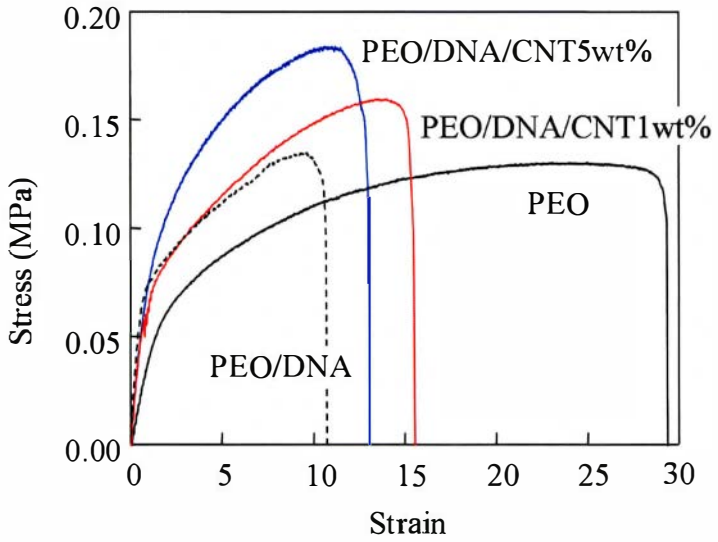

Figure 5 Stress-strain curves of pure PEO-, PEO/DNA and PEO/DNA/DWNTs-derived electrospun nanofiber webs.

7.4 Conclusion

I have fabricated long and homogenous nanofiber web by electrospinning PEO solution containing DNA-wrapped DWNTs. The individually dispersed state of DWNTs in DNA solution was confirmed by optical studies. In addition, I have confirmed that DNA and DNA-wrapped CNTs within PEO nanofiber acted as electrical path as well as the effective reinforcing filler, resulting in the largely increased electrical conductivity and mechanical strength of PEO nanofiber web. Therefore, I envisages that electrically conductive, mechanically tough nanofiber web by incorporating CNTs is an interesting multifunctional biomaterial.

7.5 References

1. H. Yoshimoto, Y. M. Shin, H. Terai, J. P. Vacanti, *Biomaterials* **24**, 2077 (2003).
2. X. Zong, H. Bien, C. Y. Chung, L. Yinc, D. Fang, B. S. Hsiao, *Biomaterials* **26**, 5330 (2005).
3. Y. Zhang, J. R. Venugopal, A. El-Turki, S. Ramakrishna, B. Su, C. Lim, *Biomaterials* **29**, 4314 (2008).
4. C. P. Barnes, S. A. Sell, E. D. Boland, D. G. Simpson, G. L. Bowlin, *Adv. Drug Deliv. Rev.* **59**, 1413 (2007).
5. S. Agarwal, J. H. Wendorff, A. Greiner, *Polymer* **49**, 5603 (2008).
6. Y. Zhang, C. T. Lim, S. Ramakrishna, Zh. Huang, *J. Mater. Sci. Mater. Med.* **16**, 933 (2005).
7. I. K. Kwon, S. Kidoaki, T. Matsuda, *Biomaterials* **26**, 3929 (2005).
8. K. S. Rho, L. Jeong, G. Lee, B. M. Seo, Y. J. Park, S. Hong, *Biomaterials* **27**, 1452 (2006).
9. B. W. Tillman, S. K. Yazdani, S. J. Lee, R. L. Geary, a. Atala, J. J. Yoo, *Biomaterials* **30**, 583 (2009).
10. J. D. Roh, G. N. Nelson, M. P. Brennam, T. L. Mirensky, T. Yi, T. F. Hazlett, *Biomaterials* **29**, 1454 (2008).
11. S. Ramakrishna, K. Fujihara, W.-E. Teo, T.-C. Lim, Z. Ma, *An Introduction to Electrospinning and Nanofibers*, World Scientific, Singapore (2005).
12. L. Huang, K. Nagapudi, R.P. Apkarian, E. Chaikof, *J. Biomat. Sci. Poly. Edi.* **12**, 979 (2001).
13. M. S. Dresselhaus, G. Dresselhaus and P. C. Eklund, *Science of Fullerenes and Carbon Nanotubes*, Academic Press, San Diego (1996).
14. K. Fu, Y. P. Sun, J. Nanosci. Nanotechnol. 3, 351 (2003).
15. L. Vaisman, H. Daniel Wagner, G. Marom, *Adv. Colloid Interface Sci.* **128-130**, 37 (2006).
16. M. S. Strano, M. Zheng, A. Jagota, G. B. Onoa, D. A. Heller, P. W. Barone, M. L. Usrey, *Nano Lett.* **4**, 543 (2004).
17. S. Niyogi, M.A. Hamon, H. Hu, B. Zhao, P. Bhowmik, R. Sen, M. E. Itkis, R. C. Haddon, *Acc. Chem. Res.* **35**, 1105 (2002).
18. S. Banerjee, T. Hemraj-Benny, S. S. Wong, *Adv. Mater.* **17**, 17 (2005).
19. M. Zheng, B.A. Diner, *J. Am. Chem. Soc.* **126**, 15490 (2004).

20. C. Fantini, A. Jorio, A. P. Santos,V. S. T. Peressinotto, M.A. Pimenta, *Chem. Phys. Lett.* **439**, 138 (2007).
21. X. Zhao, J. K. Johnson, *J. Am. Chem. Soc.* **129**, 10438 (2007).
22. S. Meng, P. Maragakis, C. Papaloukas, E. Kaxiras, *Nano Lett.* **7**, 45 (2007).
23. Y. Chen, H. Liu, T. Ye, J. Kim, C. Mao, *J. Am. Chem. Soc.* **129**, 8696 (2007).
24. S. R. Vogel, M. M. Kappes, F. Hennrich, C. Richert, *Chem. Eur. J.* **13**, 1815 (2007).
25. D. Das, A. K. Sood, P. K. Maiti, M. Das, R. Varadarajan, C. N. R. Rao, *Chem. Phys. Lett.* **453**, 266 (2008).
26. M. Endo, H. Muramatsu, T. Hayashi, Y. A. Kim, M. Terrones, M. S. Dresselhaus, *Nature* **433**, 476 (2005).
27. J. H. Kim, M. Kataoka, D. Shimamoto, H. Muramatsu, Y. C. Jung, T. Hayashi, Y. A. Kim, M. Endo, J. S. Park, R. Saito, M. Terrones, M. S. Dresselhaus, *ACS Nano* **4**, 1060 (2010).

CHAPTER 8

Exocellulase Activity of Cellobiohydrolase Immobilized on DNA-Wrapped Single-Walled Carbon Nanotubes

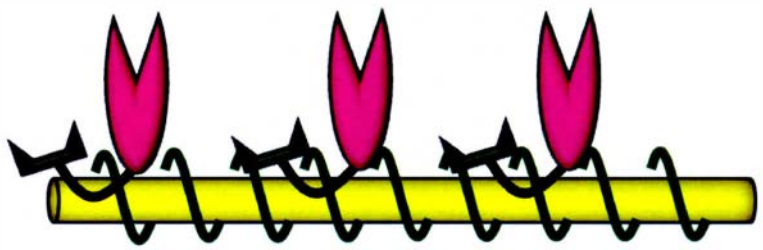

Chapter 8 Exocellulase Activity of Cellobiohydrolase Immobilized on DNA-Wrapped Single-Walled Carbon Nanotubes

8.1 Introduction

Cellulases constitute a class of enzymes that are able to catalyze the hydrolysis of cellulose.[1] Their rate-enhancing ability and selectivity[2] enable them to be commercially used in converting cellulose to ethanol, food processing and pharmaceutical applications; these enzymes are also used in the textile industry and the pulp and paper industry. Among these uses, the development of efficient means of converting cellulose into ethanol by exploiting the intrinsic activity of bacterial or fungal cellulase has been the most intensively investigated.[3] However, the enzymatic activity of cellulases strongly depends on the morphology and crystallinity of cellulose, as well as on the form of cellulase and the solution conditions.[4, 5] Although cellulases have excellent catalytic activity and low environmental impact, a major obstacle to their wider use in industry is that their activity deteriorates under harsh conditions (e.g., high temperature and pH extremes). In this chapter, I aim to address these problems, and in particular, I investigate the use of long SWNTs as substrates for cellulase.[6] However, SWNTs tend to form bundles in an aqueous medium because of their hydrophobic nature. In order to fully utilize the effects of the SWNTs, ssDNA has been used to disperse (or debundle) the individual tubes.[7-10] In this work, individually dispersed SWNTs, helically wrapped with DNA were selected as the substrate for immobilizing cellulase. In other words, by immobilizing cellulose on the sidewall of SWNTs dispersed by helically wrapped DNA, we have developed a novel type of cellulase that is both alkali- and thermo-stable. The hydrophobic interactions between the sidewall of the tubes and the cellulases are helpful for maintaining the shape of the cellulase molecules in the temperature range of 40–80 °C, while the helically wrapped DNA along the sidewall of the a tube imparts high stability at high pH. It is envisaged that this alkali- and thermo-stable form of cellulase can be used over a wide range of temperatures and environmental conditions.

8.2 Experimental Section

8.2.1 The Dispersion of Carbon Nanotubes

I prepared ssDNA solution as described in section 2.2. The HiPco-based high-purity SWNTs[10] (ca. 10 mg) were dispersed in aqueous solution (10 ml) with the aid of ssDNA wrapping under strong sonication (Kubota UP50H, ca. 470 W/cm^2) for 1 h at 4 °C.

8.2.2 Immobilization of Cellulases on DNA-wrapped Carbon Nanotubes

I prepared exocellulases (Ex-1 from *Irpex lacteus*) as described in our previous study.[11] Ex-1 (600 μl, 30 mg/ml) was mixed with 3 ml of ssDNA-dispersed SWNT suspension under mild sonication for 1 h at 4°C. The strongly bundled SWNTs were isolated by gentle centrifugation (Optima Max-XP, Beckman Coulter, 20,000 g). The supernatant (70 % by volume), enriched with individually dispersed SWNTs, was filtered through a 0.22μm membrane. The prepared suspension of cellulase immobilized on DNA-wrapped individually dispersed SWNTs did not contain free DNA.

8.2.3 The Assay of Cellulase Activity

The activity of CBH was assayed in 50 mM sodium acetate buffer (pH = 5.0) at 40 °C using PNP-lactose as substrate. The activity was monitored by measuring the release of PNP as a function of time. Concentrations of ssDNA and Ex-1 in SWNT suspension were determined on a Qubit Fluorometer. The filtered cellulase immobilized on DNA-dispersed SWNT suspension was characterized in solution by Raman spectroscopy (excitation: 785 nm) using a quartz cuvette and a Renishaw setup fitted with a macroscopic sampling kit. UV-Vis spectroscopy (SolidSpec-3700, Shimazu) was carried out to confirm the presence of individually dispersed SWNTs in the suspension.

8.3 Results and Discussion

In aqueous media, SWNTs are insoluble because of the hydrophobic nature of their sidewall and aggregate into bundles because of the strong van der Waals interactions between adjacent tubes. Thus, to fully exploit their intrinsic optical signals as well as their high specific surface in bio/medical fields, noncovalent methods using biocompatible biomolecules[13, 14] have been investigated to disperse the strongly bundled SWNT sample. However, thermally sensitive proteins have limited dispersing ability, and consequently the strongly bundled SWNT sample must generally be dispersed into solution under strong sonication for a long time. To solve this problem, SWNTs individually dispersed in suspension with the aid of DNA[9, 10] can be used as substrate for immobilizing cellulases.

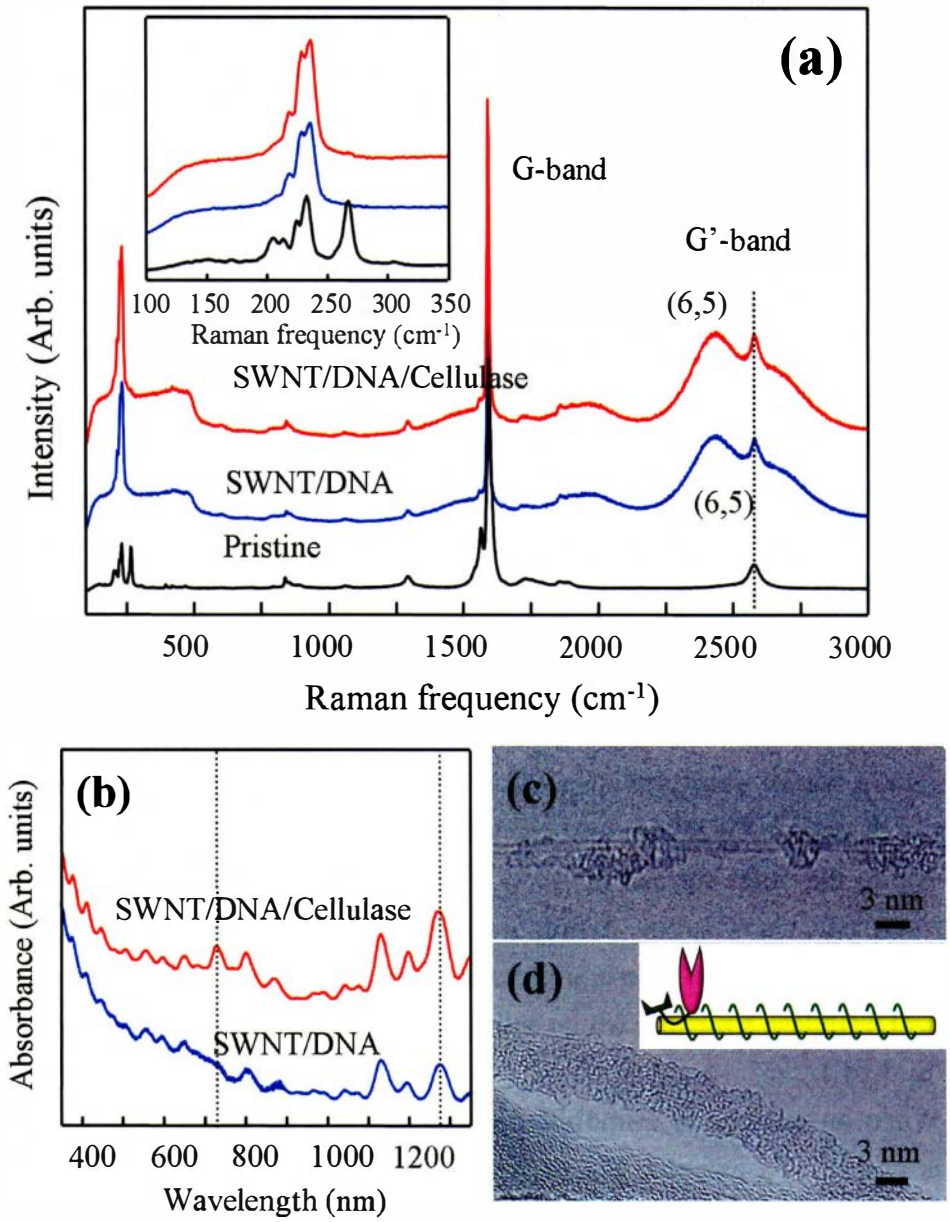

Figure 1 (a) Raman/fluorescence spectra acquired using laser excitation of 785 nm for pristine SWNTs, SWNT/DNA and SWNT/DNA/cellulase suspensions (Inset is a magnified low-frequency Raman spectra for the corresponding samples). (b) UV absorption spectra for SWNT/DNA and SWNT/DNA/cellulase suspensions. Typical TEM images (c, d) show that SWNTs are individually dispersed with the aid of DNA and cellulases. Inset shows the proposed model of the hybrid SWNT/DNA/cellulase structure.

In Raman/fluorescence spectra acquired using laser excitation of 785 nm (Fig. 1 (a)), we can see a strong G-band (E_{2g2} mode) around 1592 cm^{-1}, while several radial

breathing modes below 500 cm^{-1} can be seen along with the second-order symmetry-allowed G'-band around 2600 cm^{-1}.[15] However, upon sonication of the SWNTs in an aqueous solution with DNA, a strong luminescence peak appeared around 2500 cm^{-1}, indicating that individually dispersed SWNTs having chirality of *(6,5)* were generated through the interaction with DNA, because luminescent signals are completely quenched from the bundled sample due to the presence of entrapped metallic impurities.[16] The depression of the broad and asymmetric Breit-Wigner-Fano line could be explained by water molecule-induced transition from metallic to a p-type semiconducting SWNTs.[17, 18] More interestingly, the lack of a distinctive change in the low-frequency Raman spectra of the DNA/SWNT/cellulase suspension (see inset in Fig. 1 (a)) indicates that cellulases do not disturb the individually dispersed state of SWNTs in suspension. In addition, both DNA/SWNT and DNA/SWNT/cellulase suspensions exhibited well-resolved and sharp optical absorption peaks due to their excitonic transitions between van Hove singularities (Fig. 1 (b)), thus indicating that SWNTs were individually dispersed.[16] The new absorption peak at 720 nm as well as the intensified absorption peak at 1280 nm for DNA/SWNT/cellulase suspension indicates that cellulase has a partial ability to disperse SWNTs via a hydrophobic interaction. The individually dispersed SWNTs in low resolution TEM (Fig. 1 (c)) revealed that DNA is wrapped along the outer surface of SWNT, where cellulases are attached to the bare nanotube surfaces via a strong hydrophobic interaction, resulting in DNA-cellulase coated SWNTs (Fig. 1 (d)). Therefore, we are able to propose a model of the hybrid DNA/SWNT/cellulase structure, where cellulases cover the bare spaces of the tubes (see inset in Fig. 1 (d)).

When an enzyme is immobilized on a specific substrate, retaining cellulase activity is critical. To examine the enzymatic activity of cellulases immobilized on DNA-wrapped SWNTs, we selected Ex-1 as a model cellulase because of their ability to break down cellulosic materials into cellobiose and a small amount of glucose.[19] In the prepared SWNT suspension, the measured concentrations of ssDNA and Ex-1 were 12.3 μg/ml and 71.0 μg/ml, respectively. We observed higher initial rates for cellulases immobilized on DNA-wrapped SWNTs than for free cellulase (Fig. 2). Two possible reasons for this enhancement are (a) cellulases are attached to the highly dispersed SWNTs that have high accessible surface area (i.e., mass transfer can rapidly occur), and (b) the cellulase structure is maintained even after immobilization on SWNTs.

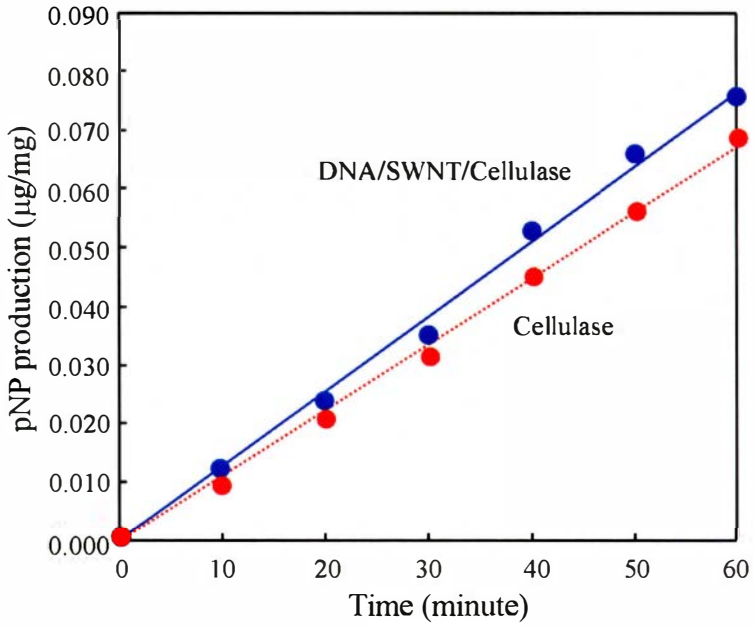

Figure 2 Initial enzymatic activity of cellulase immobilized on DNA-wrapped SWNTs compared to free cellulase

Finally, we examined the effects of temperature and pH on the stability of cellulases. We measure the relative activity of cellulase in the temperature range between 40 and 70 °C and at pH extremes. The continuous decrease in the rate of activity for free cellulase (Fig. 3 (a)) with increasing temperature is due to disruption of the intramolecular bonds (e.g., hydrogen bond) that maintain the shape of the molecule. [20] In contrast, the cellulases immobilized on DNA-wrapped SWNTs retained their relative activity of 90 % up to 50 °C, and also showed 50 % activity at 60 °C. Such improved stability of cellulase at high temperature can be explained by the strong hydrophobic interaction between cellulase and the sidewall of a SWNT, which is critical for preventing a change in the molecular structure or active sites. In addition, cellulase on DNA/SWNT showed decreased stability under acidic conditions, but improved stability under basic conditions (Fig. 3 (b)), because DNA is unstable under acidic conditions and stable under basic ones. Thus, DNA that is helically wrapped around the sidewall of the tubes provides cellulase with high stability at high pH.

8.4 Conclusion

I have successfully immobilized Ex-1 on the open sidewall spaces of SWNTs that were helically wrapped with DNA. We observed retained or enhanced enzymatic activity of cellulases when they were hybridized with individually dispersed

DNA-wrapped SWNTs. At temperatures above 40 °C, free cellulase is generally denatured, leading to change of the active site's shape. However, the hybridized cellulases exhibited highly enhanced activity at temperatures between 40 and 80 °C as well as the improved stability under basic conditions, because the hydrophobic interactions between SWNTs and cellulases partially restrict the mobility of molecular chains. Taken together, the thermostability and high activity observed in this work indicate that cellulases immobilized on individually dispersed DNA-wrapped SWNTs are promising biocatalysts for cellulose over a wide range of temperatures and environmental conditions.

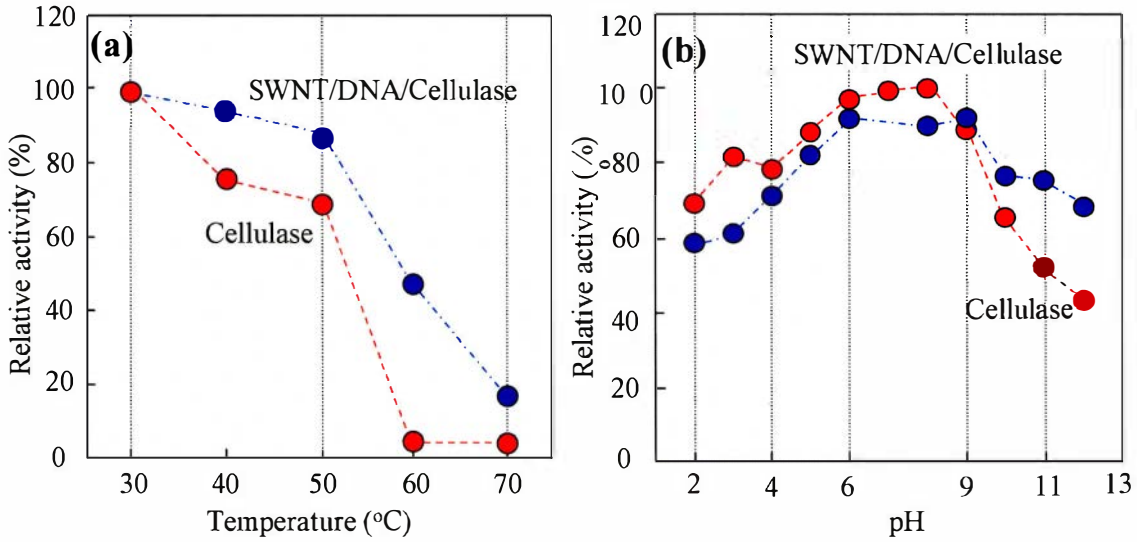

Figure 3 Activity retention of cellulase immobilized on DNA-wrapped SWNT compared to free cellulase at temperatures between 40 and 80 °C and at pH extremes.

8.5 References

1. M. L. Rabinovich, M. S. Melnik and A. V. Bolobova, *Appl. Biochem. Microbio.* **38**, 305 (2002).
2. S. J. Benkovic, S. Hammes-Schiffer, *Science* **301**, 1196 (2003).
3. M. E. Himmel, M. F. Ruth, C. E. Wyman, *Curr. Opin. Biotech.* **10**, 358 (1999).
4. N. Hayashi, J. Sugiyama, T. Okano, M. Ishihara, *Carbohydr. Res.* **305**, 261 (1998).
5. Y. Amano, K. Nozaki, T. Araki, H. Shibasaki, S. Kuga, T. Kanda, *Cellulose* **8**, 267 (2002).
6. M. S. Dresselhaus, G. Dresselhaus, P. C. Eklund, *Science of Fullerenes and Carbon Nanotubes*, Academic Press, New York, 1995.
7. N. Nakashima, S. Okuzono, H. Murakami, T. Nakai, K. Yoshikawa, *Chem. Lett.* **32**, 456 (2003).
8. M. Zheng, A. Jagota, E. D. Semke, B. A. Diner, R. S. McLean, S. R. Lustig, R. E. Richardson, N. G. Tassi, *Nat. Mater.* **2**, 338 (2003).
9. J. H. Kim, M. Kataoka, Y. A. Kim, D. Shimamoto, H. Muramatsu, T. Hayashi, M. Endo, M. Terrones, M. S. Dresselhaus, *Appl. Phys. Lett.* **93**, 223107 (2008).
10. J. H. Kim, M. Kataoka, D. Shimamoto, H. Muramatsu, Y. C. Jung, T. Tojo, T. Hayashi, Y. A. Kim, M. Endo, M. Terrones, M. S. Dresselhaus, *ChemPhysChem* **10**, 2414 (2009).
11. M. J. Bronikowski, P. A. Willis, D. T. Colbert, K. A. Smith, R. E. Smalley, *J. Vac. Sci. Technol. A* **19**, 1800 (2001).
12. Y. Amano, M. Shiroishi, K. Nisizawa, E. Hoshino, T. Kanda, *J. Biochem.* **120**, 1123 (1996).
13. P. W. Barone, S. Baik, D. A. Heller, M. S. Strano, *Nat. Mater.* **4**, 86 (2005).
14. R. J. Chen, S. Bangsaruntip, K. A. Drouvalakis, N. W. S. Kam, M. Shim, Y. Li, P. J. Utz, H. Dai, *Proc. Natl. Acad. Sci.* **100**, 4984 (2003).
15. A. M. Rao, E. Richter, S. Bandow, B. Chase, P. C. Eklund, K. W. Williams, M. Menon, K. R. Subbaswamy, A. Thess, R. E. Smalley, G. Dresselhaus, M. S. Dresselhaus, *Science* **275**, 187 (1997).
16. M. J. O'Connell, S. M. Bachilo, C. B. Huffman, V. C. Moore, M. S. Strano, E. H. Haroz, K. L. Rialon, P. J. Boul, W. H. Noon, C. Kittrell, J. Ma, R. H. Hauge, R. B. Weisman, R. E. Smalley, *Science* **297**, 593 (2002).
17. M. Shoda, S. Bandow, Y. Maruyama, S. Iijima, *J. Phys. Chem. C* **113**, 6033 (2009).
18. M. Cha, S. Jung, M.-H. Cha, G. Kim, J. Ihm, J. Lee, *Nano Lett.* **9**, 1345 (2009).
19. C. Divine, J. Stahlberg, T. Reinikainen, *Science* **265**, 524 (1994).

20. W. Parker, P. S. Song, *Biophys. J.* **61**, 1435 (1992).

CHAPTER 9

Concluding Remarks and Future Works

Chapter 9 Concluding Remarks and Future Works

9.1 Concluding Remarks

My PhD thesis is constructed based on three parts; (a) the method of functionalizing the bundled CNTs with biomolecules in order to individually disperse as well as to impart high biocompatibility, (b) the elucidation of interaction between the sidewall of CNTs and DNA, and (c) the promising end-uses of the biomolecule-decorated carbon nanotubes.

I confirmed the variation of the dispersibility of CNTs in DNA solution in terms of nanotube quality by optical spectroscopy (chapter 3). DNA was helically wrapped around the sidewall of the tubes in an irregular pattern. Structural defects on the sidewall of nanotubes were found to provide additional sites for binding with DNA. In addition, the nitrogenated sites within nitrogen-doped CNTs provided additional sites for interactions that are important to disperse nanotubes in DNA solutions (chapter 4). I demonstrated the ability of dispersing CNTs in an aqueous solution with a homogeneous coating of mussel protein on the sidewall of tubes (chapter 6).

I revealed the hidden interaction between DNA and the outer tubes in a DWNT solution, where the inner tubes are structurally shielded by outer tubes, and where a possible charge transfer occurs from the outer tubes to the inner tubes, thereby affecting the luminescence from the inner tubes (chapter 5). The luminescence signals from the inner tubes of DWNTs are intensified in the isolated state of each individual DWNT. The completely depressed RBMs associated with the outer tubes (whether semiconducting or metallic) via the mechanical wrapping and the strong charge transfer between DNA and outer tubes support our interpretation that the bright luminescence and sharp absorption spectra come from only the inner tubes, and not from isolated SWNTs. The circumferentially wrapped DNA on the outer tubes of individually isolated DWNTs in an aqueous solution gives rise to strong charge transfer to the semiconducting and metallic outer tubes as well as to generating physical strain in the outer tubes.

Finally, I demonstrated the effectiveness of DNA or DNA-wrapped CNTs as reinforcing filler in fabricating mechanically strong and electrically conductive PEO nanofiber web using the electrospinning system (chapter 7). In addition, I developed a novel type of cellulase that is both alkali- and thermo-stable by immobilizing cellulose on the sidewall of CNTs dispersed by helically wrapped DNA (chapter 8).

My future work will focus on the application of these newly designed platforms.

9.2 Future Works

9.2.1 Mussel protein coated Carbon Nanotube for Cancer Therapy

Mussel protein is an exciting biomaterial for life science and medical applications. In chapter 6, I demonstrated the homogeneous dispersion of tubes in an aqueous solution by coating mussel protein on the sidewall of tubes. Among various characteristics of mussel protein, the most fantastic feature is that specific bioactive peptides which genetically have the ability of mimicking the extracellular matrix protein for cell growth could be incorporated into the mussel protein (Fig. 1).[1] Recently, it is reported that a novel liner protein (BC-MAP) is designed and produced in *Escherichia coli* by genetically fusing mussel adhesive protein for efficient antibody immobilization on diverse surfaces.[2] Using such new technology, I have a plan to fabricate new platform, mussel protein-coated CNTs containing a specific antibody, that are optically and biologically active, and are promising tool for the targeted caner therapy.

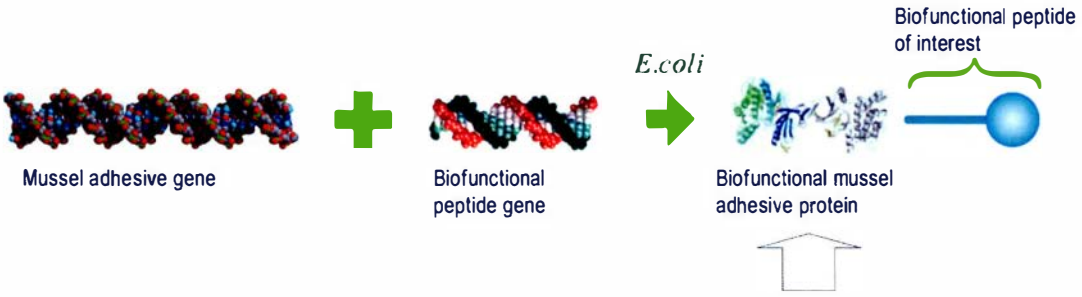

Figure 1 Novel strategy for incorporating specific bioactive peptides into the mussel protein.[1]

9.2.2 Mussel protein coated Carbon Nanofiber Web and Carbon Nanotube Buckypaper for Growing Cells

The CNTs and the electrospun carbon fiber were demonstrated to be effective as bone tissue scaffold.[3, 4] However, using a versatile biochemical activity of mussel protein, I have a plan to use mussel protein coated CNT buckypaper and the electrospun carbon nanofiber web as bone tissue scaffold.

9.3 References

1. www.kollodis.com
2. C. S. Kim, Y. S. Choi, W. Ko, J. H. Seo, J. Lee, H. J. Cha, *Adv. Funct. Mater.* **21**, 4104 (2011).
3. Y. Usui, K. Aoki, N. Narita, N. Murakami, I. Nakamura, K. Nakamura, N. Ishigaki, H. Yamazaki, H. Horiuchi, H. Kato, M. Kondo, T. Nakanishi, S. Taruta, Y. A. Kim, M. Endo, N. Saito, *Small* **4**, 240 (2008).
4. K. Aoki, Y. Usui, N. Narita, N. Ogiwara, N. Iashigaki, K. Nakamura, H. Kato, K. Sano, N. Ogiwara, K. Kametani, C. Kim, S. Taruta, Y. A. Kim, M. Endo, N. Saito, *Small* **5**, 1540 (2009).

Publications

Publications and Presentations

1. Publications

- J. H. Kim, M. Kataoka, D. Shimamoto, H. Muramatsu, Y. C. Jung, T. Tojo, T. Hayashi, Y. A. Kim, M. Endo, M. Terrones, M. S. Dresselhaus, Defect-enhanced Dispersion of Carbon Nanotubes in DNA Solutions, *ChemPhysChem* **10**, 2414–2417 (2009).
- L. Cooper, H. Amano, M. Hiraide, S. Houkyou, I. Y. Jang, Y. J. Kim, H. Muramatsu, J. H. Kim, T. Hayashi, Y. A. Kim, M. Endo, M. S. Dresselhaus, Freestanding, Bendable, Thin Film for Supercapacitors Using DNA-Dispersed Double Walled Carbon Nanotubes, *Applied Physics Letters.* **95**, 233104 (2009).
- Y. C. Jung, H. Muramatsu, K. C. Park, D. Shimamoto, J. H. Kim, T. Hayashi, S. M. Song, Y. A. Kim, M. Endo, M. S. Dresselhaus, Transparent and Conductive Polyethylene Oxide Film by the Introduction of Individualized Single-Walled Carbon Nanotubes, *Macromolecular Rapid Communications* **30**, 2084–2088 (2009)
- J. H. Kim, M. Kataoka, D. Shimamoto, H. Muramatsu, Y. C. Jung, T. Hayashi, Y. A. Kim, M. Endo, J. S. Park, R. Saito, M. Terrones, M. S. Dresselhaus, Raman and Fluorescence Spectroscopic Studies of a DNA-Dispersed Double Walled Carbon Nanotube Solution, *ACS Nano* **4 (2)**, 1060–1066 (2010).
- Y. A. Kim, H. Kakegawa, K. Fujisawa, D. Shimamoto, H. Muramatsu, J. H. Kim, Y. C. Jung, T. Hayashi, M. Endo, M. Terrones, M. S. Dresselhaus, Sensitive G-band Raman features for the electrical conductivity of multi-walled carbon nanotubes, *Journal of Nanoscience and Nanotechnology* **10**, 3940–3944 (2010).
- Y. C. Jung, H. Muramatsu, T. Hayashi, J. H. Kim, Y. A. Kim, M. Endo, M. S. Dresselhaus, Covalent Attachment of Aromatic Diisocyanate to the Sidewall of Single- and Double-Walled Carbon Nanotubes, *European Journal of Inorganic Chemistry* **24**, 4305–4308 (2010)
- Y. C. Jung, H. H. Kim, Y. A. Kim, J. H. Kim, J. W. Cho, M. Endo, M. S. Dresselhaus, Optically Active Multi-Walled Carbon Nanotubes for Transparent, Conductive Memory-Shape Polyurethane Film, *Macromolecules* **43**, 6106–6112 (2010)
- K. Fujisawa, T. Tojo, H. Muramatsu, A. L. Elías, S. M. Vega-Díaz, F. Tristán-López, J. H. Kim, T. Hayashi, Y. A. Kim, M. Endo, M. Terrones, Enhanced Electrical Conductivities of N-doped Carbon Nanotubes by Controlled Heat Treatments, *Nanoscale* **3**, 4359–4364 (2011).
- J. H. Kim, M. Kataoka, A. Kumagai, H. Nishijima, Y. Amano, Y. A. Kim, M. Endo, Exocellulase Activity of Cellobiohydrolase Immobilized on DNA-Wrapped Single-Walled Carbon Nanotubes, *ChemSusChem* **4**, 1595–1597 (2011).
- J. H. Kim, M. Kataoka, K. Fujisawa, T. Tojo, H. Muramatsu, S. M. Vega-Díaz, F. Tristán-López, T. Hayashi, Y. A. Kim, M. Endo, M. Terrones, M. S. Dresselhaus, Unusually High Dispersion of Nitrogen-Doped Carbon Nanotubes in DNA Solution, *Journal of Physical Chemistry B* **115**, 14295–14300 (2011).

- Y. C. Jung, H. Muramatsu, K. Fujisawa, J. H. Kim, T. Hayashi, Y. A. Kim, M. Endo, M. Terrones, M. S. Dresselhaus, Optically and Biologically Active Mussel Protein-Coated Double Walled Carbon Nanotube, *Small* **7**, 3292–3297 (2011).
- E. Cho, C. Kim, J.-K. Kook, Y. I. Jeong, J. H. Kim, Y. A. Kim, M. Endo, Fabrication of Electrospun PVDF Nanofiber Membrane for Western Blot with High Sensitivity, *Journal of Membrane Science* **389**, 349–354 (2012).

2. Oral Presentations

- J. H. Kim, Y. A. Kim, M. Endo, M. Kataoka, Biomolecules-Assisted Dispersion and Surface Functionalization of Carbon Nanotubes, Annual Meeting of Japan society for Bioscience, Biotechnology, and Agro-chemistry 2011, 3C38a09, March 25–28, 2011, Kyoto, Japan.
- J. H. Kim, M. Kataoka, Y. A. Kim, M. Endo, Tough, Conductive PEO Nanofiber Web by Incorporating DNA or DNA-Wrapped Carbon Nanotubes, Annual World Conference on Carbon (Carbon 2011), July 24–29, 2011, Shanghai, China.

3. Posters

- J. H. Kim, M. Kataoka, Y. A. Kim, D. Shimamoto, H. Muramatsu, T. Hayashi, M. Endo, M. Terrones, M. S. Dresselhaus, Dispersion and Diameter-selective Separation of Double Walled Carbon Nanotubes in an Aqueous DNA Solution, The 5th International Conference on Advanced Fiber/Textile Materials, S1-P-08, September 8, 2009, Ueda, Japan.
- J. H. Kim, M. Kataoka, Y. A. Kim, T. Hayashi, H. Muramatsu, D. Shimamoto and M. Endo, The Isolation and Diameter-Selective Separation of Double Walled Carbon Nanotubes via a DNA Wrapping, The 3rd Conference on Colloid and Interface Science, PO69, October 12–13, 2009, Jeju, Korea.
- J. H. Kim, M. Kataoka, Y. A. Kim, M. Endo, M. Terrones, M.S. Dresselhaus, Raman and fluorescence spectroscopic studies of DNA-dispersed double walled carbon nanotube solution, 10th International Conference on Science and Application of Nanotubes (NT10), P101, June 27–July 2, 2010, Montreal, Canada.
- J. H. Kim, M. Kataoka, Y. A. Kim, M. Endo, M. S. Dresselhaus, Optical Spectroscopic Studies of DNA-Wrapped Double Walled Carbon Nanotube Suspension, International Conference of Future Textile 2010, P-40, July 15–17, 2010, Ueda, Japan.
- J. H. Kim, Y. A. Kim, M. Endo, M. Kataoka, Decorated Biomolecules on the Sidewall of Carbon Nanotubes and Their Dispersion in an Aqueous Solution, Biochemistry and Molecular Biology (BMB2010), 3P-1256, December 7–10, 2010, Kobe, Japan.
- J. H. Kim, Y. A. Kim, M. Endo, M. Kataoka, Mechanically Tough, Electrically Conductive PEO Nanofiber through the Incorporation DNA or DNA-Wrapped Carbon Nanotubes, The 6th International Conference on Advanced Fiber/Textile Materials 2011, December 7–9, 2011, Ueda, Japan

- J. H. Kim, M. Kataoka, Y. A. Kim, M. Endo, Tough, Conductive PEO Nanofiber Web by Incorporating DNA or DNA-Wrapped Carbon Nanotubes, 2nd Nanotoday Conference, December 11–15, 2011, Hawaii, USA.

Acknowledgements

At the beginning of my doctoral course, everything (e.g., a limited knowledge about science, a lack of computer skill, a limited English proficiency and childcare duty) was very hard for me.

However, with the help of many people, I could make a first step in science field and I realized that it is a rare opportunity to have such an experience in my life.

I would like to express my gratitude to Professor Masakazu Kataoka of the Department of Environmental Science & Technology in Shinshu University for giving me this opportunity, cordial guidance, discussion during my study. I also would like to thank to Professor Morinobu Endo of the Department of Electrical & Electronic Engineering in Shinshu University for providing me highly pure and crystalline carbon nanotube sample.

I wish to thank the members of the Kataoka Laboratory in Shinshu University (Yoshnobu Nomizu, Tetsu Miyatake, Takuya Matsuda, Midori Matusnaga, Atushi Suzuki, Yukihiro Fuseya, Makiko Shida, Yuma Fujimori, Daijiro Suzuki, Yasushi Arai, and Takumi Maeda). Their kind helpful cooperation made me spend my PhD course enjoyably.

Finally, I'd like to give my special thanks to my parents, my adorable sons (Seha and Serom), especially my husband and all of my families. Without their support, I could not stand here. Thanks again.